CRITICAL OXYGEN SUPPLY AND COMBUSTION THRESHOLDS OF SMOULDERING FIRES

YUNZHU QIN

PhD

The Hong Kong Polytechnic University

This programme is jointly offered by The Hong Kong Polytechnic University and University of Technology Sydney

2025

The Hong Kong Polytechnic University
Department of Building Environment and Energy Engineering

University of Technology Sydney
School of Civil and Environmental Engineering

Critical Oxygen Supply and Combustion Thresholds of Smouldering Fires

Yunzhu Qin

A thesis submitted in partial fulfilment of the requirements for the degree of
Doctor of Philosophy

March 2025

CERTIFICATE OF ORIGINALITY

I hereby declare that this thesis is my own work and that, to the best of my knowledge and belief, it reproduces no material previously published or written, nor material that has been accepted for the award of any other degree or diploma, except where due acknowledgement has been made in the text.

_____ (Signed)

Yunzhu Qin (Name of Student)

DEDICATION

To my beloved parents.

ABSTRACT

Critical Oxygen Supply and Combustion Thresholds of Smouldering Fires

by

Yunzhu Qin

Doctor of Philosophy in Department of Building Environment and Energy Engineering

The Hong Kong Polytechnic University, October 2024

Supervised by Dr. Xinyan Huang

Smouldering is a slow, low-temperature, and flameless form of combustion, primarily governed by two key mechanisms: system heat loss and **oxygen supply**. The path and rate of oxygen supply are critical for sustaining the heterogeneous oxidation reactions that generate the heat required to balance endothermic processes such as drying, preheating, environmental cooling, and pyrolysis during smouldering propagation. This thesis addresses the fundamental issue of oxygen thresholds in near-limit smouldering combustion and examining the effects of fuel properties and environmental conditions. Both experimental and computational studies were conducted to investigate the characteristics of limiting oxygen supply under forced internal flow. In addition, large-scale laboratory experiments (1 metre in height) were performed to demonstrate persistent deep smouldering fires under natural diffusion. The insights gained from this work deepen our understanding of smouldering combustion, contribute to more effective prevention strategies for smouldering fires, and help optimise applied smouldering systems.

The thesis is structured in a manuscript-style format, beginning with an introduction to the literature review and objectives in the first chapter. The following chapters each stand alone as an independent paper, which have been published in journals. In the final chapter, the overall outcomes are summarised and potential ideas for future research are outlined.

Chapter 1 reviewed the current methodologies and insights of limiting oxygen supply characteristics of smouldering. The knowledge gaps were identified, and general research objectives and methodologies were determined to address these gaps.

Chapter 2 experimentally determined the limiting oxygen supply to sustain smouldering propagation in peat soil. Oxidiser flow velocities (up to 14.7 mm/s) and oxygen concentrations ranging from 2% to 21% were controlled as forced internal flow to feed smouldering zone. The findings reveal a transition in smouldering behaviour: at higher velocities, smouldering propagates bidirectionally (forward and opposed), while reducing the velocity results in unidirectional propagation. At a velocity as low as 0.3 mm/s, smouldering ceases, with the minimum temperature recorded at around 300°C. As internal flow velocity increases, the limiting oxygen concentration (LOC) for sustaining smouldering decreases, reaching a minimum value below 2%. When the oxygen concentration exceeds 10%, the minimum oxygen supply rate stabilizes at 0.08 ± 0.01 g/m^2·s. However, for oxygen concentrations below 10%, the required oxygen supply rate rises significantly due to enhanced convective cooling caused by the higher internal flow velocities.

Chapter 3 investigated how bulk density and particle size control smouldering in porous pine needle beds (55–120 kg/m^3) and wood samples of particle size (1–50 mm). The experiments demonstrate that the critical airflow velocity for self-sustained smouldering rises when bulk density decreases or particle size grows. At elevated flow rates, smouldering initially advances only against the oxidiser stream, then transitions to simultaneous forward and opposed spread. However, for larger pore geometries, either from coarser particles or lower packing density, oxygen readily penetrates the opposed reaction front, leading to persistent bidirectional propagation. A simplified thermochemical model further reveals that interparticle conductive heat transfer plays important roles on the oxygen flux needed to maintain smouldering.

Chapter 4 presents a one-dimensional, physics-based simulation coupling multicomponent heat and mass transport with a five-step heterogeneous reaction scheme to quantify the oxygen thresholds for smouldering under forced internal flows. The model predicts that, for fixed flow velocity, the LOC for smouldering propagation is 3%, agreeing well with the experimental observations and theoretical analysis. Furthermore, the required flow rate increases with decreasing fuel density, lower ambient temperature, or higher moisture content, and the predicted maximum moisture content capable of supporting smouldering was about 110 %. At the smothering limit, the computed peak reaction-zone temperature and propagation rate are around 300 ^{o}C and 0.5 cm/h.

Chapter 5 conducts large-scale laboratory experiments demonstrating that, under purely

diffusive conditions, smouldering persists in deep peat layers for over ten days, independent of ignition depth. Four distinct propagation modes appear as the ignition point moves downward: (I) downward propagation, (II) upward-and-downward propagation, (III) in-depth propagation, and (IV) no propagation (local burning). Modes III and IV produce neither visible smoke nor surface collapse, underscoring the challenge of detecting subsurface peat fires. For ignition depths shallower than -40 cm, peak reaction-zone temperatures decline with depth. However, temperatures remained stable near 300 °C when initial ignition depth deeper than -40 cm, indicating that oxygen availability predominantly governs deep-layer dynamics. Despite persistent combustion, overall mass loss remains low owing to incomplete oxidation at these moderate temperatures. Near-surface CO levels span tens to hundreds of ppm, suggesting that real-time CO monitoring could serve as a pilot detection method for underground fire activity.

Chapter 6 summarises the overall outcomes of oxygen thresholds and smouldering dynamics in oxygen-limited conditions. According to the present findings, the challenges the researcher need to overcome in the future are also discussed.

ACKNOWLEDGEMENTS

It has been a wonderful journey during my PhD study. I am deeply thankful to my mentors, friends, and family for all the support, encouragement, and inspiration they have provided me during this period.

First and foremost, I want to express my deepest gratitude to Dr. Xinyan Huang, for your unreserved guidance and encouragement throughout my time at PolyU Firelab. I am immensely proud to have been your student and to have explored the fascinating smouldering research together with you. The insights and skills I gained from you have shaped my academic growth, and I will always cherish the experience.

I would like to express my sincere gratitude to Dr. Yuhan Huang, my supervisor at University of Technology Sydney, for your invaluable mentorship. Thanks for been so supportive and encouraging all the time. I will never forget the lessons I've learned from you, both in science and beyond.

I wish to thank Dr. Shaorun Lin, my big brother at PolyU, for supporting me every step of the way, from guiding me in designing my experiments to helping me build numerical models. I am deeply grateful for your encouragement and meticulous help over the past years.

For this thesis, I would like to thank all the co-authors, Dr. Yuying Chen (Chapter 2, 3, 4, assistance in formal analysis), Mr. Yichao Zhang (Chapter 3, 4, assistance in experiments), and Dr. Dayang Nur Musa (Chapter 5, assistance in experiments). I wish to thank Prof. Rory Hadden (University of Edinburgh) and Prof. Nieves Fernandez Anez (Western Norway University of Applied Sciences) for serving as my external examiners and your advice to improve this thesis.

I would like to thank to all the peers and friends at PolyU Firelab: Xiqiang, Shaorun, Anwar, Aatif, Caiyi, Zhirong, Han, Peiyi (Sally), Tianhang, Yuying, Zilong, Xiaoning, Lingchu (Sue), Yanhui, Yanfu, Yizhou, Ho Yin, Gulzhan, Wilson, Rahul, Shakeel, Congliang, Yuxin Zhang, Diane, Yifei, Yuxin Zhou, Lei, Yichao, Weikang, Meng, Jacub, Zifan, Zonghao, Fuqiu, Xinghao, Jin, Tianwei, Cheng Chen, Chang Tian, Yuchen (Eleni). It is my honour to be in the academic family with all of you.

I want to thank the mentors during these years: Dr. Mohd Zahirasri Mohd Tohir (UPM), Dr. Dejian Wu (Umicore), Dr. Zeyang Song (Xi'an University of Science and Technology), Dr. Jian Gao (Shenzhen Technology University). Thank you for helping me grow, I will always

learn from each of you.

I am grateful to my friends who inspired me: Tao and Shiyu (PolyU), Xiuqi (WPI), Cong Gao and Aoran (HKU), Enzo (CityU), Wenyuan (UNSW), Weidong (USTC), Lehan, Qingyun, Chao, Yihao, Jingping, Jibin (UTS), Siyan (UC Berkeley), Peng Zhao (Otto von Guericke University Magdeburg), Iffah and Michael (UPM), Dayang (UMS), Picha (Tokyo University of Science), Afi (Imperial College) for the beautiful memories in Hong Kong, Sydney, Canberra, Kuala Lumpur, Milan, Magdeburg, and Coimbra. I would like to express my special thanks to my old friends, Xiongtian, Shijie, Sicheng, and Tengxiang for your time and encouragement.

I want to acknowledge the financial support from National Natural Science Foundation of China (NSFC Grant No. 52322610 and 51876183), General Research Fund Scheme of Hong Kong Research Grants Council (RGC-GRF Grant No. 15221523), and Inner Mongolia Science and Technology Department (No. 2021CG0002), as well as scholarships from The Hong Kong Polytechnic University and University of Technology Sydney.

Finally, and most importantly, a BIG thank you to my family for your love, patience, and unconditional support. I could not have accomplished this without your constant belief in me. Thank you to my sister for always being a guiding light in my life. Lastly, my heartfelt gratitude goes to my beloved partner, Qing Yu. I deeply appreciate our shared efforts and mutual support during these years, which have made the entire journey feel passionate and hopeful.

Yunzhu Qin
Hong Kong
October 2024

TABLE OF CONTENTS

LIST OF TABLES

LIST OF FIGURES

NOMENCLATURE

Symbols

A	condensed phase species *A* (reactant)
B	condensed phase species *B* (product)
c	specific heat capacity (J/kg·K)
D	diffusivity (m^2/s) /pore size (m)
d_p	characteristic pore size (m)
E	activation energy (J)
F	fuel (-)
ΔH	heat of reaction (MJ/kg)
h	specific enthalpy (J/kg)
h_c	convective coefficient (W/m^2·K)
h_r	radiative coefficient (W/m^2·K)
K	permeability (m^2)
k	thermal conductivity (W/m·K)
L	fuel length
M	molar mass (g/mol)
m	mass (g)
$\dot{m}''$	mass flux (g/m^2·s)
Nu	Nusselt number (-)
n_k	reaction order (-)
p	pressure (Pa)
$\dot{q}''$	heat flux (kW/m^2)
S	spread/surface area (m^2)
T	temperature (^{o}C)
t	time (s)
U	flow velocity (mm/s)
X	volume fraction (-)
Y	mass fraction (-)
Z	pre-exponential factor (s^{-1})
ΔZ	cell size (m)

Greeks

α	thermal diffusivity (m^2/s)
β	local fire spread probability
γ	radiative conductivity coefficient (m)
ε	emissivity (-)
μ	local fire extinction probability
ν	viscosity/stochiometric factor (Pa·s/-)
ρ	density (kg/m^3)
σ	Stefan–Boltzmann constant ($kg/s^3 \cdot K^4$)
ψ	porosity (-)
$\dot{\omega}''$	volumetric reaction rate ($kg/m^3 \cdot s$)

Subscripts

cond	conduction
conv	convection
cp	cellulose pyrolysis
d	destruction
dr	drying process
e	environmental
ev	evaporation
f	formation
g	gas
hp	hemicellulose pyrolysis
i	species number
k	reaction number
min	minimum
lp	lignin pyrolysis
o	original/bulk
O_2	oxygen
ox	oxidation or oxidiser
r	radiation
s	solid
sm	smouldering

lp	lignin pyrolysis
∞	ambient

Abbreviations

AI	Artificial intelligence
CA	Cellular automaton
DSC	Differential scanning calorimetry
EA	Elementary analysis
ESR	Electron spin resonance
FPA	Fire Propagation Apparatus
FTIR	Fourier-transform infrared spectroscopy
GHG	Greenhouse gases
Gpyro	Generalized pyrolysis model for combustible solids
LiDAR	Light Detection and Ranging
LOC	Limiting oxygen concentration
MC	Moisture content
MOC	Minimum oxygen concentration
PM	Particulate matter
PMMA	Polymethyl methacrylate
TC	Thermocouple
TGA	Thermogravimetric analysis

PUBLICATIONS

List of Journal Papers included in the Thesis

1. Y. Qin, Y. Chen, Y. Zhang, S. Lin* and X. Huang* (2024). Modeling Smothering Limit of Smouldering Combustion: Oxygen Supply, Fuel Density, and Moisture Content. ***Combustion and Flame***, 269, 113683.
2. Y. Qin, Y. Zhang, Y. Chen, S. Lin* and X. Huang* (2024). Minimum oxygen supply rate for smouldering propagation: Effect of fuel bulk density and particle size. ***Combustion and Flame***, 261, 113292.
3. Y. Qin, Y. Chen, S. Lin* and X. Huang* (2022). Limiting Oxygen Concentration and Supply Rate of Smouldering Propagation. ***Combustion and Flame***, 245, 112380.
4. Y. Qin, D. Musa, S. Lin* and X. Huang* (2022). Deep Peat Fire Persistently Smouldering for Weeks: A Laboratory Demonstration. ***International Journal of Wildland Fire***, 32, 86-98.

List of Journal Papers not included in the Thesis

1. Y. Qin[#], Y. Zhang[#], Y. Chen, S. Lin*, Y. Shu*, Y. Huang, X. Huang* and M. Zhou (2025). Impact of Snow on Underground Smouldering Wildfire in Arctic-Boreal Peatlands. ***Environmental Science & Technology*****,** 59, 8, 3915–3924 *(selected as supplemental cover paper)*.
2. S. Lin, W. Cui, S. Wang, Y. Qin, Y. Chen, Y. Zhang, X. Huang, SL. Quarles, and M.J. Gollner* (2025). Susceptibility to ignition of landscaping mulches exposed to firebrand piles or radiation. ***Fire Safety Journal***, 104388.
3. Y. Zhang, Y. Shu, Y. Qin, Y. Chen, S. Lin*, X. Huang*, M. Zhou (2024). Resurfacing of underground peat fire: smouldering transition to flaming wildfire on litter surface. ***International Journal of Wildland Fire***. 33(2).
4. S. Lin, Y. Qin and X. Huang*, M. Gollner (2023). Use of pre-charred surfaces to improve fire performance of wood. ***Fire Safety Journal***, 136, 103745.
5. Y. Chen, S. Lin, Y. Qin, N.C. Surawski* and X. Huang* (2023). Carbon distribution and multi-criteria decision analysis of flexible waste biomass smouldering processing technologies. ***Waste Management***, 167. 183-193.
6. Y. Chen, Z. Wang*, S. Lin, Y. Qin and X. Huang* (2023) A review on biomass thermal-oxidative decomposition data and machine learning prediction of thermal analysis. ***Cleaner Materials***, 100206.

[#] *indicates equal contribution; * indicates corresponding author.*

Selected Conference Communications

1. Y. Qin, Y. Chen, Y. Zhang, S. Lin* and X. Huang* (2024). Influence of fuel and ambient conditions on the smouldering oxygen limits. ***Combustion Institute's 40th International Symposium***, Milan, Italy, July 21-26. [Poster]
2. Y. Qin, Y. Zhang, Y. Shu*, S. Lin* and X. Huang* (2023). Interaction between Snow Layer and Smouldering Peat Fire under Extreme Environment. ***9th Conference on Fire Effects on Soil Properties***, The Netherlands, 20 - 22 June 2023. [Oral].
3. Y. Qin, Y. Zhang, Y. Chen, Y. Shu*, S. Lin*, X. Huang*, M. Zhou (2024). How do snow weathers influence smouldering peat fires? ***7th International Fire Behaviour and Fuels Conference***, Canberra, April 15-19, 2024 [Poster]
4. Y. Qin, Y. Zhang, Y. Chen, Y. Shu*, S. Lin*, X. Huang*, M. Zhou (2023). The role of snow in Arctic-boreal peatland fires. ***The 23rd Cross-strait and Hong Kong Macao Symposium on Environment, Resources and Ecological Conservation***, Hong Kong SAR, December 18-23, 2023. [Oral]
5. Y. Qin, Y. Zhang, Y. Chen, S. Lin, X. Huang, The Role of Fuel Properties on Oxygen Thresholds of Smouldering Fire, ***14th International Symposium on Fire Safety Science***, Tsukuba, Japan, October 23-27, 2023. [Poster]
6. Y. Qin, Y. Chen, S. Lin* and X. Huang* (2023). Minimum Oxidizer Supply of Smouldering Combustion in Biomass Fuels. ***The 14th Asia-Pacific Conference on Combustion (ASPACC 2023) Program***, Taiwan, China, 14 - 18 May 2023. [Oral].
7. Y. Qin, D. Musa, S. Lin* and X. Huang* (2022). Persistent Underground Smouldering Fire in Deep Peat Layer. ***IX International Conference on Forest Fire Research***, Coimbra, Portugal, 11 - 18 Nov 2022. [Oral]
8. Y. Qin, Y. Chen, S. Lin* and X. Huang* (2022). What is the limiting oxygen condition for smouldering fire? ***39th International Symposium on Combustion***, Vancouver, Canada, 24 -29 July 2022. [Poster].

Patents

1. X. Huang, S. Lin, Y. Qin, Y. Chen, System and method of measuring the limiting oxygen supply and index for smouldering ignition and fire spread, China Patent, Application No. 202211154962.3 (Under review).

2. X. Huang, Y. Qin, S. Lin, Y. Liu, An underground smouldering fire detection and firefighting system based on heat pipes, China Patent, Application No. 202310284750.5 (Under review).
3. X. Huang, Y. Qin, S. Lin, A fireproof cigarette based on the quenching principle of smouldering. China Patent, Application No. 202410179598.9 (Under review).

Chapter 1 Introduction

1.1 Background and motivation

From the perspective of combustion, wildfires can be divided into two types: flaming and smouldering [1]. Smouldering is a slow, low-temperature, and flameless phenomenon that occurs in charring porous fuels such as peat, coal, wood, and forest litter. It is primarily sustained by exothermic oxidations when oxygen molecules directly attack the hot surface of condensed-phase reactive media. As a typical incomplete combustion, its reaction temperature (~450–700 °C), fire spread rate (~1 mm/min), and combustion heat (~6–15 MJ/kg) are lower than those of flaming combustion that occur in gas phase. The smouldering process involves numerous chemical reactions and intricate heat and mass transfer mechanisms. To summarise these processes, smouldering is simplified into two steps: pyrolysis and char oxidation, as shown in Fig. 1-1a.

Pyrolysis is a prerequisite for the occurrence of smouldering reactions:

$$\text{Solid fuel} + \text{Heat} \rightarrow \text{Pyrolysis gases} + \text{Char} \tag{1.1}$$

In this process, charring solid fuels undergo endothermic decomposition (even in the absence of oxygen), producing pyrolysis gases, particulate matter (PM), and char. The pyrolysis temperature is influenced by fuel properties. Thermogravimetric analysis (TGA) shows that the lowest pyrolysis temperature (the threshold temperature at which pyrolysis reactions begin) of common fuels (such as wood products and peat) is about 200 °C, while the peak pyrolysis temperature (the threshold temperature causing the maximum rate of mass loss) is about 320 °C [2].

The products of pyrolysis in both gas (pyrolysis gases) and solid (char) phases can undergo further oxidation. Flaming occurs when the exothermic reactions are dominated by homogeneous reactions between pyrolysis gases and oxygen:

$$\text{Pyrolysis gases} + \text{Oxygen} \rightarrow \text{Gaseous products} + \text{Heat} \quad \textbf{(Flaming)} \tag{1.2a}$$

The occurrence of flaming requires sufficient concentrations of pyrolysis gases and oxygen, as well as adequate heat and temperature to initiate flaming combustion [3]. By contrast, smouldering occurs when the oxidation of solid-phase char dominates the process:

$$\text{Char} + \text{Oxygen} \rightarrow \text{Gaseous products} + \text{Ash} + \text{Heat} \quad \textbf{(Smouldering)} \tag{1.2b}$$

The characteristic temperatures of char oxidation are slightly higher than those of pyrolysis; the lowest oxidation temperature (the threshold temperature at which oxidation reactions begin) is about 300–350 °C, and the peak oxidation temperature (the threshold temperature causing

the maximum rate of mass loss due to char oxidation) is about 440 °C [2]. Notably, metal and minerals contained in the char can catalyse oxidation reactions [4], and the inorganic contents which cannot be oxidised become ash as combustion residues. Throughout the smouldering process, the heat released by oxidation reactions is used to balance system heat losses, evaporate fuel moisture, maintain and preheat fuel temperature, and sustain the endothermic pyrolysis reactions.

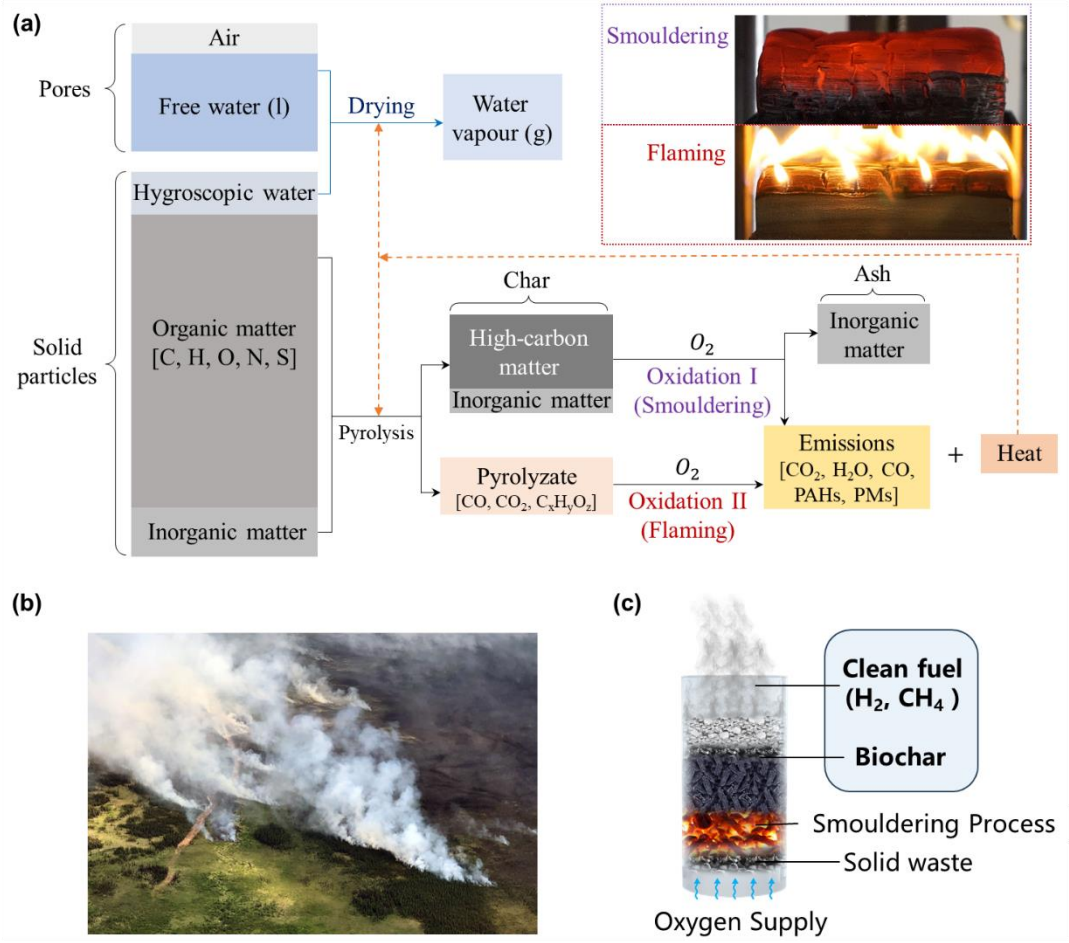

Fig. 1-1 Schematic diagram of the chemical pathways of flaming and smouldering in charring solid fuels, with examples of smouldering and flaming in wood (b) smouldering peatland fire around the Swan Lake in Alaska, 2019 (photo by Kale Casey, Alaska Division of Forestry). (c) Diagram of the clean smouldering technology for biowaste removal and biofuel production [5].

Smouldering fires can be a natural disaster or clean technology. On the one hand, it causes catastrophic fires (see Fig. 1-1b). Smouldering can be sustained under extreme conditions of high moisture content (dry basis MC >100%) and can burn at very low oxygen concentrations. Some experiments have measured its critical oxygen concentration to be less than 10% [6]. In

contrast, sustaining flaming combustion usually requires at least 14–16% oxygen concentration, and flame-retardant materials need environments with oxygen concentrations higher than atmospheric levels (21%) to maintain combustion [3]. Even if the oxygen concentration is high, flames are difficult to sustain without sufficient airflow, such as in microgravity environments [7,8]. Smouldering peat fires and underground coal fires are among the largest and longest-lasting fire phenomena on Earth [9]. For example, influenced by climate change, Southeast Asia has frequent smouldering peat fires since 1991, with the most severe incidents occurring in 1997, 2006, 2009, 2013, and 2015 [10]. During the 1997 El Niño event alone, massive peat fires in Indonesia triggered a notorious transboundary haze event that lasted over half a year, resulting in severe air pollution in densely populated areas and significantly affecting public health [11,12]. Smouldering peat fires also occur in northern and boreal regions such as Siberia and North America (Fig. 1-1b). In recent years, increasing remote sensing monitoring [13–15] and experimental evidence [16,17] have confirmed the existence of "overwintering fires": smouldering fires in cold regions can hibernate underground in low temperature environment and re-emerge to the surface when temperatures rise and fuels dry out in the following year, and even igniting surface flaming fires [17]. Even during underground propagation, smouldering fires continuously emit large amounts of greenhouse gases (GHGs) like CO_2 and CH_4 into the atmosphere, exacerbating climate change and the greenhouse effect in the Arctic region, leading to global issues such as glacier melting and permafrost thawing [18,19]. Although smouldering fires on a global scale have attracted some attention, our current understanding of them is still limited. Considering the natural oxygen supply in underground smouldering fires, oxygen diffuses from the fuel surface to deeper layers, resulting in an inverse correlation between actual oxygen supply and fuel depth [20]. However so far, no experimental observations or theoretical analyses have demonstrated the maximum depth at which smouldering can be sustained under natural oxygen supply. Moreover, due to the incomplete understanding of the oxygen supply limits of smouldering, there is a lack of research on smouldering wildland fires suppression methods based on restricting oxygen supply. **Therefore, an in-depth understanding of the critical oxygen conditions for smouldering is of great significance for understanding the characteristics of smouldering wildland fires and controlling large-scale natural disasters.**

On the other hand, well-controlled applied smouldering processes offer promising avenues for biofuel production [21], biowaste removal [22], and pollution reduction [23], playing an important role in the context of our increasing attention to carbon neutrality and sustainable

development. For example, with the accelerated growth of the world's population and economy in recent years, urban solid waste has increased significantly, including kitchen waste, wood scraps, and paper debris. Traditional solid waste treatment methods mainly include landfilling, biotransformation, and thermochemical treatments [5,24]. It is estimated that nearly 50% of major organic waste in Australia in 2020 was simply disposed of through landfilling [25]. However, this method leads to large amounts of GHG emissions, which accounts for 10–15% of total anthropogenic methane emissions [26]. At the same time, other solid waste treatment methods often face challenges such as low conversion efficiency and high energy consumption. In contrast, smouldering-based solid waste treatment technologies (Fig. 1-1c) have many advantages: (1) self-sustaining, without the need for continuous injection of nitrogen and large amounts of heat energy as in pyrolysis processes [27]; (2) The gaseous (CO, CH_4, etc.), liquid (tar), and solid-phase products (biochar) can all be collected and utilized as clean energy (Fig. 1-1c) [5]; (3) relatively low reaction temperatures (~500 °C), resulting in lower equipment safety risks; (4) simple pretreatment steps, requiring only drying and grinding [27,28]. Currently, although the application of smouldering solid waste treatment technology already has substantial theoretical and experimental support [29–31] and promising prospects, improving its processing efficiency and optimising energy efficiency remains challenging. Particularly, oxygen supply, as the dominant mechanism in smouldering reactions, can effectively control the intensity and efficiency of reactions [32], but our understandings are still limited. Therefore, **an in-depth investigation of the critical oxygen characteristics and influencing mechanisms of smouldering is beneficial for optimising the application of smouldering solid waste treatment systems**. In summary, whether from the perspective of controlling large-scale smouldering wildland fires or advancing efficient and clean solid waste treatment technologies, more in-depth and systematic fundamental research on smouldering oxygen supply is needed.

1.2 Literature review

1.2.1 Smouldering oxygen supply modes

Oxygen supply modes in smouldering are typically divided into two categories: natural oxygen supply (Fig. 1-2a) and forced oxygen supply (Fig. 1-2 (b-d)). In the case of natural diffusion oxygen supply, air (oxygen) can be transported from the external environment to the smouldering reaction zone driven by natural/free convection and diffusion. For example,

natural convection due to buoyancy plays a dominant role in oxygen supply for surface smouldering fires where the environmental wind is neglected. In contrast, in underground fires that spread in deeper layers, the concentration gradient formed after the consumption of limited oxygen makes oxygen diffusion the dominant form of oxygen supply [4,20]. In the one-dimensional (1-D) deep underground smouldering scenario,

$$\dot{m}''_{ox}(y) = -\bar{\psi} D \frac{\partial Y_{O_2}}{\partial y} \qquad \text{(Diffusion)} \qquad (1.3)$$

where y represents the distance between the smouldering front and the free surface. The term $\dot{m}''_{ox}(y)$ denotes the diffusive oxygen supply flux driven by the concentration gradient at different depths (in g/m^2·s). $\bar{\psi}$ is the average porosity within the porous medium. D is the diffusion coefficient of oxygen in the porous fuel, influenced by factors such as temperature and the porosity of the porous material. The expression $\frac{\partial Y_{O_2}}{\partial y}$ represents the oxygen concentration gradient at depth y.

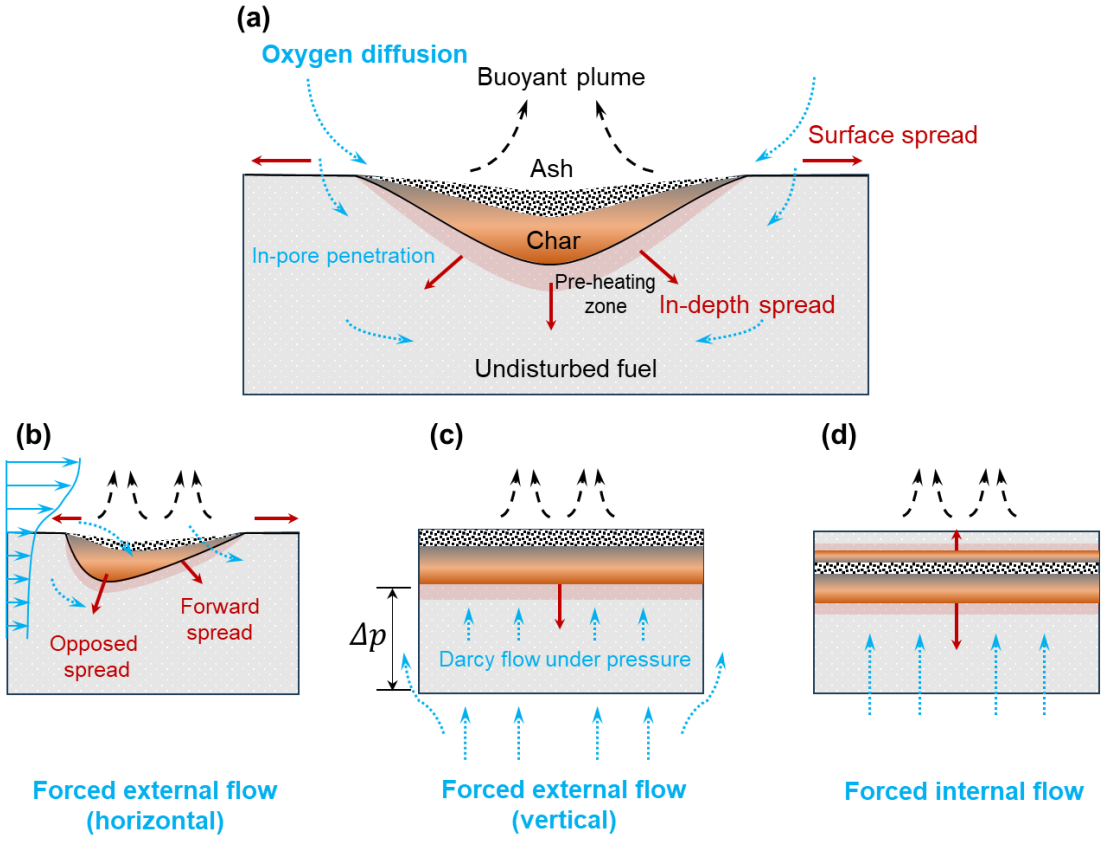

Fig. 1-2 Two different oxygen supply scenarios of smouldering combustion: (a) natural diffusion; (b) forced horizontal external flow; (c) forced vertical external flow; (d) forced internal flow.

Forced oxygen supply includes **(1) forced external flow**: convection where airflow passes over (Fig. 1-2b) or toward the fuel surface (Fig. 1-2c), such as in surface smouldering fires under the influence of environmental wind, and **(2) forced internal flow**: directly introducing air into the porous fuels (e.g., controlling oxygen supply variables in laboratory smouldering experiments or airflow introduced in smouldering solid waste treatment devices). In the scenarios of forced external flow on the fuel surface (Fig. 1-2c), the actual oxygen flux at depth y, denoted as $\dot{m}''_{ox}(y)$ can be estimated using Darcy's law:

$$\dot{m}''_{ox}(y) = \frac{K\Delta p}{\mu y} \cdot Y_{O_2} \qquad (Forced\ external\ \ flow) \qquad (1.4a)$$

where $\dot{m}''_{ox}(y)$ is the oxygen flux at depth y. K is the permeability of the porous fuel, which is related to properties such as material porosity and pore shape. μ is the dynamic viscosity of the gas, influenced by factors like gas temperature, concentration, and composition. Y_{O_2} is the mass fraction of oxygen in the gas. Δp is the pressure difference between depth y and the fuel surface caused by the external forced flow.

In the scenarios of forced internal flow (Fig. 1-2d), the oxygen supply obtained by the smouldering reaction is directly controlled by the gas flow rate:

$$\dot{m}''_{ox} = \psi \rho_g Y_{O_2} U \qquad (Forced\ internal\ flow) \qquad (1.4b)$$

where $\dot{m}''_{ox}$ is the oxygen flux within the pores. ψ is the porosity of the porous fuel. ρ_g is the density of the incoming gas. Y_{O_2} is the mass fraction of oxygen in the gas. U is the gas flow velocity.

Based on the fundamental smouldering oxygen supply models discussed above, several existing experiments and numerical simulations at different scales have explored the oxygen supply limits of smouldering. In the following section, current research methods and results will be reviewed, respectively.

1.2.2 Current methodology

Currently, experiments are the primary approaches for exploring the oxygen supply characteristics of smouldering combustion, which can be categorised into micro-scale and small-scale studies based on the experimental scale. However, to date, no studies have investigated the effects of critical oxygen conditions for smouldering through field combustion

experiments. This is because such experiments require strict control of oxygen supply conditions, and it is challenging to avoid the influence of environmental wind during on-site field tests.

Micro-scale experiments primarily include methods based on thermogravimetric analysis (TGA), electron spin resonance (ESR), and their couples with Fourier-transform infrared spectroscopy (FTIR) to explore the kinetics mechanisms of pyrolysis and smouldering. TGA analysis is an important approach for studying pyrolysis chemistry in combustion and fire [33]. In these experiments, milligram-level samples are placed in a controlled oxygen concentration environment, and a controlled temperature ramp is provided (Fig. 1-3a) to obtain the mass loss rate of the fuel at different temperatures. This is often coupled with FTIR to analyse gas emissions [34,35]. In TGA analysis, mass loss curves under air and inert atmospheres are typically compared to infer the oxidation reaction rates at different oxygen concentrations, thereby determining whether smouldering reactions occur. The ESR method is used for reaction analysis at the molecular scale. By measuring the area of the spin resonance spectrum, it indirectly quantifies the concentration of free radicals in the fuel under specific oxygen environments, thus inferring the likelihood of combustion reactions occurring [36].

Methods for small-scale research on smouldering have been systematically elaborated previously [33]. However, small-scale experimental studies on the critical oxygen supply characteristics of smouldering typically require introducing an oxygen supply system capable of controlling flow rate and concentration based on the original experiments. External forced oxygen supply experiments usually direct the oxidiser onto the fuel surface (Fig. 1-3b) [37], or utilise standard fire testing methods based on the Fire Propagation Apparatus (FPA) to provide external forced convective oxygen supply and control radiant ignition power (Fig. 1-3c) [38]. Nevertheless, this approach makes it difficult to determine the actual amount of oxygen reaching the smouldering front within the porous fuel and cannot eliminate the influence of natural oxygen diffusion at the surface of the fuel container. Therefore, small-scale experiments often employ internal forced oxygen supply methods, directly measuring the total oxygen supply introduced into the smouldering system using a flow meter (Fig. 1-3d) [39].

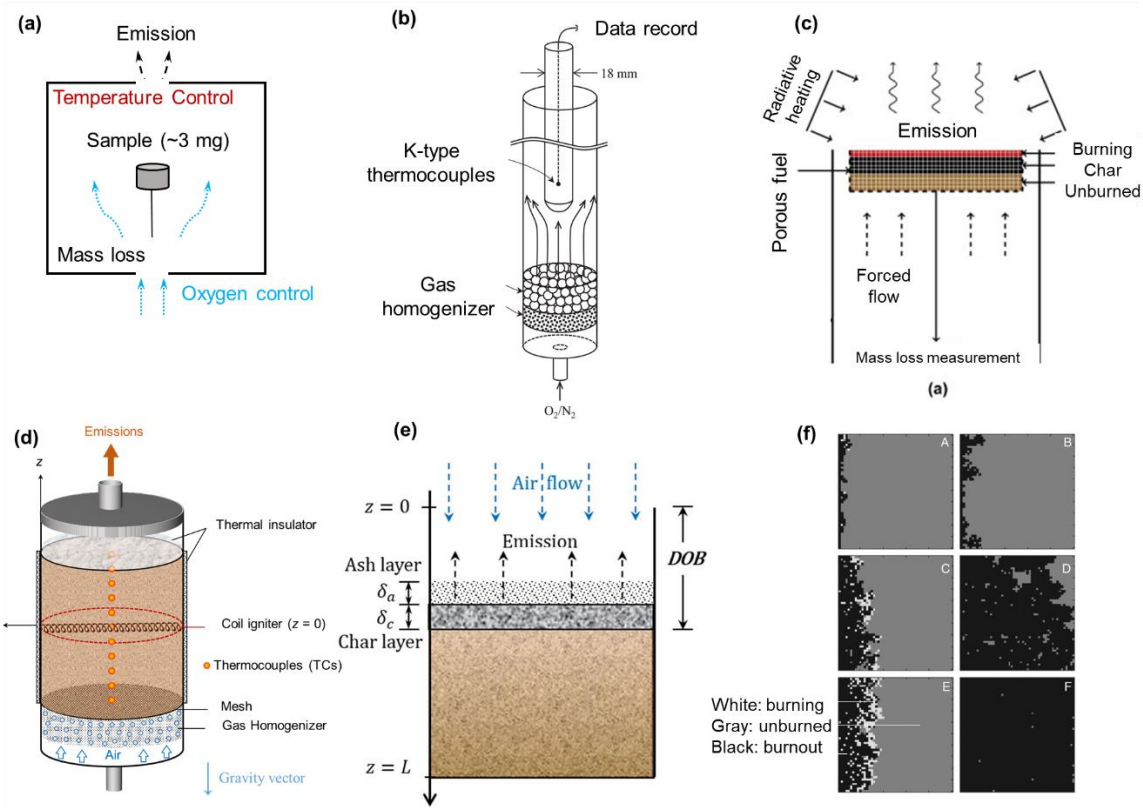

Fig. 1-3 Current representative experimental and computational setup on smouldering oxygen supply limits: (a) microscale (~mg) thermogravimetric analysis; (b) external forced oxygen supply [37]; (c) external forced oxygen supply based on FPA [38]; (d) forced internal oxygen supply [39]; (e) numerical study based on physical-based model [40]; (f) discrete event statistical simulation by CA [41].

In small-scale experiments, oxidiser flows of various concentrations are usually obtained by mixing pure air with nitrogen or argon gases. To ensure the uniform flow of the mixed gases within tubular containers, gas homogenising layers composed of metal mesh, glass beads, or gravel are typically installed at the inlet or before the gases enter the container. For near-limit critical smouldering experiments, precise control of ignition protocol is also crucial for exploring the critical oxygen supply conditions. Common ignition methods in small-scale experiments include radiant ignition [38], variable power coil ignition [39,42], and heated rod ignition [43]. Different ignition methods can achieve various smouldering ignition intensities by controlling the applied radiation intensity (radiant heat flux) or the conductive temperature of the metal igniter. In addition to directly observing combustion phenomena, thermocouples and infrared cameras are also commonly used to detect temperatures, indirectly inferring whether the current oxygen supply conditions are sufficient to sustain smouldering. In terms of large-scale experiments, there are very few large-scale experimental studies on smouldering

combustion and fires in the literature due to the challenges in monitoring and extinguishing smouldering fires. The existing largest study is the GAMBUT experiment conducted in Indonesia (10 m × 10 m) [44]. However, it is difficult to effectively control environmental wind in natural settings to explore the impact of oxygen supply. Therefore, such studies only focus on the ignition, propagation, extinction, and emission dynamics of smouldering fires.

Numerical simulations of the oxygen supply characteristics of smouldering are relatively limited and can be categorised into physical models based on heat and mass transfer and statistical models using discrete event simulations. A typical 1-D smouldering physics-based model is shown in Fig. 1-3e, which has been used to simulate ignition, fire spread, and extinction in smouldering [45,46]. This model includes heterogeneous chemical reactions and heat and mass transfer processes between the gas and solid phases within a porous medium. It assumes thermal equilibrium at the same location in the system, that is, efficient heat exchange within the porous medium, where the gas and solid phases share the same temperature within the same grid cell. The main governing equations in the model are consistent with those used in the open-source software Gpyro [47], including the conservation of (1.5) mass, (1.6) species, and (1.7) energy in the condensed phase, as well as the conservation of (1.8) mass, (1.9) species, and (1.10) momentum (Darcy's law) in the gas phase.

$$\frac{\partial \bar{\rho}}{\partial t} = -\dot{\omega}_{fg}''' \tag{1.5}$$

$$\frac{\partial (\bar{\rho} Y_i)}{\partial t} = \dot{\omega}_{fi}''' - \dot{\omega}_{di}''' \tag{1.6}$$

$$\frac{\partial (\bar{\rho} \bar{h})}{\partial t} + \frac{\partial (\dot{m}'' \bar{h}_g)}{\partial z} = \frac{\partial}{\partial z}\left(k \frac{\partial T}{\partial z}\right) + \sum \dot{\omega}_{di,k}''' \Delta H_k \tag{1.7}$$

$$\frac{\partial (\rho_g \bar{\psi})}{\partial t} + \frac{\partial \dot{m}''}{\partial z} = \dot{\omega}_{fg}''' \tag{1.8}$$

$$\frac{\partial (\rho_g \bar{\psi} Y_j)}{\partial t} + \frac{\partial (\dot{m}'' Y_j)}{\partial z} = -\frac{\partial}{\partial z}\left(\rho_g \bar{\psi} D \frac{\partial Y_j}{\partial z}\right) + (\dot{\omega}_{fj}''' - \dot{\omega}_{dj}''') \tag{1.9}$$

$$\dot{m}'' = -\frac{\bar{K}}{\nu}\frac{\partial \bar{p}}{\partial z} \quad (\rho_g = \frac{P\bar{M}}{RT}) \tag{1.10}$$

In addition to traditional physical models, discrete statistical models based on Cellular Automata (CA) have also been used to study the critical oxygen conditions for smouldering combustion Fig. 1-3f [41]. CA consist of a large number of regular units, and they exhibit complex global behaviour by simulating local interactions between adjacent cells [48]. CA

models have been widely applied not only in natural system simulations, image processing, and crowd behaviour modelling, but their characteristic of "neighbour cell interactions" also makes them highly suitable for simulating fire spread phenomena. For example, existing smouldering CA models have already achieved simulations of smouldering fire spread under varying moisture content [49,50], field-scale simulations [51], and complex fire spread behaviours such as fingering spread [52]. In the study of critical oxygen conditions based on CA [41], a grid of 50 × 50 cells is first established, where each cell can be in one of three states: "unburned", "burning", and "burned out". The model also includes two parameters: the local fire spread probability β and the local fire extinction probability μ. Through extensive simulations with random values of these two parameters to compare with experimental results, the optimal parameter choices are finally determined, and the model's applicability is validated.

Table 1-1 summarises the micro-scale and small-scale experimental and simulation studies in the existing literature related to the critical oxygen supply characteristics of smouldering combustion, including the types of fuels used, configurations, and oxygen supply modes.

Table 1-1 Experimental information on the limiting oxygen concentration (LOC) of smouldering combustion, sorted by fuel type and study scale. The critical oxygen concentration of flaming combustion for common solid fuels: 18% (paper) [53] and 19-20% (PMMA) [54,55].

Fuel	Configurations	Study type	Oxygen supply mode	LOC	Ref.	Remarks
Peat	Disclosed cylindrical reactor, H=30 mm, D=125 mm	Small-scale experiment	Forced external flow concentration 9-35% fixed flow rate 20-150 mm/s	10%	Hadden et al. 2013 [38]	Burning rate after ignition is independent of external heating
Peat	1D mode, H=12 cm	Numerical simulation	Diffusion under different oxygen concentration	13%	Huang and Rein. 2016 [40]	Relationship between critical oxygen concentration and critical water content of fuel
Peat	Simulation domain 10 × 10 cm, grid 50 × 50	Numerical simulation (CA)	Diffusion under different oxygen concentration	16%	Belcher et al. 2010 [41]	Verification based on combustion rate and time in experiments
Pine dust	Disclosed square reactor, H=12 cm, l=3.8 cm	Small-scale experiment	Forced internal flow concentration 5-21%	5%	Wang et al. 2017 [56]	Relationship between limiting concentration and external heating

			fixed flow rate 15 mm/s			
Moxa rod	Fuel rod, D=18 mm	Small-scale experiment	Forced external flow Fixed flow 18L/min	13.5 %	Kadowaki et al. 2021 [37]	Quenching is due to the limited char oxidation rate in the absence of oxygen.
Wood brick	Dimension 8 × 8 × 3 cm	Small-scale experiment + Numerical simulation	Exp: Forced external flow concentration 0-21% flow rate: 200L/min Sim: natural diffusion	4% (ig.)	Richter et al. 2021 [6]	LOC is affected by external radiation intensity
Paper scraps	Disclosed cylindrical reactor, H=15 mm, D=20 mm	Small-scale experiment	Forced internal flow Concentration 21% Max. flow rate 18 cm/s	N. A.	Yan and Fujita, 2019 [43]	Influence of density and heating rod temperature
Coal	5 mg	ESR Micro-scale experiment	Forced external flow Concentration 3-21% Fixed flow 50 mL/min	9%	Zhou et al. 2021 [36]	Determining the oxygen limit by measuring free radicals and reaction rates
PMMA	Cylindrical fuel, D=13.2 cm, l=15 cm	Small-scale Experiment (microgravity)	Forced internal flow Max. flow 3.66 $g/m^2 \cdot s$	N. A.	BAR-ILAN et al., 2004 [57]	Microgravity experiment; explored the role of buoyancy in smouldering

1.2.3 Findings from existing studies

In small-scale studies, it is challenging to experimentally explore the critical oxygen concentration under natural diffusion. Therefore, the limiting diffusive oxygen supply is usually solved by numerical simulation. One study on wood blocks identified the oxygen concentration ranges required for pyrolysis, smouldering, and flaming under different heat fluxes (Fig. 1-4a): < 4% for pyrolysis, 4-15% for smouldering, and > 15% for flaming. It is important to note that the smouldering limits this study only focuses on ignition phase.

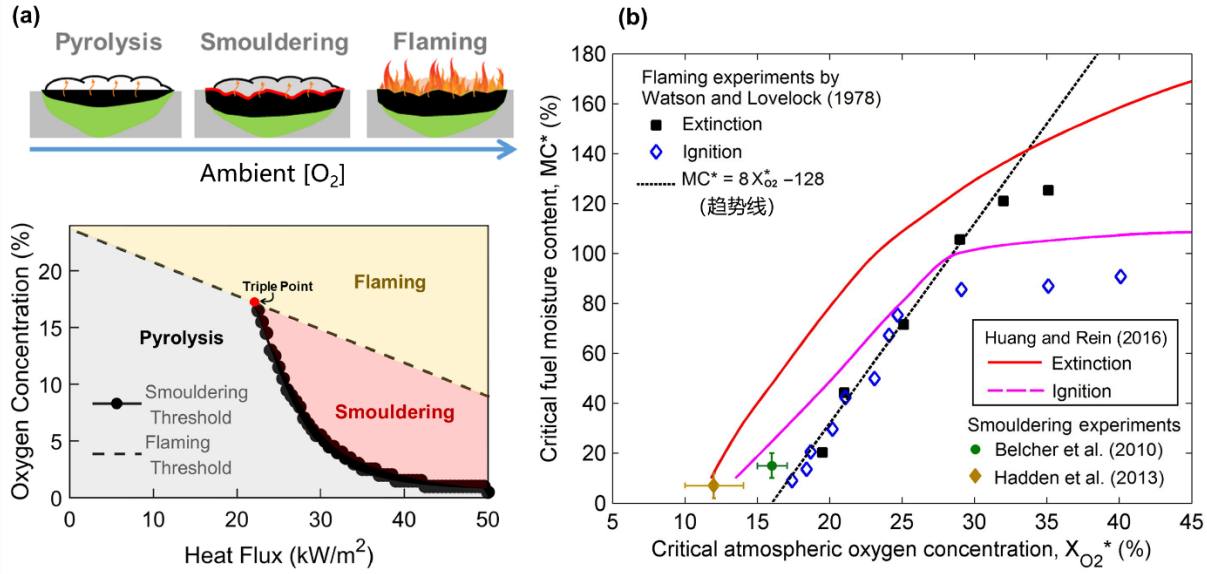

Fig. 1-4 (a) Increasing ambient oxygen concentration with the same external heating flux, the phenomenon transitions from pure pyrolysis to smouldering, then to flaming [6]. (b) Critical moisture content (MC^*) vs. critical ambient oxygen concentration ($X_{O_2}^*$) found in experiments of flaming paper [53] and smouldering peat [38,41], and new predictions [40].

Another computational study based on physical model also identified the relationship between the critical oxygen concentration ($X_{O_2}^*$) and the critical moisture content (MC^*) [40] (Fig. 1-4b). The results indicate that as moisture content increases, the critical oxygen concentration for smouldering ignition and fire spread rises significantly. Compared to flaming combustion, smouldering can sustain under higher fuel moisture content (with a conventional oxygen concentration of X_{O_2} =21%, the $MC^*$for smouldering reaches up to 100%, while for flaming it is only 40%) and lower oxygen concentration (smouldering $X_{O_2}^*$ =13%, flaming 16%). However, CA simulations yielded higher results: it showed that smouldering reactions are suppressed at oxygen concentrations below 18.5% and completely cease at concentrations below 16%. The study also re-assessed Earth's flammability limits over the past 350 million years based on these findings [41].

Furthermore, there is a study employed an internal forced oxygen supply model in smouldering pine sawdust [56]. It found that the critical oxygen concentration required for smouldering is related to external heating. Self-sustained smouldering can only be initiated when the oxygen concentration is between 10% and 21%. When the oxygen concentration decreased below 7.5%, sustaining smouldering combustion requires additional external radiant

heating. At oxygen concentrations of 5% or lower, smouldering cannot occur, even with the assistance of external heating.

Studies under forced external supply is found to have critical oxygen concentration than that observed with internal oxygen supply. Representative studies include directly applying airflow to the surface of ignited fuel [37] (Fig. 1-3b) and using the FPA to control ignition intensity and oxygen supply conditions [38] (Fig. 1-3c). These studies determined critical oxygen concentrations of 13.5% (Fig. 1-5a) and 10% (Fig. 1-5b) for external forced oxygen supply. Similarly, both studies found that char content was higher in quenched fuel when oxygen concentration was insufficient (Fig. 1-5b), indicating that the limited char oxidation to release sufficient heat is the primary reason for smouldering extinction. As the oxygen concentration increased, both experiments observed higher fire spread rates, burning temperatures, and fuel mass loss rates. The study in smouldering peat also revealed that the duration of smouldering decreased as oxygen concentration increased [38]. This helps explain the phenomenon of persistent smouldering fires in deep underground peat layers.

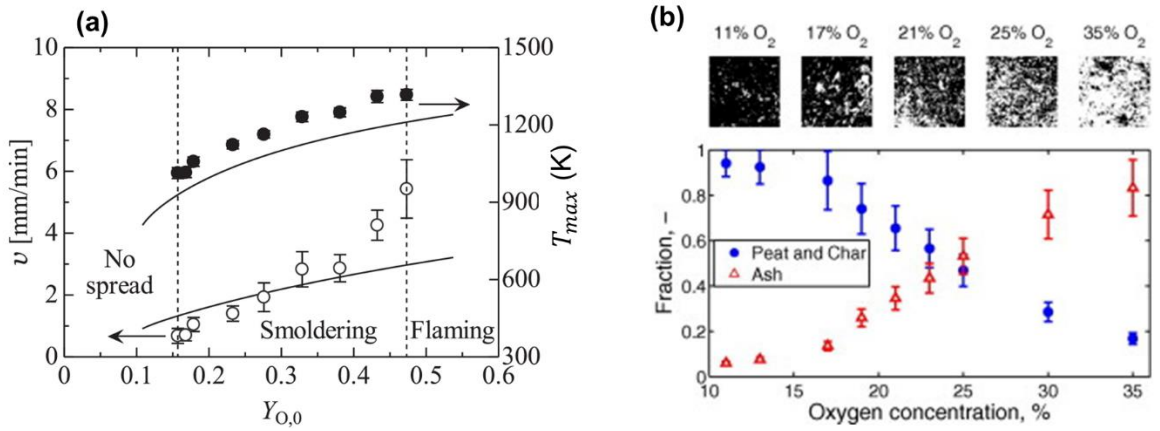

Fig. 1-5 Critical oxygen supply under forced external flow of (a) moxa rod (~13.5%) [37] and (b) peat soil (~10%) [38].

Although there are relatively few studies on critical oxygen supply rates in the literature, it plays important role in the ignition and extinction of smouldering combustion. The critical oxygen supply rates can be influenced by both fuel properties and environmental conditions. A study on smouldering ignition in paper scraps found that in low-density fuel, there is sufficient oxygen within the gaps of the porous material during ignition. As a result, ignition can occur successfully even without additional oxygen supply. However, excessively high airflow rates can enhance internal convective heat loss, leading to failed ignition (Fig. 1-6a). When the fuel density increases, oxygen supply becomes the primary factor controlling ignition

success, as shown by the U-shaped trend in Fig. 1-6 (b-c), where ignition fails both under insufficient oxygen supply and excessive airflow rates.

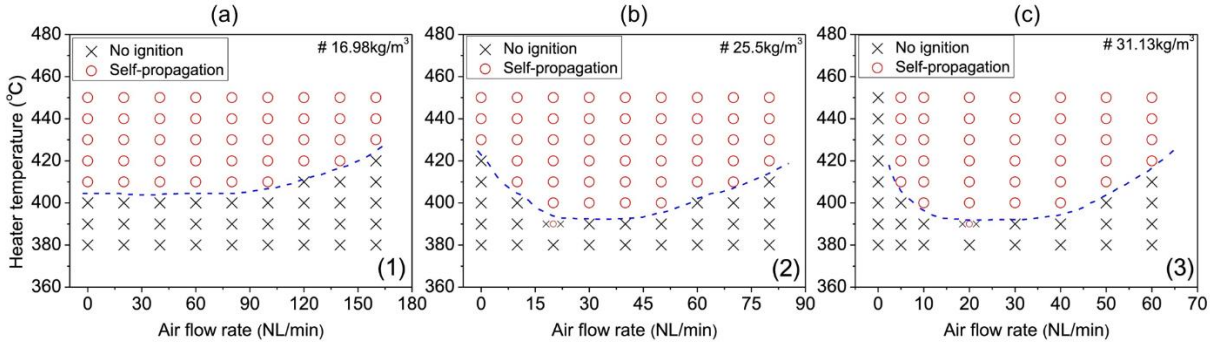

Fig. 1-6 Effects of ignition temperature and air flow rate on ignition behaviour in the smouldering ignition experiment of waste paper with different densities [43].

The influence of environmental conditions on the critical oxygen supply rate for smouldering is primarily reflected in the heat loss at system boundaries [28,58]. However, no previous studies have systematically explored the impact of boundary heat loss on the smouldering oxygen supply limit. Additionally, gravity and buoyancy may also influence smouldering in porous fuels. One study used polyurethane foam as fuel, and compared the results of forced flow tests under normal gravity with those in microgravity [57]. The results showed that under normal gravity, self-sustained propagation required approximately 0.5-0.8 g/m²·s of air mass flux. In contrast, this critical air mass flux decreased to 0.3 g/m²·s under microgravity conditions. This is due to the removal of gravity reduces buoyancy-driven heat loss, allowing smouldering to be sustained under lower oxidation rates.

In summary, even though numerous experimental and numerical studies have explored limiting oxygen supply characteristics in near-limit smouldering, most have been conducted under quiescent ambient conditions or with external wind, which cannot completely isolate oxygen diffusion from the surroundings. This has led to knowledge gaps: (1) the fundamental research problem of the actual minimum oxygen rate required to sustain smouldering remains unclear. (2) the roles of fuel properties and environmental conditions are still not well understood. (3) Even for the same fuel, varying values of LOC are reported due to different setup and boundary conditions. Hence, further systematic investigation in smouldering oxygen thresholds is required.

1.3 Aims and Objectives

In view of the above issues, this thesis aims to systematically study the oxygen supply limits in near-limit smouldering through both experimental and computational methods. The objectives of this thesis are as follows:

(1) To explore the oxygen threshold for smouldering combustion, including the limiting oxygen concentration and minimum oxygen supply rate, using a newly designed forced internal oxygen supply reactor.
(2) To quantitatively analyse the influence of fuel properties (bulk density, particle size, MC) and environmental conditions on the oxygen thresholds of smouldering.
(3) To establish a numerical model and validate it using previous experimental data, enabling the model to explore the critical oxygen supply characteristics of smouldering.
(4) To conduct laboratory large-scale laboratory experiments and observe smouldering behaviour under oxygen-limited conditions driven by natural diffusion in deep-layer scenarios.

1.4 Structure of this thesis

This thesis is a compilation of four publications achieved during the Ph.D. study. Overall, this thesis is presented in a manuscript style: ***Chapter 1*** introduces the background, research motivation, and reviews current methodologies and insights in literature.

Chapter 2 presents the design of a novel reactor that allows precise control and measurement of the oxidiser flow entering the smouldering reaction zone. This enables the definition of the oxygen threshold, including both the limiting oxygen concentration and flow rate, for a representative porous fuel.

Peer reviewed paper associated with *Chapter 2*: Y. Qin, Y. Chen, S. Lin* and X. Huang* (2022). Limiting Oxygen Concentration and Supply Rate of Smouldering Propagation. ***Combustion and Flame***, 245, 112380.

Chapter 3 conducts more experiments in typical natural fuels to analyse and explain the role of fuel properties, such as bulk density and particle size, in smouldering oxygen thresholds.

Peer reviewed paper associated with *Chapter 3:* Y. Qin, Y. Zhang, Y. Chen, S. Lin* and X. Huang* (2024). Minimum oxygen supply rate for smouldering propagation: Effect of fuel bulk density and particle size. ***Combustion and Flame***, 261, 113292.

Chapter 4 attempts to develop a computational model and validate it using previous experimental data. This enables the prediction of the influence of additional fuel properties and environmental temperatures on smouldering oxygen thresholds.

Peer reviewed paper associated with *Chapter 4:* Y. Qin, Y. Chen, Y. Zhang, S. Lin* and X. Huang* (2024). Modeling Smothering Limit of Smouldering Combustion: Oxygen Supply, Fuel Density, and Moisture Content. ***Combustion and Flame***, 269, 113683.

Chapter 5 performs large-scale laboratory experiments (1 metre in height) to demonstrate persistent smouldering phenomena and observe fire behaviour under oxygen-limited conditions.

Peer reviewed paper associated with *Chapter 5:* Y. Qin, D. Musa, S. Lin* and X. Huang* (2022). Deep Peat Fire Persistently Smouldering for Weeks: A Laboratory Demonstration. ***International Journal of Wildland Fire***, 32, 86-98.

Chapter 6 summarises the conclusions and suggests some ideas for future research.

Chapter 2 Experimental Study on Oxygen Thresholds: Limiting Oxygen Concentration and Supply Rate under Internal Forced Flow

Summary

This chapter presents experimental measurements of the minimum oxidiser flux required to sustain different smouldering modes. After centrally igniting the fuel bed, increasing the flow rate drives a transition from unidirectional (opposed) spread to bidirectional (opposed + forward) propagation. For both regimes, the critical flow velocity decreases as the oxygen fraction rises, and the corresponding oxygen flux converges on 0.08 ± 0.01 g/m^2·s under ambient air. Notably, smouldering persists even at an extremely low O_2 volume fraction of 2%.

With higher O_2 concentration or flow velocity, both the overall mass loss and the peak reaction-zone temperature increase, while the minimum smouldering temperature remains near 300 °C regardless of supply conditions. A simplified heat-and-mass transfer model explained the observed relationship between the required oxygen flux and the ambient oxygen concentration.

This chapter is based on "Y. Qin, Y. Chen, S. Lin* and X. Huang* (2022). Limiting Oxygen Concentration and Supply Rate of Smouldering Propagation. ***Combustion and Flame***, 245, 112380."

2.1 Introduction

Smouldering combustion is slow, low-temperature, and flameless that is driven by exothermic heterogeneous oxidations when oxygen molecules directly attack the hot fuel surface [4,9,59]. In porous media, smouldering can be triggered by weak heating or even self-ignition, and may transition to flaming [60–63]. Once initiated, it persists under extreme conditions such as poor oxygen supply and high moisture, making it the dominant combustion mode in many residential, industrial, and natural fires [40,64]. For example, underground peat fires endure in oxygen-limited soil for months [1], while engineered smouldering reactors efficiently treat wet organic wastes [28,65,66]. A deeper understanding of smouldering is therefore essential both for hazard mitigation and for advancing its industrial applications.

Two key factors dominates the spread and extinction of smouldering: oxygen availability and systematic heat loss [4,9,59]. Heat loss effects, including wall quenching [45,67,68], moisture evaporation [68–72], and wind cooling [60] are now well characterized. By contrast, despite the effect of oxygen levels on smouldering has been explored since the 1970s [73], the oxygen threshold behaviour remains poorly quantified. Early work showed smouldering spread at O_2 levels down to 6% in self-ignition tests [74], but another work showed that 5% ambient O_2 wasn't sufficient to extinct smouldering on coal and wood chips [75]. However, reported limiting oxygen concentrations (LOCs) vary widely, even for the same fuel, depending on experimental configuration [6,38,40,41]. Peat smouldering failed below 16% O_2 without forced flow [41], yet persisted at 11% under flow conditions [38]. Wood LOCs range from 10% with internal airflow [56] to 4–6% under intense irradiation [6] and increase further with moisture content [40]. The physical basis for these disparate LOC values remains unresolved.

Moreover, reducing ambient pressure or gravity further lowers the oxygen threshold for smouldering [57,76–78]. Experiments report minimum pressures of 10–20 kPa, comparable to quenching pressures in flames [77,78]. Furthermore, microgravity tests reveal that smouldering polyurethane foam demands less oxygen flow in space than under 1 g [57]. Yet the precise oxygen mass flux through porous media at these extremes remains unknown.

Oxygen supply into a porous bed depends on both concentration and internal flow velocity. In quiescent ambient studies, diffusion and natural convection provide oxygen to sustain smouldering, but uncontrolled ambient exchange makes it difficult for accurate flux quantification. To address this, we isolate a peat column from external air and impose a controlled oxidiser flow oxidiser flow with velocity (U) up to 14.74 mm/s and oxygen

concentration (X_{O_2}) of 2%-21%. We then measure total mass loss and peak reaction-zone temperature across varying supply rates. Finally, we develop a theoretical framework to predict the minimum oxygen flux and corresponding limiting oxygen concentration for robust smouldering propagation.

2.2 Experimental method

2.2.1 Porous peat soil

The experiments employed organic peat soil, a porous fuel prone to smouldering, as described in our previous work (Fig. 2-1) [62,68,71,79]. This moss peat has approximately 97% organic content, uniform density, and consistent particle size, ensuring excellent reproducibility [79]. Samples were oven-dried at 90 °C for 48 h and then equilibrated at roughly 5% moisture upon exposure to ambient air. This level has been shown to exert negligible impact on smouldering propagation [40,80]. Measured bulk density and porosity were 145 ± 10 kg/m^3 and 0.90 ± 0.01 [45], respectively. Particle diameters of about 1 mm create pore space for oxygen transport. Elemental analysis yielded mass fractions of C, H, O, N, and S equal to 45.6, 6.0, 48.0, 0.5, and 0.3%, respectively. Thermogravimetric tests using a PerkinElmer STA 6000 were performed at five oxygen concentrations of 21% (air), 10%, 5%, 2%, and 0 (pure nitrogen), and selected mass-loss rates and heat-flow data are provided in Appendix 1 (Fig. A1).

2.2.2 Experimental setup

Fig. 2-1 shows the experimental setup, which comprises a tubular smouldering reactor, an ignition system, and an oxidiser supply system. The reactor is constructed from 2 mm thick quartz glass, with an internal diameter of 12 cm to minimise wall quenching, and a depth of 30 cm [45,67]. A 1 cm thick ceramic insulation layer covers the outer surface to reduce heat losses. To ensure uniform gas flow, a steel mesh is positioned 3 cm above the base, topped by a 5 cm layer of glass beads. The fuel bed, maintained at a constant height of 20 cm, is placed on the beads.

Five K-type thermocouples (1 mm bead) are inserted into the fuel at 5 cm vertical intervals, recording temperature every minute. A coil igniter located at the centre (z = 0) initiates smouldering. Oxidiser is introduced from the reactor bottom at a flow rate controlled to within

± 5 percent by a flow meter. At the top, a 1 cm diameter outlet restricts ambient air diffusion, so that oxygen reaches the smouldering front only via the forced flow from below.

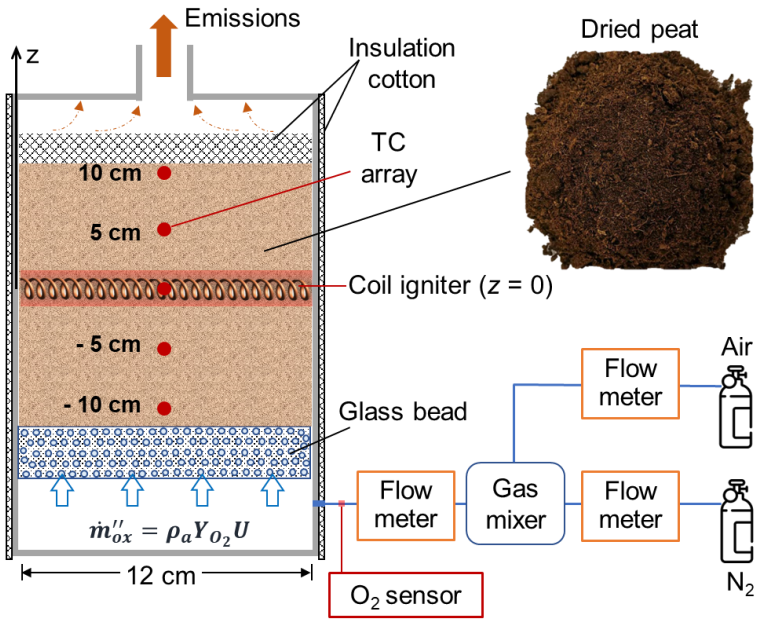

Fig. 2-1 Schematic diagram of experimental setup and photo of tested organic peat soil sample.

2.2.3 Test procedure and controlled parameters

The ignition protocol used a 100 W coil for 15 minutes, sufficient to ignite the dry peat and establish stable smouldering under ambient conditions. After ignition, a 1 cm layer of insulation cotton was placed on the fuel surface to minimise heat losses. The oxidiser, with prescribed oxygen concentration (X_{O_2}) and flow velocity (U) was introduced from the reactor base. Oxygen supply rate was defined as the mass flux through the reactor cross section:

$$\dot{m}''_{ox} = \rho_g Y_{O_2} U \tag{2.1}$$

where U is the average cross-sectional velocity; ρ_g is the gas density; Y_{O_2} is the oxygen mass fraction. The relationship between X_{O_2} and Y_{O_2} is given as:

$$X_{O_2} = \rho_g \frac{Y_{O_2}}{\rho_{O_2}} \tag{2.2}$$

Each test began at X_{O_2} = 21%. If the smouldering propagation can self-sustain after ignition, the flow velocity for was decreased for another individual test until extinction, so that the

minimum flow velocity (U_{min}) was found. Subsequently, the value of X_{O_2} was reduced to conduct tests with fresh samples and find the relationship between X_{O_2} and U_{min}. In this work, the oxygen concentration changes from 21% to 2%, and the flow velocity changes from 0.1 mm/s to 14.7 mm/s. Laboratory conditions were 22 ± 2 ^{o}C, the humidity was 50 ± 10%, and the pressure was 101 kPa. Each scenario was repeated at least twice to ensure reproducibility.

2.3 Results and discussion

2.3.1 Smouldering propagation phenomena

Fig. 2-2 presents thermocouple results for self-sustained smouldering and extinction at different flow velocities when X_{O_2}= 21%. During the 15 min ignition phase, the coil heater raises the reaction zone above 500 °C in every test, confirming robust ignition.

In the high-flow case (U = 4.4 mm/s, Fig. 2-2a) shows the smouldering propagation when the oxygen supply is abundant. After the 15-min ignition, the gas flow was supplied from the bottom end of the reactor. The temperature first decreases but soon increases again, indicating a self-sustained smouldering propagation [71]. Temperatures exceed 300 °C both above (z > 0) and below (z < 0) the ignition plane, indicating bidirectional spread (see Fig. 2-3a). Here, the downward front benefits from direct oxygen influx and exhibits higher peak temperatures and propagation rates, while the upward front, fed by residual oxygen, shows lower temperatures at z > 0. Once all temperatures return to ambient, only a thin mineral ash layer remains, signifying nearly complete fuel consumption and maximal mass loss.

When the flow is reduced to U = 1.2 mm/s, Fig. 2-2b shows that as the airflow velocity is decreased to 1.2 mm/s, the forward spread ceases: temperatures above z < 0 stay below the smouldering threshold (~250 °C) [67]. In addition, the smouldering front only propagates towards the gas flow from the bottom (opposed), as illustrated in Fig. 2-3b. In this oxygen-limited regime, the downward front consumes nearly all incoming O_2. The post-test bed contains an ash layer under a thick layer of virgin fuel, yielding lower mass loss (Section 2.3.3).

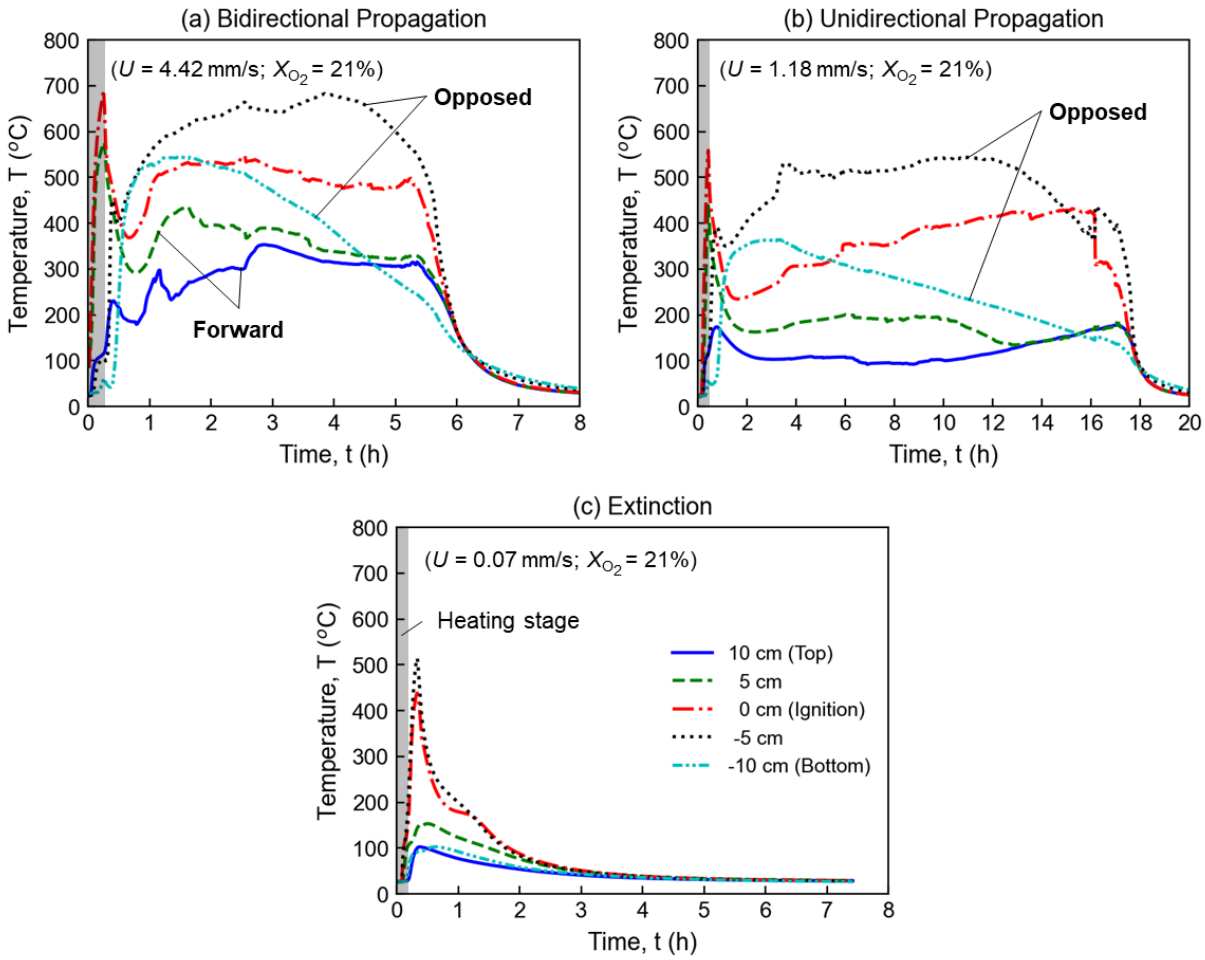

Fig. 2-2 Temperature profiles at different airflow (X_{O_2}= 21%) velocities, (a) U = 4.42 mm/s with a bidirectional propagation, (b) U=1.18 mm/s with a unidirectional propagation, and (c) U=0.07 mm/s without smouldering propagation.

Reducing the airflow velocity further leads to extinction of smouldering propagation. Fig. 2-2c shows temperature data for a non-propagating case at U = 0.07 mm/s. Although the coil heater raises the local temperature to approximately 500 °C during ignition, the temperature declines monotonically to ambient once the heater is switched off, with no fluctuations. Extending ignition to 30 or 45 minutes does not initiate propagation, confirming that this flow rate lies below the smouldering threshold for the peat fuel.

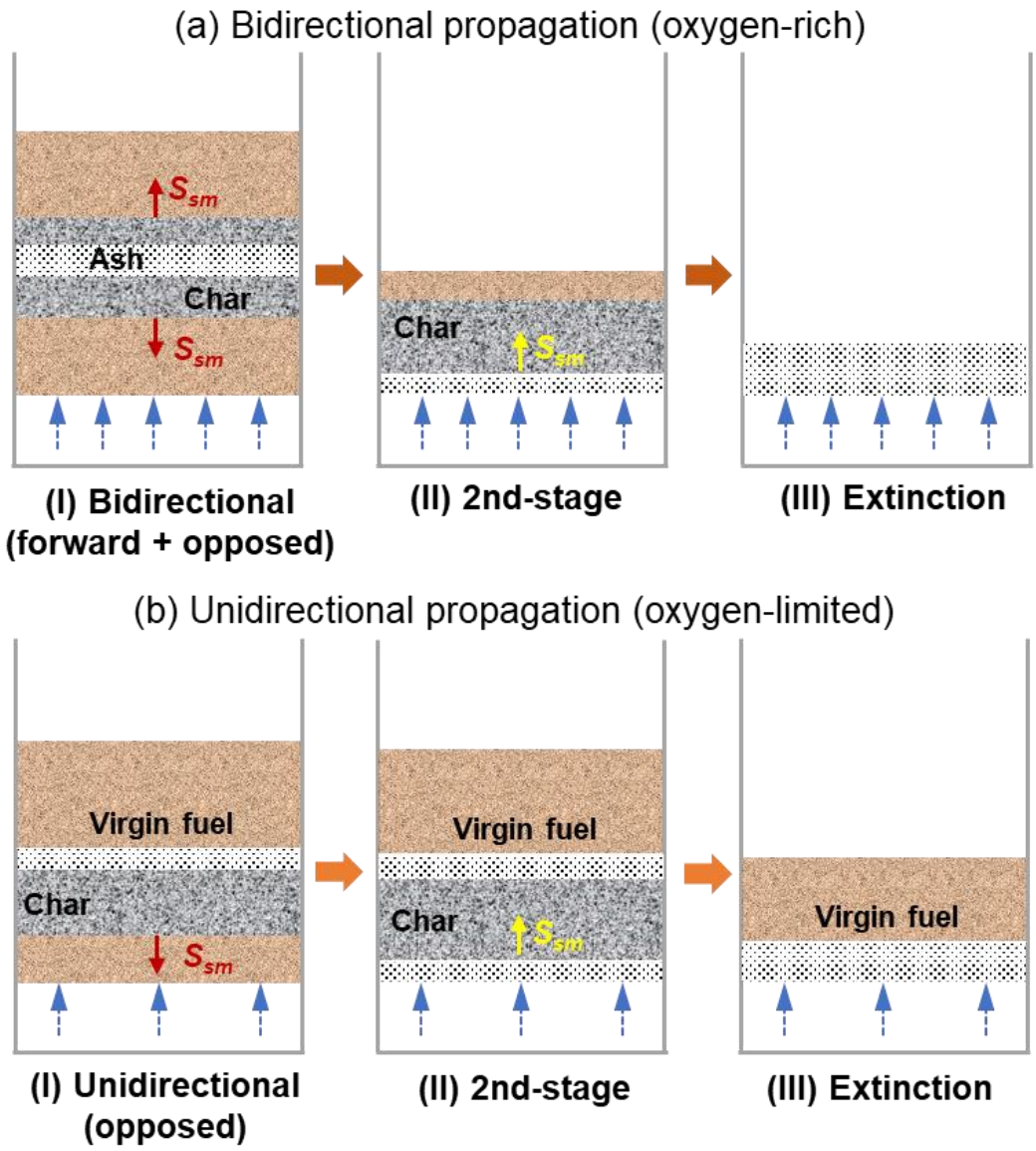

Fig. 2-3 Schematic diagrams of (a) bidirectional smouldering propagation and (b) unidirectional propagation under different oxygen conditions.

2.3.2 Oxygen supply limit for smouldering

Fig. 2-4a presents the measured minimum flow velocity (U_{min}) required to sustain smouldering under varying oxygen mole fractions (X_{O_2}). Hollow symbols denote tests with no propagation, semi-filled symbols indicate unidirectional spread, and solid symbols correspond to bidirectional spread. As anticipated, bidirectional propagation demands substantially higher flow rates than unidirectional propagation. For example, with a forced airflow ($X_{O_2} = 21\%$), the minimum velocities for bidirectional and unidirectional modes are 2.9 mm/s and 0.3 mm/s,

respectively.

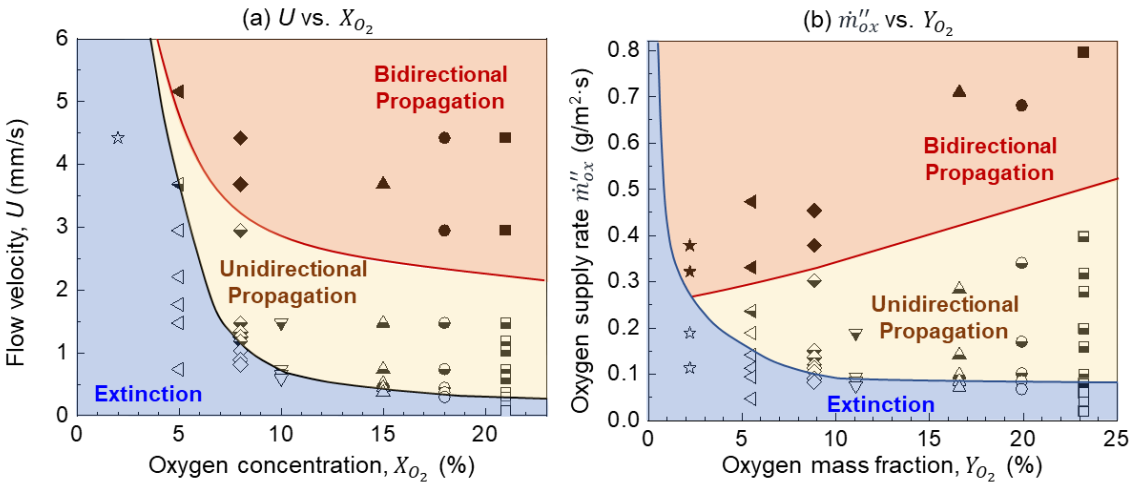

Fig. 2-4 (a) Minimum flow velocity (U_{min}) vs. oxygen concentration (X_{O_2}) and (b) minimum oxygen mass flow rate ($\dot{m}''_{ox,min}$) vs. oxygen mass fraction (Y_{O_2}).

The required oxidiser flow velocity for both unidirectional and bidirectional smouldering modes increases as the oxygen fraction declines. For example, reducing X_{O_2} from 21% to 10% raises the minimum velocity for unidirectional propagation from 0.3 mm/s to 0.7 mm/s. Even at extremely low X_{O_2} of 2%, self-sustained smouldering persists when the flow exceeds 12.5 mm/s. Fig. 2-5 shows temperature profiles of a successful smouldering propagation under 2% oxygen volume fraction. To the best of the authors' knowledge, this is the lowest oxygen concentration reported for smouldering fire. Thermogravimetric data (Fig. A1) confirm that exothermic char oxidation remains vigorous at 2% oxygen, implying that the limiting oxygen concentration for peat smouldering lies below this level. We estimate the minimum oxygen concentration at approximately 1.5 ± 0.5%. Such a low threshold helps explain the longevity of subsurface peat fires in oxygen-poor deep soils [9].

Empirical correlations between the minimum flow velocity and oxygen fraction are expressed as follows:

$$U_{min} = \begin{cases} \dfrac{0.06}{X_{O_2} - MOC} & \text{(unidirectional)} \quad (2.3a) \\ \dfrac{0.06}{X_{O_2} - MOC} + 2 & \text{(bidirectional)} \quad (2.3b) \end{cases}$$

where the unit of the internal flow velocity is mm/s, and R^2 of the fitting is 0.97. This empirical form was adopted in accordance with the theoretical analysis of Section 2.3.4. It is valid only for oxygen mole fractions above the minimum oxygen concentration (around 1.5 %); below

that value, the correlation lacks physical meaning.

At 2% oxygen, unidirectional propagation no longer occurs. Under rapid flow rates, the reaction zone at the downward front does not retain oxidiser long enough for complete char oxidation, so excess oxygen leaks upstream and sustains bidirectional spread. As a result, the thresholds for the two propagation modes converge at high oxygen fluxes (see Fig. 2-4b).

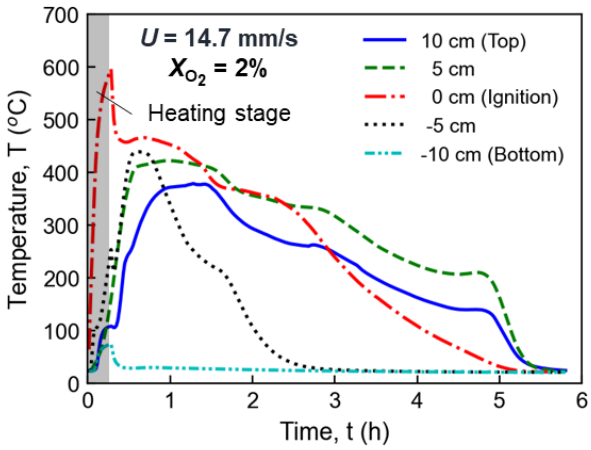

Fig. 2-5 Temperature profile at a flow velocity of U = 14.7 mm/s and oxygen concentration of X_{O_2}= 2%.

Fig. 2-4b compares the minimum oxygen mass flux ($\dot{m}''_{O_2,min}$) required to sustain unidirectional and bidirectional smouldering as a function of oxygen mass fraction (Y_{O_2}). Above Y_{O_2}=10%, the extinction threshold remains nearly constant at 0.08 ± 0.01 g/m^2·s, which we define as the minimum oxygen supply rate for sustained smouldering propagation. It is possible that this threshold decreases for Y_{O_2} above atmospheric levels, but further verification is needed. As the oxygen mass fraction further drops below 10%, the minimum oxygen supply rate for (unidirectional) smouldering propagation gradually increases to 0.25 ± 0.05 g/m^2·s at X_{O_2}=2%.

Combining equations (2.1-2.3), we have an empirical correlation between the minimum oxygen supply rate and oxygen level as

$$\dot{m}''_{O_2,min} = \rho_g Y_{O_2} U_{min} \approx \begin{cases} \dfrac{0.08 Y_{O_2}}{Y_{O_2} - MOC} & \text{(unidirectional)} \quad (2.4a) \\ \dfrac{0.08 Y_{O_2}}{Y_{O_2} - MOC} + 2.5 Y_{O_2} & \text{(bidirectional)} \quad (2.4b) \end{cases}$$

where MOC = 1.5 ± 0.5% for the test peat fuel, and R^2 of the fitting is above 0.9 because the

difference between oxygen volume and mass fractions are relatively small ($X_{O_2} \approx Y_{O_2}$).

The transition boundary between bidirectional and unidirectional propagation, plotted in Fig. 2-4a, shifts to higher flow velocities as Y_{O_2} decreases, maintaining a nearly constant offset of about 2 mm/s. This suggests that a minimum residence time of oxidiser is required for the forward smouldering front to ignite. Furthermore, as Y_{O_2} declines, both the extinction threshold and the width of the unidirectional regime narrow, as shown in Fig. 2-4b.

2.3.3 Mass loss and Smouldering temperature

Fig. 2-6a also presents mass-loss fractions and peak smouldering temperatures to clarify near-limit behaviour and extinction thresholds. Panel 2.6a shows mass loss for all tests, with filled symbols for bidirectional propagation, half-filled symbols for unidirectional propagation, and hollow symbols for extinction. The forced ignition phase alone consumed about 9% of the fuel mass (24.3 g of 270 g). Subsequent mass loss falls into three distinct regimes corresponding to the observed propagation modes: **Bidirectional propagation** achieved over 70% mass loss. Excess oxygen supply enabled a more complete combustion process, leaving only a thin ash residue at the reactor base, which is close to the 97% organic fraction of the peat. **Unidirectional propagation** consumed 35-70% of the fuel. Limited oxygen supplies halted spread beyond the downward front, so a residual layer of unburnt peat remained. The mass-loss range in this regime increases with oxygen concentration, mirroring the trend in required oxygen flux (Fig. 2-4b). Extinction (no propagation) still produced 10-35 % mass loss. Here, weak char oxidation persisted in the preheated ignition region but lacked sufficient oxygen to develop the reaction front.

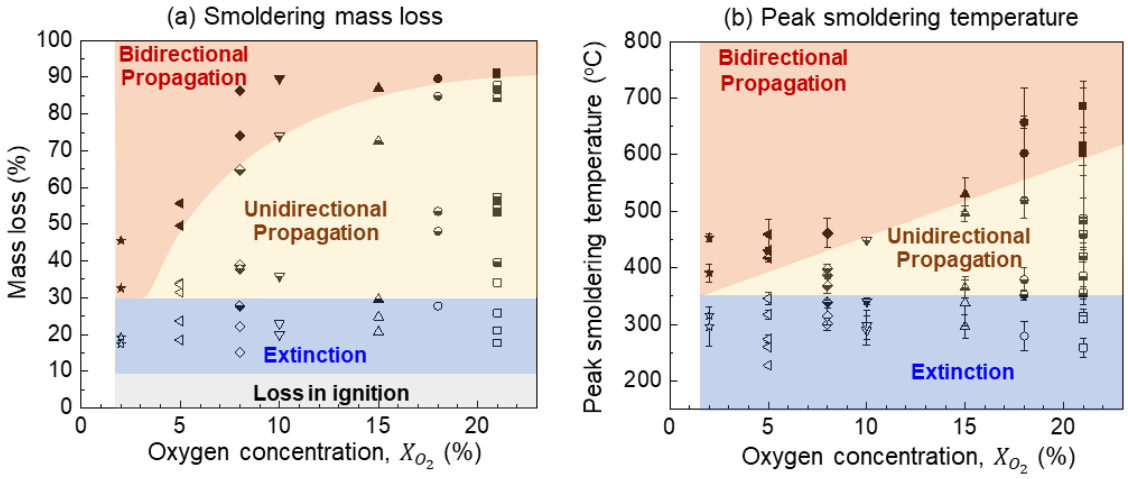

Fig. 2-6 (a) Mass loss and (b) the peak temperature during different smouldering-propagation modes.

Fig. 2-6b illustrates how peak smouldering temperatures respond to changes in flow velocity and oxygen concentration. For this peat soil, maximum temperatures reach approximately 700 °C, in agreement with previous reports [67,71,81]. Increasing either the oxygen fraction or the flow velocity elevates the reaction-zone temperature. For example, given an oxygen concentration of 18%, raising the flow rate from 0.4 mm/s to 4.4 mm/s, increases the peak temperature from 352 °C to 658 °C by enhancing char oxidation. Conversely, as oxygen and flow decrease, the peak temperature declines until, at the extinction threshold, it converges on a global minimum of about 300 °C. This value closely matches the char-oxidation onset observed in thermogravimetric analysis and corresponds to literature thresholds for sustaining smouldering [67,82].

2.3.4 Analysis of minimum oxygen supply

To explain the relationship between the minimum flow velocity (U_{min}), minimum oxygen mass flow rate ($\dot{m}''_{O_2,min}$) and oxygen fraction (X_{O_2} or Y_{O_2}), a simplified energy conservation equation is applied to a propagating smouldering front, as shown in Fig. 2-7. At the extinction limit, the heat generated from the net heterogenous smouldering reactions ($\dot{q}''_{sm}$) should just balance the heat loss from water evaporation ($\dot{q}''_{MC}$), internal flow convection ($\dot{q}''_{conv}$), and environmental heat losses ($\dot{q}''_{e}$) such as cold walls as

$$\dot{q}''_{sm,min} = \dot{q}''_{MC} + \dot{q}''_{conv} + \dot{q}''_{e} \tag{2.5}$$

where the minimum oxidation heat generated is

$$\dot{q}''_{sm,min} = \dot{m}''_{O_2,min}\Delta H_{ox} = \rho_g (UY_{O_2})_{min}\Delta H_{ox} \tag{2.6}$$

where ρ_g is the density of oxidiser flow, and ΔH_{ox} is the heat of oxidation. Therefore, we can derive the minimum oxidiser flow velocity as

$$U_{min} = \frac{\dot{q}''_{MC} + \dot{q}''_{conv} + \dot{q}''_{e}}{\rho_g Y_{O_2}\Delta H_{ox}} \propto \frac{1}{Y_{O_2}} \tag{2.7}$$

which shows that the minimum gas flow velocity is inversely proportional to the oxygen concentration ($X_{O_2} \approx Y_{O_2}$). Thus, the trend of experimental data in Fig. 2-4a is successfully explained.

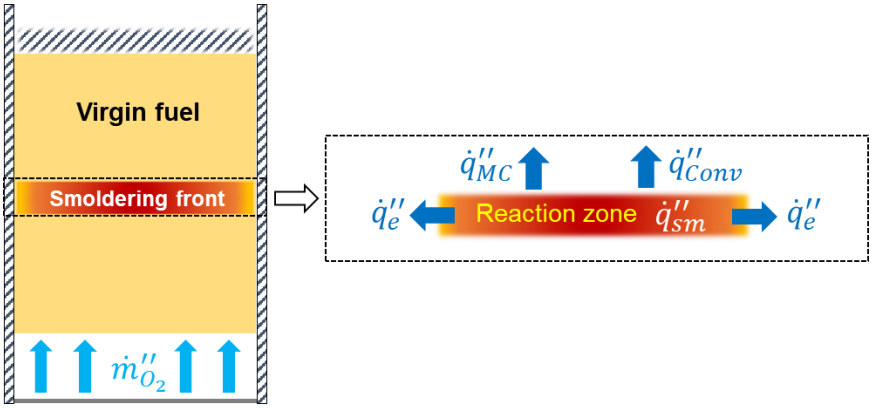

Fig. 2-7 Schematics for energy conservation in propagating smouldering front.

Further reorganising the energy equation, the minimum oxygen supply rate can be expressed as

$$\dot{m}''_{O_2,min} = U_{min}\rho_g Y_{O_2} = \frac{\dot{q}''_{MC} + \dot{q}''_{conv} + \dot{q}''_e}{\Delta H_{ox}} \tag{2.8a}$$

As the oxygen concentration decreases, the required internal flow velocity increases significantly (Fig. 2-4a), and its convective cooling ($\dot{q}''_{conv}$) becomes important [83], as

$$\dot{q}''_{conv} = h(T_{sm} - T_\infty) = Nu\left(\frac{k}{D}\right)(T_{sm} - T_\infty) \tag{2.9}$$

$$Nu \propto Re^m Pr^n \propto (UD/\nu)^m (\nu/\alpha)^n \propto U^m \tag{2.10}$$

where h is convective heat transfer coefficient, T_∞ is ambient temperature, D is the pore size, ν is kinematic viscosity, α is thermal diffusivity, and $0 < m < 1$ [84]. In the low-concentration, high-flow regime, convective cooling by the internal flow cannot be neglected. In that case, the minimum oxygen mass flux required to sustain smouldering must supply both the chemical consumption and the heat losses. It can therefore be expressed as

$$\dot{m}''_{O_2,min} = U_{min}\rho_g Y_{O_2} \propto \dot{q}''_{conv} \propto U_{min}^m \propto \left(Y_{O_2}\right)^{\frac{m}{m-1}} \quad (Y_{O_2} < 10\%) \tag{2.8b}$$

Specifically, with $m = 0.5$, we have $U_{min} \propto 1/Y_{O_2}^2$ and $\dot{m}''_{O_2,min} \propto 1/Y_{O_2}$. Therefore, the minimum oxygen supply rate increases with the flow velocity and decreases with the oxygen concentration. This successfully explains the experimental trend in Fig. 2-4b, when the oxygen mass fraction (Y_{O_2}) is smaller than 10%.

On the other hand, as the oxygen mass flux further increases, the required flow velocity will gradually decrease (see Fig. 2-4a). Eventually, the minimum required flow velocity will be tiny, so the convective heat loss becomes negligible as

$$\dot{m}''_{O_2,min} = \frac{\dot{q}''_{MC} + \dot{q}''_{conv} + \dot{q}''_{e}}{\Delta H_{ox}} \approx \frac{\dot{q}''_{MC} + \dot{q}''_{e}}{\Delta H_{ox}} = \text{const.} \quad (Y_{O_2} \geq 10\%) \qquad (2.8c)$$

With fixed fuel properties (for example, moisture content) and reactor geometry, the minimum oxygen flux converges to a constant value. This explains the experimentally observed threshold of $\dot{m}''_{O_2,min} = 0.08$ g/m^2·s at oxygen mass fractions above 10% (see Fig. 2-4b).

Equation (2.8c) also shows that this threshold varies with fuel characteristics. For example, the oxidation enthalpy (ΔH_{ox}) depends on fuel composition, and the fuel bed's thermal conductivity alters environmental heat losses ($\dot{q}''_e$). Increased moisture evaporation losses $\dot{q}''_{MC}$ likewise demand higher oxygen fluxes. Systematic measurements across different fuel types and bed conditions are therefore needed to develop a database for evaluating and ranking smouldering-fire hazards.

2.4 Conclusions

In this chapter, we experimentally determine the oxygen flux thresholds required for different smouldering modes. Following central ignition, increasing the oxidiser velocity drives a transition from opposed (unidirectional) to simultaneous opposed-and-forward (bidirectional) propagation. The critical flow rate for each mode decreases as oxygen concentration rises, and the minimum oxygen flux for self-sustained smouldering converges on 0.08 g/m^2·s under ambient conditions. Smouldering persists at oxygen levels as low as 2%, implying an even lower limiting concentration. Both mass loss and peak reaction-zone temperature increase with higher oxygen fraction and flow rate, while the minimum propagation temperature remains near 300 °C regardless of supply. A simplified heat-and-transfer analysis successfully captures the relationship between oxygen flux and concentration. Future numerical simulations are needed to reveal the detailed thermo-chemical mechanisms under varied flow regimes. These results provide crucial insights into peat fire persistence and applied smouldering systems.

Acknowledgments

This research is funded by the National Natural Science Foundation of China (NSFC) No. 51876183.

Chapter 3 The Roles of Fuel Properties in Oxygen Thresholds: Bulk Density and Particle Size

Summary

This chapter investigates how fuel bulk density and particle size govern the oxygen threshold for smouldering propagation under internal flow up to 5 mm/s. Pine needle beds (bulk densities of 55-120 kg/m^3) and wood samples (particle diameters of 1-50 mm) were tested, revealing that the critical airflow velocity for sustained smouldering rises as bulk density decreases or particle size increases. At low flow rates, the reaction front spreads only against the flow (opposed propagation). However, as velocity increases, it transitions to simultaneous opposed and forward spread. Moreover, in loosely packed or coarse-packed beds, where pore apertures are large, oxygen infiltrates the forward propagation front, enforcing bidirectional propagation even at minimal velocities. A simplified thermochemical model demonstrates that interparticle conductive heat transfer principally sets the minimum oxygen flux required for smouldering propagation.

This chapter is based on "Y. Qin, Y. Zhang, Y. Chen, S. Lin* and X. Huang* (2024). Minimum oxygen supply rate for smouldering propagation: Effect of fuel bulk density and particle size. ***Combustion and Flame***, 261, 113292."

3.1 Introduction

Smouldering combustion is a slow, low-temperature, flameless process sustained by exothermic, heterogeneous oxidation at the hot surfaces of reactive porous media [9,28,59,85]. It involves a complex interplay of chemical reactions and heat-and-mass transfer, which can be globally represented in two lumped steps: fuel pyrolysis followed by char oxidation [85,86]. Smouldering poses significant hazards across residential environments (bedding, upholstered furniture, mattresses), industrial settings (silos, storage piles), and natural fuels (coal seams, peatlands, forest floor litter), see Fig. 3-1a [1,9,87–92]. At the same time, controlled smouldering offers sustainable routes for energy recovery and waste treatment [27,93], so advancing fundamental knowledge is essential both for fire prevention and for optimising applied smouldering technologies [28,94].

Propagation and extinction of smouldering are governed primarily by two factors: heat loss and oxygen supply [9,59,95]. Adequate oxygen availability must balance endothermic processes such as drying, pyrolysis, and convective cooling in order to sustain the exothermic reactions that drive the smouldering front [42]. Because smouldering is an incomplete oxidation process, it requires less oxygen than flaming combustion and exhibits a lower limiting oxygen concentration (LOC) [6,42]. This enables smouldering sustaining in oxygen-poor environments such as deep peat and coal deposits [16,96].

Most prior investigations of smouldering oxygen limits have been conducted under quiescent or forced external wind conditions, which cannot isolate oxygen diffusion to the reaction zone [42]. As a result, reported LOC values vary widely even for the same material [38,40,41], and the true minimum oxygen mass flux necessary for sustained smouldering remains unclear. Accurate measurement of oxygen flux through the porous bed is therefore required to establish reliable LOC thresholds.

In our previous work [42], we introduced a tubular reactor that delivers controlled oxidiser flow through the fuel without ambient intrusion. For high-organic peat, we found an LOC below 2% and a minimum internal oxygen flux of 0.08 ± 0.01 g/m^2·s, constant for oxygen mass fractions (Y_{O_2}) above 15% (see Fig. 3-1b). However, LOC and flux thresholds for common fuels such as wood [27,94,97], coal [70], and biowastes [98,99], remain to be determined. Furthermore, fuel properties that includes particle size, bulk density, and moisture content may alter the oxygen requirements near extinction [100].

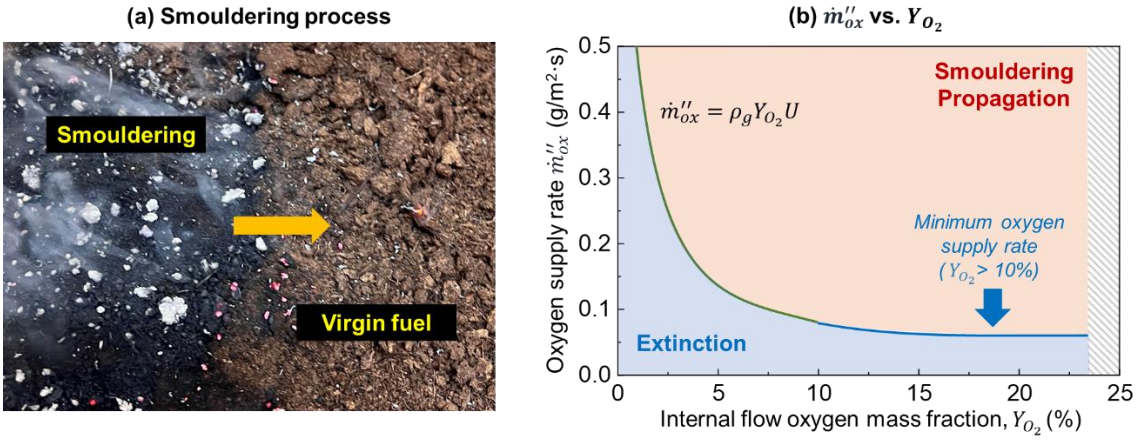

Fig. 3-1 (a) Smouldering, the flameless combustion, in organic peat soil. (b) minimum oxygen mass flow rate for supporting smouldering in peat at different oxygen mass fraction [42], where the oxygen limit achieve a minimum value of 0.08 ± 0.01 g/m^2·s when $Y_{O_2} > 15\%$.

Accordingly, this study examines the influence of fuel particle size and bulk density on the minimum oxygen supply rate required for smouldering. Experiments use pine needle and wood beds under a fixed oxygen mole fraction of $X_{O_2} = 21\%$ and impose internal flow velocities up to 5 mm/s. We quantify mass loss and temperature profiles across varied fluxes, and we develop a heat-transfer analysis to explain how fuel parameters control the minimum oxygen flux for sustained smouldering.

3.2 Experimental method

3.2.1 Fuel samples and processing

Wood and pine needles were chosen as representative porous fuels prone to smouldering combustion (Fig. 3-2a) [27,101,102]. Duff and peat also support smouldering but exhibit variable composition, so they were not used here. Homogeneous wood chips (fine dust, medium chips and large chips) were supplied by ECO-Greentech Ltd., and pine needles were collected from the Saihanwula Biosphere Reserve, China. Thermogravimetric analyses performed on a PerkinElmer STA 6000 under air and nitrogen atmospheres yield representative degradation profiles Fig. A2.

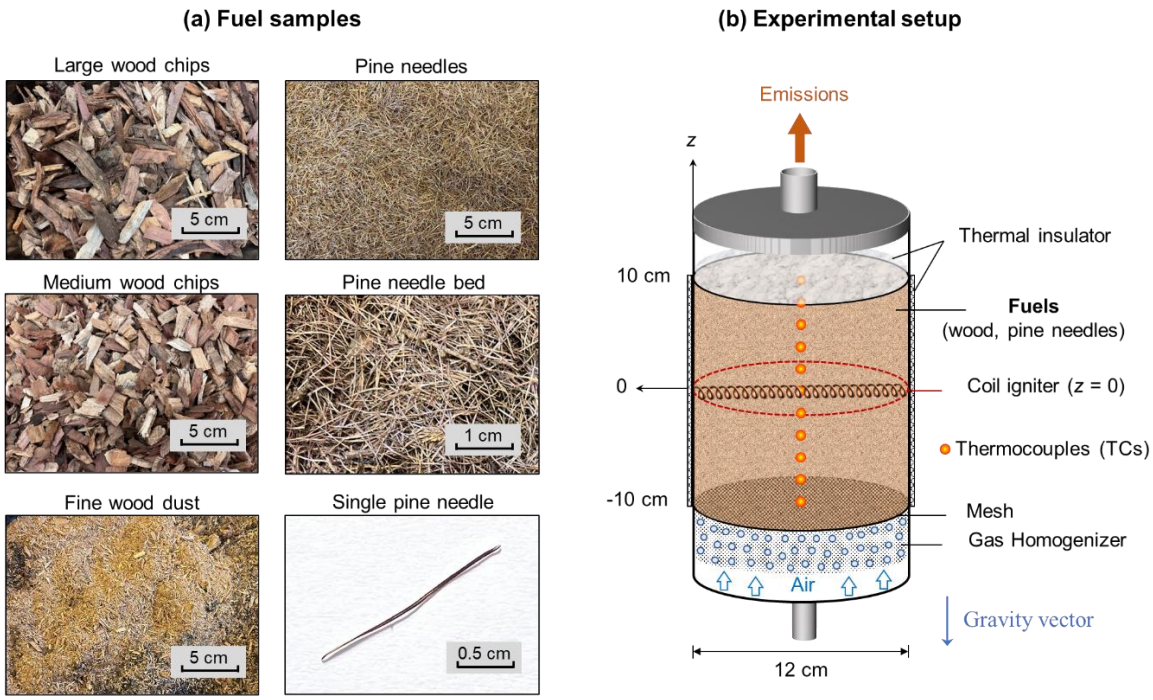

Fig. 3-2 (a) Tested samples of wood (large, medium chips and fine dust) and pine needles (in different observation views) and (b) schematic diagram of the experimental setup.

Prior to testing in the reactor (Fig. 3-2b), all fuels were oven-dried at 90 °C for at least 48 h and equilibrated to moisture contents below 5%, a level shown to exert negligible influence on smouldering propagation [40,80]. In general, wood chips were relatively stiff, and it is more feasible to control the fuel size. Comparatively, pine needles were relatively loose, and it is easier to change the bulk density. Thus, two groups of experiments were designed:

(I) woods with three particle sizes (d) of 1 (fine dust), 25 (medium), 50 mm (large), and

(II) pine needles with the same size (diameter (d) of 0.2 mm and length (L) of 25 mm) but three bulk densities of 55, 80, and 120 kg/m^3.

Note that the bulk densities (ρ_b) of medium (162 ± 20 kg/m^3) and large chips (178 ± 30 kg/m^3) were close to each other, while the bulk density of fine wood dust (325 ± 20 kg/m^3) doubled. A larger measurement error in bulk density is attributed to the strong dependency on stacking situation (e.g., the direction of chips), particularly in cases where particle size is relatively large. Since the solid density (ρ_s) of the wood material was about 600 kg/m^3 [27], the porosities ($\psi = 1 - \rho_b/\rho_s$) of the large, medium, and fine wood samples were 0.7 ± 0.02, 0.73 ± 0.03 and 0.46 ± 0.03, respectively. Table 3-1 summarises all fuel properties. Fig. 3-3 plots the relationship between particle size and bed density.

Table 3-1 Properties of dry fuel samples in the experiments

Fuel	Particle size d (mm)	Bulk density ρ_b (kg/m^3)	Solid density ρ_s (kg/m^3)	Porosity ψ (-)	Volatile (%)	Fix carbon (%)	Ash (%)
Wood	1 ± 0.5 (Fine)	325 ± 20	600 ± 20	0.46 ± 0.03	58.8	38.9	1.1
	25 ± 5 (medium)	162 ± 20		0.73 ± 0.03			
	50 ± 10 (large)	178 ± 30		0.70 ± 0.02			
Pine needle	d = 0.2 ± 0.1 L = 25 ± 5	55 ± 5	607 ± 30	0.91 ± 0.01	47.1	35.7	14.3
		80 ± 10		0.87 ± 0.02			
		120 ± 15		0.80 ± 0.02			

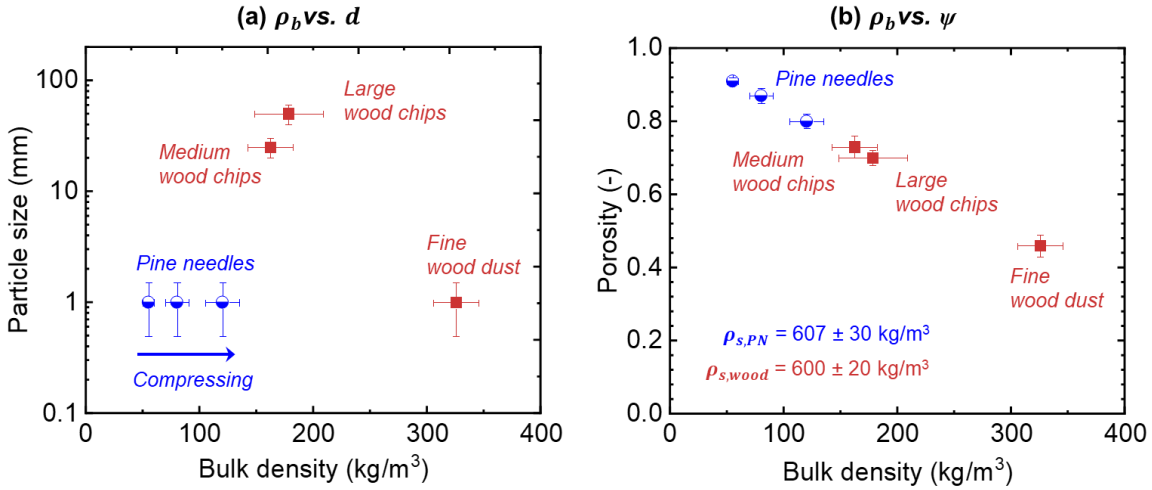

Fig. 3-3 Bulk density versus (a) fuel size and (b) fuel bed porosity of tested pine needles and wood samples

3.2.2 Experimental setup and procedure

The smouldering experiments were carried out in a vertical tubular reactor fitted with an ignition system and an air-supply module, see Fig. 3-2b. The reactor is made of 2 mm-thick quartz glass and has a total depth of 35 cm, an update from our previous design [42]. Its internal diameter is 12 cm, giving a cross-sectional area $A_c = 113$ cm^2, which minimises lateral wall cooling [45,67].

Purified air was fed from the base at velocities up to 5 mm/s. Since that gravity and buoyancy can affect extinction limits [57], future studies should explore different flow orientations. Here, the average velocity ($U = m/\rho_g A_c$) represents the bulk flow rate divided by gas density and reactor area, not the local pore velocity. A flow homogeniser, comprising mesh, a 5 cm glass-bead layer, and a second mesh ensures uniform supply. Above this, a 20

cm layer of dried fuel is installed.

To reduce heat loss to the environment, a 1 cm thermal-insulation cotton was applied around the reactor. An array of eleven K-type thermocouples (1 mm bead) is inserted at 2 cm intervals to record temperature profiles every minute. A 100 W coil igniter at mid-height (z = 0) runs for 20 min to initiate smouldering; once ignition ends, the heater is switched off and the controlled airflow is begun.

All probe and igniter ports are sealed to prevent leaks. A 1 cm outlet at the reactor top vents exhaust gases while blocking ambient air [42]. Laboratory conditions were 25 ± 3 ^{o}C, 50 ± 20% relative humidity (equivalently 1.5 ± 0.6% mole fraction of water in the air), and 101 kPa pressure. Each condition was tested in at least three replicates, where consistent ignition or extinction confirms reproducibility [42,67].

3.3 Results and discussion

3.3.1 Smouldering propagation phenomena

Fig. 3-4 presents thermocouple measurements for medium wood chips at decreasing internal flow rates, showing a progression from bidirectional propagation to unidirectional propagation and then to extinction. Similar trends were also observed for wood dust and pine needles in this work and for organic soil in our previous work [42].

Under an internal airflow of 4.4 mm/s (Fig. 3-4a), the ignition zone temperature rose above 300 °C by the end of the ignition period, establishing a stable reaction front. After ignition, airflow induced two separate smouldering fronts: one moving downward against the flow and one moving upward with the residual oxygen. The downward front exhibited higher peak temperatures and produced a thicker ash layer, indicating more complete combustion. At high flow rates, most oxygen is consumed by the downward front while the excess supports the upward front. The heat-transfer processes governing these peak temperatures are analysed in Section 3.3.4.

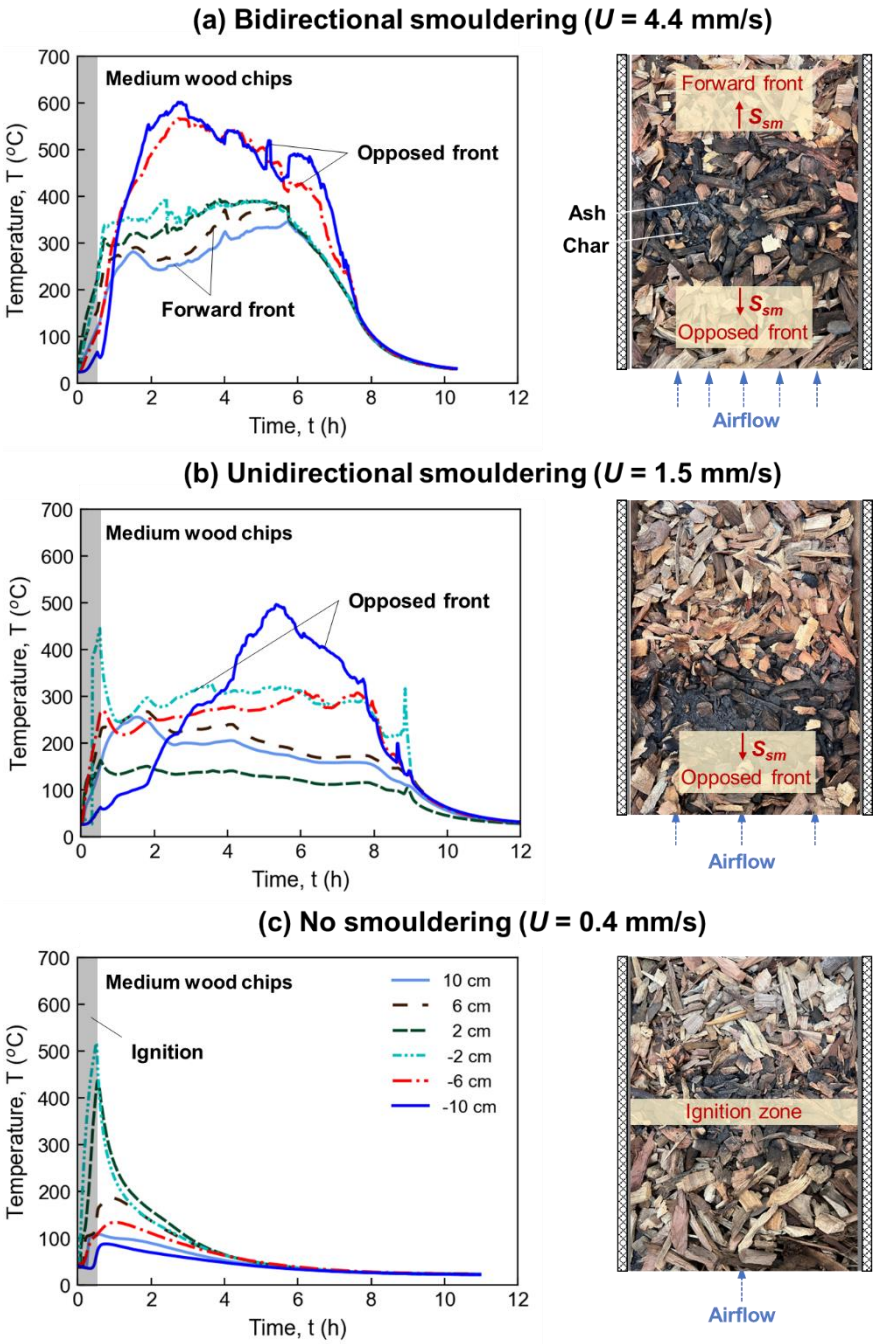

Fig. 3-4 Thermocouple measurements and schematic diagrams of (a) bidirectional smouldering, (b) unidirectional smouldering and (c) no smouldering in medium-size wood chips with internal airflow supply rate of 4.4 mm/s, 1.5 mm/s and 0.4 mm/s, respectively.

Under the same ignition protocol and air supply timing, reducing the flow to 1.5 mm/s (Fig. 3-4b) sustained only the opposed smouldering front above 250 °C, as all supplied oxygen was consumed by the downward reaction zone. During ignition, the 6 cm thermocouple recorded higher temperatures than the 2 cm sensor, likely because of nonuniform thermal conduction in the fuel bed or because the 2 cm bead sat in a pore rather than solid material. After burnout,

the fuel surface decreased sharply, leaving a clear interface between virgin fuel above and ash and unburned char below.

Further reduction of the airflow extinguished smouldering, as shown in Fig. 3-4c. Once ignition ended, temperatures throughout the reactor fell directly to ambient with no secondary rise. Neither extending the ignition period nor increasing coil power sustained smouldering propagation at this flow rate.

3.3.2 Smouldering oxygen supply limits vs. fuel-bed bulk density

Fig. 3-5 correlates the internal airflow velocity required for smouldering with (a) fuel bulk density (ρ_b) and (b) porosity (ψ) in pine-needle beds. Three regimes: bidirectional propagation, unidirectional propagation, and extinction, define two different oxygen-supply thresholds. On the one hand, Fig. 3-5a shows the minimum oxygen supply decreases with the fuel dry bulk density, indicating that denser beds require less oxygen to sustain smouldering. Specifically, when the bulk density was increased from 55 kg/m^3 to 120 kg/m^3, the U_{min} decreased significantly from 0.5 mm/s to 0.2 mm/s.

Conversely, the boundary separating bidirectional and unidirectional modes shifts to higher velocities at greater bulk densities. At ρ_b = 120 kg/m^3, bidirectional propagation in the vertical direction can only be observed at a larger airflow velocity (near 3 mm/s). In contrast, for pine needles close to their natural bulk density (~ 45 kg/m^3), as long as the provided airflow is larger than the minimum supply limit, both upward and downward smouldering fronts can be formed and sustained. The reason behind this "bidirectional smouldering propagation" is not the excessive O_2 supply to a uniform front (as illustrated Fig. 3-6a and detailed in our previous work [42]). As illustrated in Fig. 3-6b, two leakage scenarios: high porosity (B1) and large particle size (B2) produce localized oxygen entry that ignites a second front. Consequently, lower-density beds (higher porosity) are more prone to bidirectional propagation.

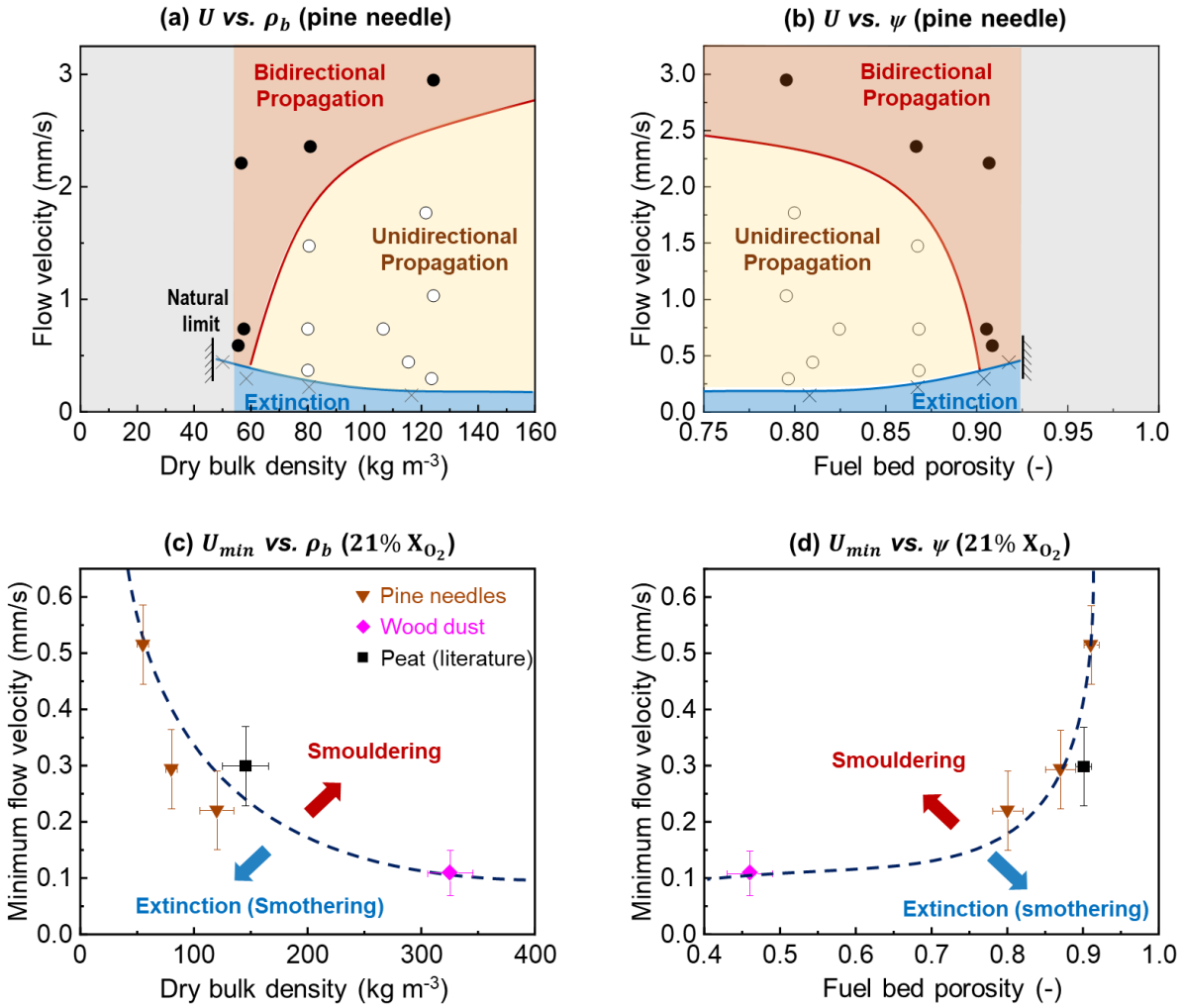

Fig. 3-5 Internal airflow velocity vs. (a) pine needle bulk density and (b) porosity, where ●: bidirectional, ○: unidirectional, and ×: extinction. Minimum internal airflow velocity vs. (c) fuel bulk density and (d) porosity for different fuel beds.

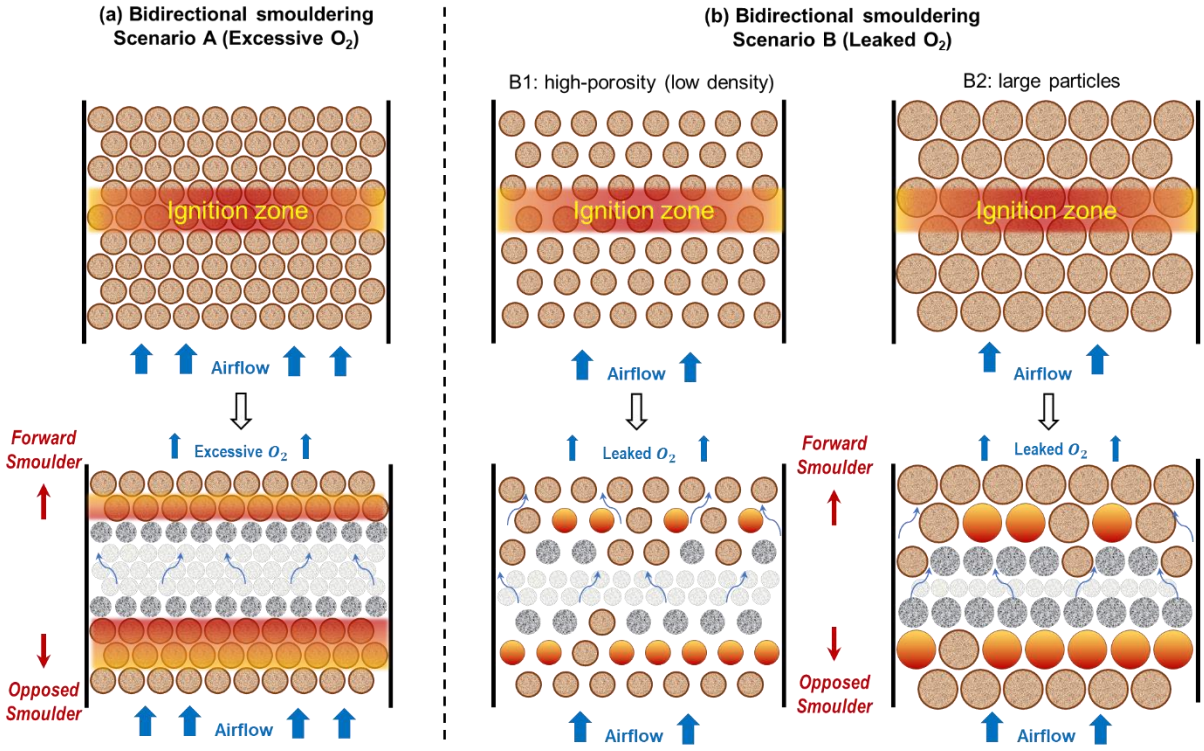

Fig. 3-6 Two scenarios of bidirectional smouldering propagation, (a) excessive oxygen not fully consumed by the opposed front; and (b) leaked oxygen due to B1: high-porosity (low-density) fuel bed or B2: large fuel particles.

Fig. 3-5 (c-d) compile the minimum flow velocities U_{min} required for smouldering across fuels of similar particle size (0.5-2 mm): pine needles, wood dust, and peat soil [42] as a function of porosity. Although these materials differ in organic content, heat of combustion, and other physical properties (Table 3-1 and Appendix 2), the trends show that, with particle size held constant, bulk density is the primary determinant of the oxygen flux needed for sustained smouldering. Further experimental data spanning diverse fuels, together with theoretical analyses, are needed to reveal the contributions of porosity, composition, thermal conductivity, and other parameters.

3.3.3 Smouldering oxygen supply limits vs. fuel particle size

Based on the experimental results, the effect of density on the U_{min} can also be applied to wood samples to some extent, as shown in Fig. 3-7a. In general, wood samples with higher bulk densities require less oxygen to support unidirectional smouldering combustion, but a larger flow rate for bidirectional propagation. However, an anomaly was found when focusing on bulk density between 150 and 200 kg/m^3, that is, the relationship between ρ_b and U_{min}

shows no clear trend; this variability reflects sensitivity to chip orientation and packing in that density range. Consequently, we recast the wood data in terms of particle size rather than bulk density.

Fig. 3-7b summarises U_{min} for pine-needle beds of varying needle lengths (0.5-2 mm diameter, length at 25 mm). As particle size decreases, the minimum flow velocity for sustained smouldering declines, mirroring the effect of increased bulk density. Large wood chips (50 mm) only exhibited bidirectional propagation at velocities above 1 mm/s, attributable to oxygen leakage through interstices (Fig. 3-6 (B2) and Fig. 3-7). Thus, both increased particle size and reduced bed density promote local oxygen bypass that ignites a secondary, forward-propagating front.

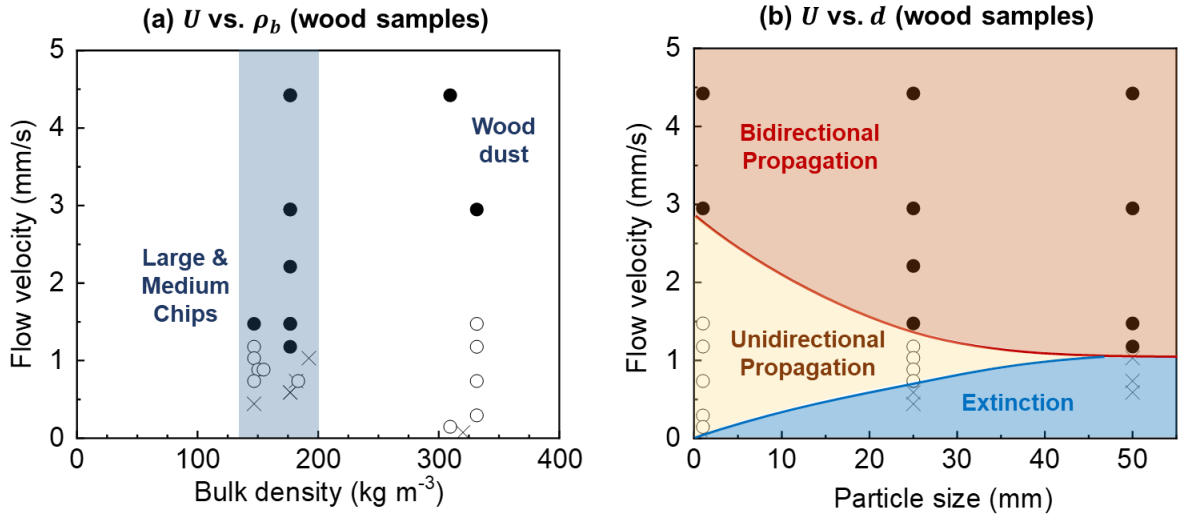

Fig. 3-7 Internal airflow velocity vs. (a) dry bulk density and (b) particle size of wood samples, where ●, ○ and × represent “bidirectional propagation”, “unidirectional propagation” and “no propagation”, respectively.

3.3.4 Smouldering mass loss and temperature

Mass loss and peak temperature are key indicators of smouldering behaviour near extinction. Fig. 3-8 presents the total mass loss after smouldering, using hollow symbols for unidirectional propagation and solid symbols for bidirectional propagation. Each data point reflects a separate test at a given airflow velocity. Although pine needles lose more mass during the ignition phase than wood chips, at higher flow rates wood achieves greater overall mass loss due to its lower ash fraction (determined by TG test, see Table 3-1 and Appendix 2). In both fuels, mass loss rises with increasing airflow regardless of particle size, bulk density or propagation mode, highlighting the need for precise oxygen control in biomass smouldering

applications [22,27,94].

Importantly, bidirectional spread does not consistently produce higher mass loss than unidirectional spread, so mass loss alone cannot identify the propagation mode, but temperature profiles must also be analysed. Moreover, Fig. 3-8 (c-d) compare how bulk density and particle size influence mass loss, showing that conditions favouring bidirectional propagation (namely low bulk density or large particle size) tend to reduce overall combustion completeness.

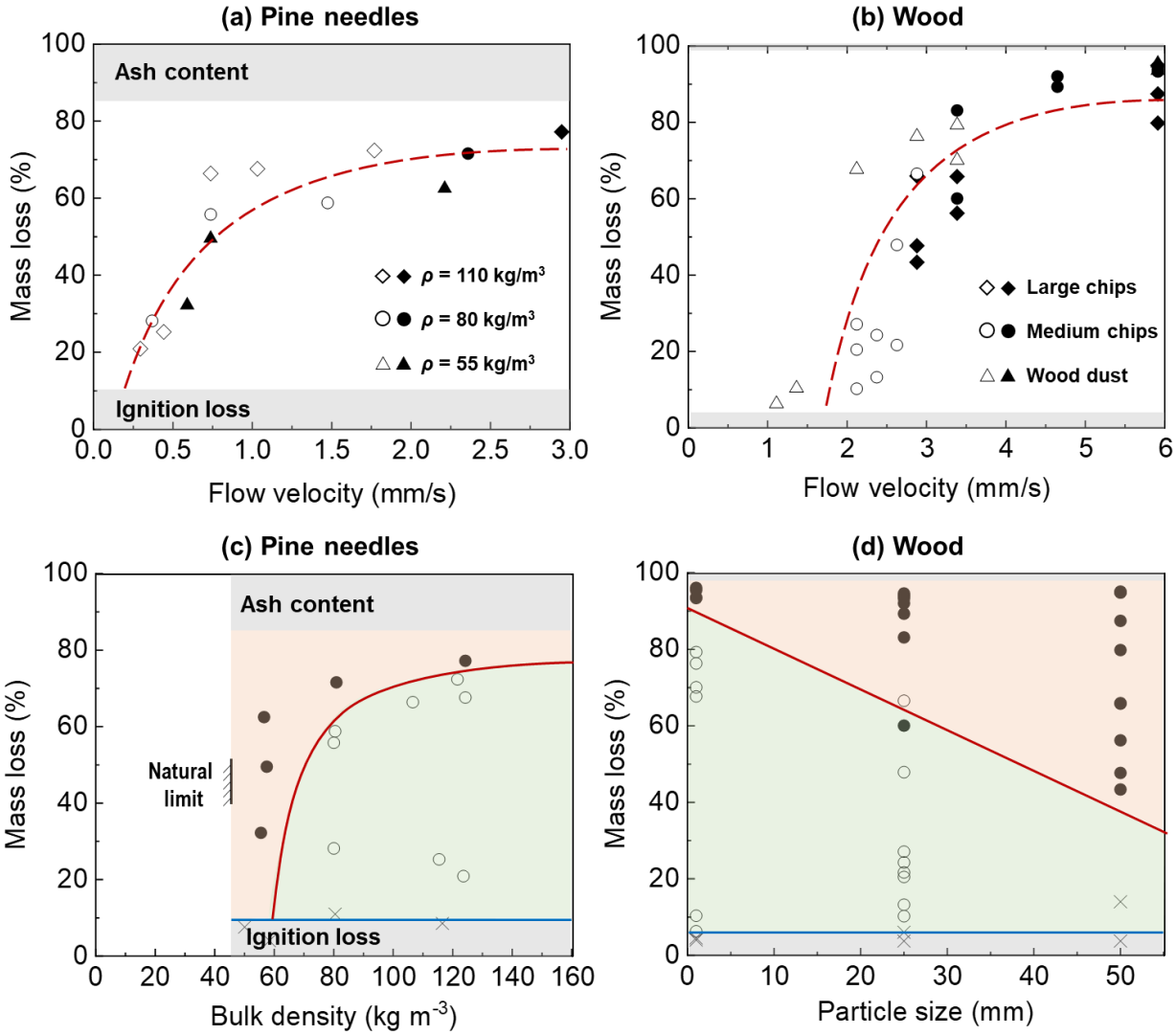

Fig. 3-8 The effect of (a-b) internal airflow velocity, (c) bulk density and (d) particle size on mass loss during smouldering, where ○ is unidirectional propagation, and ● is bidirectional propagation.

Fig. 3-9 presents the peak smouldering temperatures measured in both fuels. For unidirectional propagation, the value is the mean peak temperature of the single reaction front; for bidirectional propagation, it is the mean of the two fronts across repeated tests, with

standard deviations shown as error bars. Peak temperature rises with increasing oxidiser flow rate, reflecting improved oxygen availability and greater heat release during char oxidation. This behaviour mirrors the mass-loss trends in Fig. 3-8.

Peak temperature alone does not distinguish propagation mode. For example, large wood samples at 1.2 mm/s airflow exhibited bidirectional spread despite a relatively low peak temperature (see Fig. 3-8b). This indicates that bidirectional propagation can result not only from excess oxygen [42] but also from oxygen bypass through non-uniform fronts caused by low bulk density or large particle size (see Fig. 3-6).

Pine needles display a slightly higher minimum peak temperature, around 300 °C, compared to 250 °C for wood samples. Although neither bulk density nor particle size substantially alters peak temperature under the same oxygen supply (see Fig. 3-9 (a-b)). In addition, Fig. 3-9 (c-d) show that bidirectional spread in low-density or large-particle beds corresponds to lower peak temperatures.

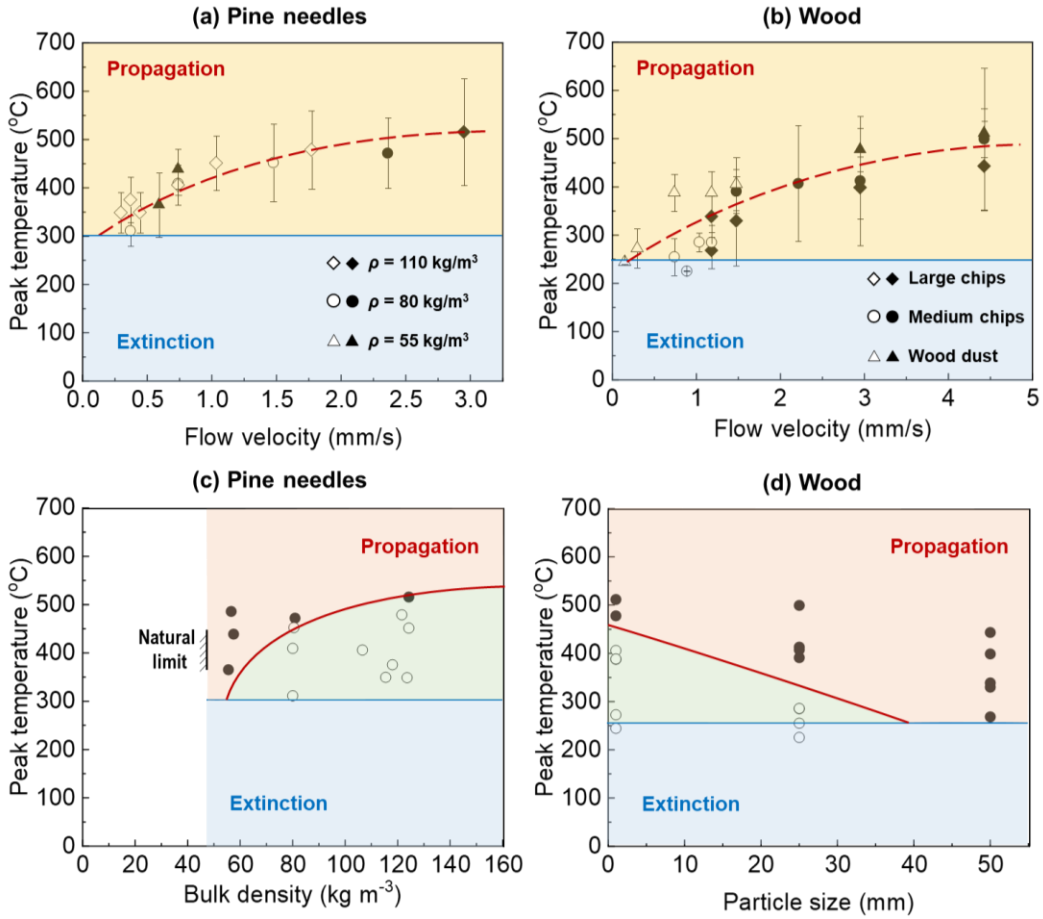

Fig. 3-9 The effect of (a-b) flow velocity, (c) bulk density and (d) particle size on peak smouldering temperatures, where the hollow (○) and solid (●) symbols represent uni- and bidirectional propagation, respectively.

3.3.5 Heat and mass transfer analysis

Smouldering propagation is governed by three heat-transfer modes: conduction, convection and radiation. We applied energy conservation to the reaction front under near-limit conditions (Fig. 3-10), which yields a simplified heat-balance. At the threshold of propagation or extinction, the net heat flux released by the smouldering front ($\dot{q}''_{sm}$) must exactly balance the total heat loss ($\dot{q}''_{loss}$) as

$$\dot{q}''_{sm} \geq \dot{q}''_{loss} \tag{3.1}$$

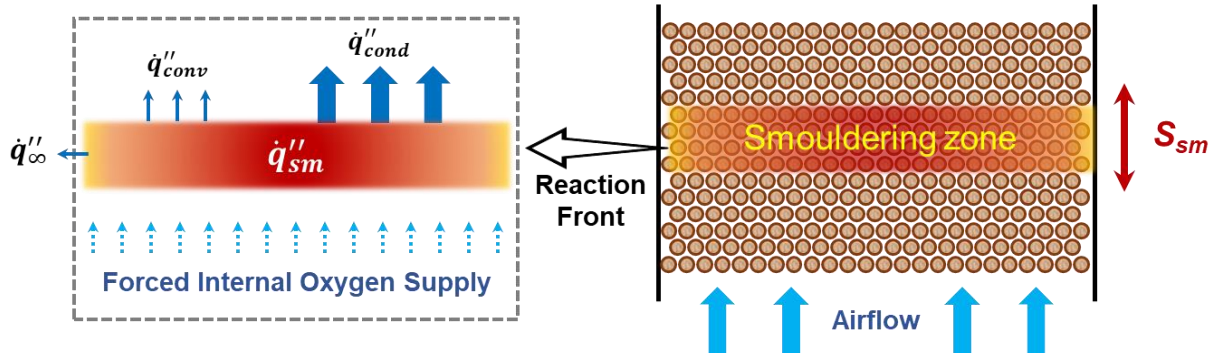

Fig. 3-10 Schematics for the energy balance for a propagating smouldering front at near-limit conditions.

As smouldering propagation is primarily controlled by thermal conduction in this porous fuel system with a low-velocity forced airflow (<1 mm/s) [103], by rearranging Eq. (3.1), we obtain

$$\dot{q}''_{sm} = \dot{m}''_{O_2,min}\Delta H_{ox} = \rho_g U_{min} Y_{O_2}\Delta H_{ox} \approx \dot{q}''_{cond} = k\frac{(T_{sm} - T_0)}{\Delta x} \tag{3.2}$$

where k is the effective thermal conductivity in porous media (as a solid-fluid system), T_{sm} is the smouldering temperature, T_0 is the temperature of virgin fuel, Δx is the characteristic length of conductive heat transfer. Therefore, the minimum flow velocity U_{min} can be derived as

$$U_{min} = \frac{k(T_{sm} - T_0)}{\rho_g Y_{O_2}\Delta H_{ox}\Delta x} \tag{3.3}$$

Furthermore, the effective thermal conductivity k includes a solid and a radiative component [47,104]:

$$k = k_s(T) + k_r(T) = k_0\left(\frac{T}{T_r}\right)^{n_k} + \gamma\sigma T^3 \tag{3.4}$$

where n_k is the temperature dependence, σ is the Stefan-Boltzmann constant, γ is the radiative conductivity parameter (with units of length) that depends on pore morphology and other considerations and can be estimated by characterized pore size d_p as $\gamma = 3d_p$ [105,106]. The characterized pore size relates to the particle surface area (S, m^2/g) and bulk density (ρ_b, kg/m^3) as $d_p = 1/S\rho_b$ [105]. Therefore, from Eqs. (3.3-3.4), as the bulk density of fuel increases, d_p, γ and k will decrease accordingly, leading to a lower minimum flow velocity (U_{min}) as

$$U_{min} \sim k \sim \gamma \propto d_p \propto \frac{1}{\rho} \tag{3.5}$$

On the other hand, as the particle size (d) increases, the specific surface area (S) will decrease and the characterized pore size (d_p) will increase. As a result, both γ and k will increase simultaneously, leading to a larger minimum flow velocity (U_{min}) as

$$U_{min} \sim k \sim \gamma \propto d_p \propto \frac{1}{S} \propto d \tag{3.6}$$

In other words, increased fuel bulk densities or smaller fuel particle sizes can both lower the minimum oxygen supply required for smouldering propagation by enhancing heat conduction between the burning zone and virgin fuels. Thus, the proposed heat transfer analysis successfully explains the experimental data (Fig. 3-5a and Fig. 3-7b) and indicates the important role of radiation heat transfer across pores in affecting the oxygen supply limit of smouldering propagation over porous media.

Although these experiments and analyses have clarified the influence of bulk density and particle size on the minimum oxygen flux for smouldering, further experimental and numerical work is needed to quantify the dependence of U_{min} on additional fuel properties such as moisture content, organic fraction, and combustion enthalpy. The current theoretical model also assumes a constant solid density, which is valid for single-component fuels (pine needles or wood chips) but may not apply to heterogeneous mixtures with variable ρ_s. Future studies should therefore investigate how complex fuel compositions affect smouldering thresholds. These efforts will both advance our fundamental understanding of smouldering combustion and provide the basis for a database to optimise oxygen delivery in waste-treatment systems and to assess smouldering fire hazard.

3.4 Conclusions

In this chapter, we experimentally quantified how fuel bulk density and particle size influence the minimum oxygen flux required for smouldering combustion. Pine-needle beds of varying bulk densities and wood samples of differing particle sizes were tested in a vertical tubular reactor with controlled airflow. Following central ignition, three regimes emerged as the flow rate was reduced: bidirectional propagation, unidirectional propagation, and extinction. Bidirectional spread arose either from surplus oxygen that the opposed front could not consume or from oxygen bypass through non-uniform pore networks created by large particles or low packing density. We found that the critical flow velocity for sustained smouldering rises as bulk density decreases or particle size increases. At extreme porosities, propagation thresholds converge, and only bidirectional smouldering persists due to oxygen leakage. Finally, a simplified heat-transfer model is introduced to demonstrate the role of radiative heat transfer across pore spaces in setting the oxygen-supply limit for smouldering over porous media.

Acknowledgments

This research is funded by the National Natural Science Foundation of China (NSFC) No. 52322610 and RGC Hong Kong GRF Scheme No. 15221523.

Chapter 4 Computational Study on Predicting the Smouldering Oxygen Thresholds

Summary

In this chapter, we develop a one-dimensional, physics-based model that couples heat and mass transport with a five-step heterogeneous reaction scheme to determine the smothering limit of smouldering in porous pine-needle beds under forced internal oxidiser flow. Simulations indicate that the critical oxidiser velocity (or equivalently the oxygen flux) rises as inlet O_2 concentration falls, leading to a limiting O_2 concentration (LOC) of 3%, in satisfactory agreement with experiments results. Furthermore, the required flow rate increases with decreasing fuel bulk density, lower ambient temperature, or elevated moisture content, with the model predicting a maximum moisture content of 110%. At the smothering threshold, the peak reaction-zone temperature and propagation speed are approximately 300 °C and 0.5 cm/h, respectively.

This chapter is based on "Y. Qin, Y. Chen, Y. Zhang, S. Lin* and X. Huang* (2024). Modeling Smothering Limit of Smouldering Combustion: Oxygen Supply, Fuel Density, and Moisture Content. ***Combustion and Flame***, 269, 113683."

4.1 Introduction

Smouldering combustion is a slow, low-temperature, flameless process sustained by heterogeneous oxidation at hot solid surfaces, involving complex interactions of chemical reactions and heat-mass transfer [4,9,28,34,59,107]. It poses severe hazards in peatlands, coal seams and forest litter layers [9,16,108,109], and contributes substantially to residential and industrial fires [110,111]. At the same time, controlled smouldering offers routes to energy production, waste removal, and pollution control [21–23]. A deeper understanding of its fundamental mechanisms is therefore essential for both hazard mitigation and optimisation of applied systems.

Smouldering initiation, spread and quenching depend on the interplay of heat losses and oxygen availability [59]. Previous experiments [22,67] and computational studies [95] have systematically characterized how heat losses governs smouldering propagation, establishing a foundation for both hazard mitigation and the design of industrial smouldering processes. Equally, oxygen drives the surface oxidation reactions, supplying the heat needed to offset endothermic sinks such as pre-heating, drying, pyrolysis and convective cooling [112]. Thus, defining the critical oxygen concentration and smothering limit is essential for setting ignition, propagation and extinction criteria [6,113]. Despite this importance, the detailed mechanisms controlling the minimum oxygen requirement for self-sustaining smouldering remain only partially understood.

In the literature, reports of limiting oxygen concentration (LOC) for biomass smouldering under wind-driven or quiescent conditions vary widely: from 10% [38], 13% [40], and 16% [41] for peat, 4% [6] for wood, to 13.5% [37] for cellulosic material. Because ambient diffusion could not be fully excluded, the exact oxygen flux reaching the reaction zone was uncertain. To address this, we recently developed a tubular reactor that delivers a controlled oxidiser flow—with prescribed oxygen content and flow rate through the porous bed [42]. Using high-organic peat, we found LOC below 2% and a minimum internal oxygen flux of 0.08 ± 0.01 $g/m^2 \cdot s$. However, LOC in porous fuels likely depends on intrinsic properties (density, moisture, mineral content) and environment conditions (system heat loss, ambient temperature, gravity), requiring further investigation [45,57,82].

Pine needle litter is a widespread wildland fuel in coniferous forests, forming highly porous beds that ignite with low energy input and may transition to flaming under wind, posing significant hazards [114–117]. Numerous studies have examined smouldering kinetics [118],

ignition thresholds [119], propagation dynamics [120–122], flammability [117], and smouldering-to-flame transitions [116,123] for pine needles and related litters. Nevertheless, the role of controlled oxygen supply near extinction remains poorly defined. Our prior work measured the minimum oxygen flux for smouldering propagation in pine needle beds and quantified bulk-density effects [39], but the influence of other physicochemical and environmental factors is still unknown. To date, no computational model has been established specifically to predict oxygen thresholds and smothering limits under forced internal oxidiser flow, highlighting a critical knowledge gap.

In this work, we extend our experimental findings by developing a one-dimensional smouldering model using the open-source Gpyro framework [47] coupled to a five-step kinetic scheme for pine needles [124]. We simulate forced internal oxidiser flows to determine smothering limits and to validate our previous reactor experiments and theoretical analyses. We further explore how moisture content, bulk density and ambient temperature affect smouldering dynamics and oxygen thresholds. These efforts aim to fill critical gaps in our understanding and to support the design of both fire-safe environments and efficient smouldering-based technologies.

4.2 Computational model

4.2.1 Experiment description and model establishment

Most investigations of smouldering limits have been conducted under external wind or quiescent ambient conditions, making it difficult to precisely quantify the oxygen requirement [6,38,40,41]. To overcome this, our recent experiments used an enclosed tubular reactor that delivers a controlled oxidiser flow through the porous fuel [39,42]. Because model validation relies on data from this setup, its configuration is summarised here.

The reactor (Fig. 4-1a) has an internal diameter of 12 cm which is large enough to suppress wall quenching effects [45,67]. Meanwhile, the tubular reactor was further wrapped in a 2-cm thick thermal-insulation material and an aluminium foil layer to minimise the lateral heat loss. Its total height is 30 cm, divided into three zones: a 5 cm insulation section at the top, a 15 cm combustion section in the middle, and a 10 cm gas-homogenisation section at the bottom (see Fig. 4-1a). Oxidiser flows with various flow velocities (U, mm/s) and oxygen concentrations (X_{O_2} (volume fraction) or Y_{O_2} (mass fraction), %) were fed from the bottom. Eight K-type thermocouples (1 mm bead) are spaced every 2 cm along the fuel's central axis to record

temperature.

Notably, the ignition protocol here differs from that in [39]: we employ top ignition (Fig. 4-1 (b-c)) to avoid the complex bidirectional fronts of mid-bed ignition (Fig. 4-1d), and the confined local burning seen with bottom ignition (Fig. 4-1e). To ensure a uniform and self-sustained front, a 1 cm layer of pine needles (pre-ignited with a propane flame for 1 min) was placed at the top the sample as the ignition source.

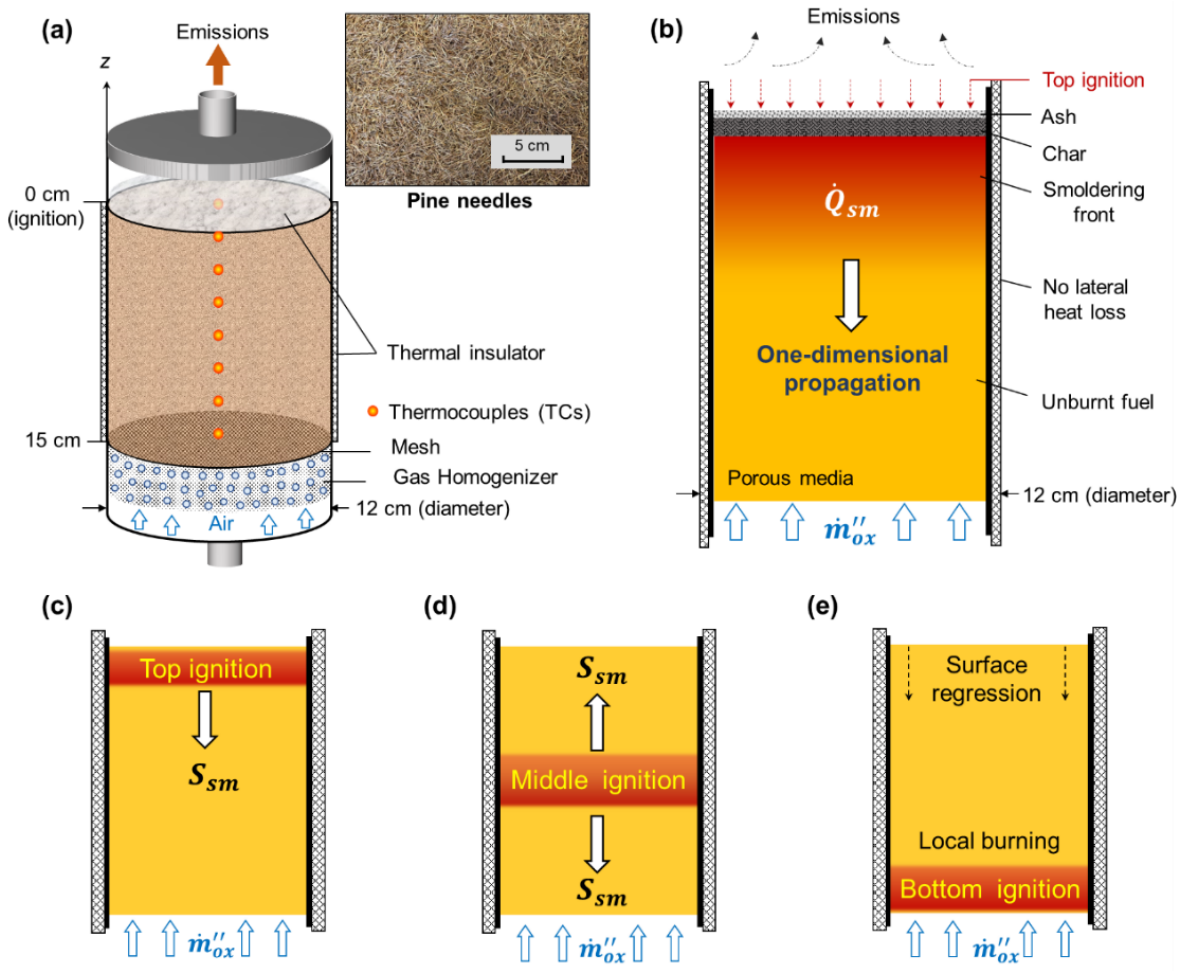

Fig. 4-1 (a) Experimental setup to explore the oxygen supply thresholds (or smothering limits) of smouldering combustion, where pine needles were selected as representative porous fuel; (b) schematic diagram of the one-dimensional smouldering model; (c-e) common ignition locations (top, middle, and bottom ignition protocol) used in the studies of in vertical smouldering propagation.

Pine needles (Fig. 4-1) from a larch forest in Saihanwula Biosphere Reserve, China, serve as the model porous medium. The native needle pack has porosity 0.90 ± 0.02 and, by

thermogravimetric analysis, > 80% organic content with ~ 15% mineral matter. Needles were oven-dried at 75 °C for ≥ 48 h to < 5% moisture, which shown to have negligible effect on propagation [69]. By compressing the fuel bed, bulk densities ranging from 50 ± 10 to 150 ± 30 kg/m^3 were achieved.

With lateral heat loss minimised and ignition applied uniformly, vertical spread is effectively one-dimensional [42]. We therefore implemented a 1-D model in Gpyro v0.7, matching the 30 cm sample depth (refer to Fig. 4-1a) [47]. Gpyro is a generalized open-source code for combustible solids and has been used to simulate the pyrolysis and smouldering of various porous media such as peat [45], wood [6], PU foam [47], and coal [125]. Simulations begin with excess oxidiser; if smouldering propagates, the flow is reduced stepwise until extinction, thus identifying the minimum oxygen flux. Subsequent runs vary X_{O_2} by adjusting the N_2/O_2 ratio to explore limiting oxygen conditions across different concentrations.

4.2.2 Governing equations

The one-dimensional model computes the transient conservation equations for both condensed and gas phases, neglecting gravity and buoyancy effects within the small porous sample [40,45]. In the condensed phase, it includes mass conservation (4.1), species conservation (4.2), and energy conservation (4.3). In the gas phase, it solves mass conservation (4.4), species conservation (4.5), and momentum conservation via Darcy's law (4.6). All variables are defined in the Nomenclature, and the full mathematical formulation is available in the Gpyro technical reference [126]. The model assumes local thermal equilibrium between gas and solid, unit Schmidt number, identical diffusion coefficients and specific heats for all gas species, and a constant gas density (ρ_g) of 1.161 kg/m^3, independent of oxygen fraction (Y_{O_2}) or gas temperature (T_g). Solid-phase shrinkage is omitted, as it has a negligible effect on the limiting oxygen supply for smouldering. More details of the mathematical form of these equations can be found in [47].

$$\frac{\partial \bar{\rho}}{\partial t} = -\dot{\omega}'''_{fg} \tag{4.1}$$

$$\frac{\partial (\bar{\rho} Y_i)}{\partial t} = \dot{\omega}'''_{fi} - \dot{\omega}'''_{di} \tag{4.2}$$

$$\frac{\partial (\bar{\rho}\bar{h})}{\partial t} + \frac{\partial (\dot{m}''\bar{h}_g)}{\partial z} = \frac{\partial}{\partial z}\left(k\frac{\partial T}{\partial z}\right) + \sum \dot{\omega}'''_{di,k}\Delta H_k \tag{4.3}$$

$$\frac{\partial(\rho_g\bar{\psi})}{\partial t}+\frac{\partial\dot{m}''}{\partial z}=\dot{\omega}_{fg}''' \tag{4.4}$$

$$\frac{\partial(\rho_g\bar{\psi}Y_j)}{\partial t}+\frac{\partial(\dot{m}''Y_j)}{\partial z}=-\frac{\partial}{\partial z}\left(\rho_g\bar{\psi}D\frac{\partial Y_j}{\partial z}\right)+(\dot{\omega}_{fj}'''-\dot{\omega}_{dj}''') \tag{4.5}$$

$$\dot{m}''=-\frac{\bar{K}}{\nu}\frac{\partial\bar{p}}{\partial z}\quad(\rho_g=\frac{P\bar{M}}{RT}) \tag{4.6}$$

4.2.3 Smouldering chemical kinetics and parameter selection

The heterogeneous chemistry of the smouldering pine needles was described by a 5-step kinetic scheme with three major components: hemicellulose, cellulose, and lignin [124]. The 5-steps included (4.7) drying [*dr*]; (4.8-4.10) pyrolysis of hemicellulose, cellulose, and lignin (the typical temperature at ~250 ^{o}C, ~300 ^{o}C, and ~350 ^{o}C, respectively) [*hp*], [*cp*], [*lp*]; (4.11) char oxidation [*co*], expressed as:

$$Water\rightarrow Water\ vapor\ [dr] \tag{4.7}$$

$$Hemicellulose\rightarrow Char+Pyrolyzates\ [hp] \tag{4.8}$$

$$Cellulose\rightarrow Char+Pyrolyzates\ [cp] \tag{4.9}$$

$$Lignin\rightarrow Char+Pyrolyzates\ [lp] \tag{4.10}$$

$$Char\ +\ O_2\rightarrow Ash+gas\ [co] \tag{4.11}$$

The normalized destruction rate of condensed-phase species *A* in reaction *k* can be expressed by Arrhenius law as

$$\dot{\omega}_k^*=Z_k\exp\left(-\frac{E_k}{RT}\right)f(m_A^*)g(Y_{O_2}) \tag{4.12}$$

where Z_k is the pre-exponential factor, and E_k is the activation energy. The function for mass action of reactant A is

$$f(m_A^*)=(m_A^*)^{n_k}=\left(\frac{m_A}{m_{sA,0}}\right)^{n_k} \tag{4.13}$$

where $m_{sA,0}$ is the original mass of the species A, and n_k is the reaction order. The oxidation model considers oxidative pyrolysis as

$$g\left(Y_{O_2}\right)=\begin{cases}1 & (n_{k,O_2}=0)\\ (1+Y_{O_2})^{n_{k,O_2}}-1 & (n_{k,O_2}\neq 0)\end{cases} \tag{4.14}$$

Physical properties of all condensed-phase species were obtained from [127] and listed in Table 4-1, where the subscript *s* and *o* represents the solid physical properties (i.e., $\psi = 0$) and bulk physical properties, respectively. Although pine-needle beds are intrinsically more heterogeneous than fine particulate fuels such as wood dust, the model treats them as uniform porous media. As a result, the effective thermal conductivity in the porous medium includes both bulk conduction and radiative transfer across pore voids:

$$k_i = k_{s,i}(1 - \psi_i) + \gamma_i \sigma T^3 \tag{4.15}$$

where γ is dependent on the pore size (d_p) as $\gamma \sim d_p = 1/S\rho$. The permeability ($K \sim {d_p}^2$) of all solid species: hemicellulose, cellulose, lignin, char, and ash, was assumed to be independent and estimated on the scale of 10^{-12}~10^{-10} [105]. The averaged properties of condensed-phase species in each cell were calculated by weighting appropriate mass or volume fractions as

$$\bar{\rho} = \sum X_i \rho_i \,, \bar{k} = \sum X_i k_i \,, \bar{c} = \sum Y_i c_i \,, X_i = \bar{\rho}\frac{Y_i}{\rho_i} \tag{4.16}$$

The kinetic and stoichiometric parameters of the 5-step reactions were also obtained from [127] and listed in Table 4-2.

Table 4-1 The physical parameters of condensed-phase species

Species (*i*)	Y_0 (-)	$\rho_{s,i}$ (kg/m^3)	$\rho_{o,i}$ (kg/m^3)	$k_{s,i}$ (W/m·K)	$c_{p,i}$ (J/kg·K)
Water	0.05	1000	1000	0.6	4186
Hemicellulose	0.2	782	150	0.2	1500
Cellulose	0.5	694	150	0.2	1500
Lignin	0.25	454	150	0.2	1500
Char	0	500	100	0.05	3000
Ash	0	150	15	0.1	3000

Table 4-2 Chemical kinetic parameters of 5-setp reaction for pine needles, where the reaction expression is $A_k + \nu_{O_2,k}\, O_2 \rightarrow \nu_{B,k}\, B_k + \nu_{g,k}$ gas, and $\Delta H_k > 0$ means endothermic.

Parameter	*dr*	*hp*	*cp*	*lp*	*co*
$lgZ_k(\mathrm{lg(s^{-1})})$	8.12	8.2	12.4	14.7	11.9
E_k (kJ/mol)	67.8	106	160	236	184
$n_k(-)$	3	1.49	0.95	8.7	1.27

$n_{k,O_2}(-)$	0.252	454	150	0.2	1500
$\nu_{B,k}$(kg/kg)	0	0.24	0.27	0.40	0.06
ΔH_k (MJ/kg)	2.26	0.2	0.5	0.5	-20
$\nu_{O_2,k}$(kg/kg)	0	0.5	0.5	0.5	1.5

The initial fuel temperature was set to 300 K. To replicate the dried pine needles from the experiments, a moisture content of 5% was assumed and the composition was specified as 0.209 *hemicellulose*, 0.529 *cellulose* and 0.262 *lignin* [127]. A convective heat-transfer coefficient of $h_c = 10\ W/m^2K$ represented cooling at both the top and bottom surfaces, and the biomass emissivity was 0.95. The gas-phase specific heat capacity (c_g) was fixed at 1100 J/kg·K for all gas species [47]. A prescribed oxidiser flow entered from the bottom of the domain. To initiate smouldering, 30 kW/m^2 of heat flux was applied at the top for 5 minutes. Propagation was deemed successful if the smouldering front moved steadily downward to the base without observable deceleration or temperature decline [67]. In cases of ignition failure, the heat flux was increased to 50 kW/m^2 for 30 minutes. Ambient pressure and temperature were 1 atm and 300 K. Grid convergence was achieved with ΔZ = 0.1 mm and Δt = 0.01 s. Further reducing the cell size and time step by a factor of two gave no significantly different results, so the calculation was sufficiently resolved.

4.3 Computational results and discussions

4.3.1 Base cases and model validation

Two representative cases: one with successful self-sustained smouldering and one with extinction were compared between experiment and simulation. In both cases, pine-needle beds were prepared at a bulk density of $\rho_o = 120 \pm 20$ kg/m^3 and MC = 5%, and oxygen mass fraction was set at Y_{O_2} = 23%. The example temperature profiles of successful and failed smouldering propagation from experimental and simulation results are compared in Fig. 4-2. Fig. 4-2a shows the experimental measurements under an internal airflow velocity of 2.6 mm/s, and the simulated temperature profile is presented in Fig. 4-2b for comparison. Despite the complexity of smouldering, the model reproduces the key features observed experimentally. The data exhibit a two-stage opposed-to-forward propagation, in agreement with previous findings [16,82]. After top ignition, a robust reaction front forms and propagates downward,

reaching the base within one hour. Thereafter, smouldering advances upward with the oxidiser stream, characteristic of char oxidation with longer residence time and higher temperature. Post-burnout residues form a fragile char-ash matrix that resists collapse, limiting surface regression compared to fuels such as peat or fine wood chips [128].

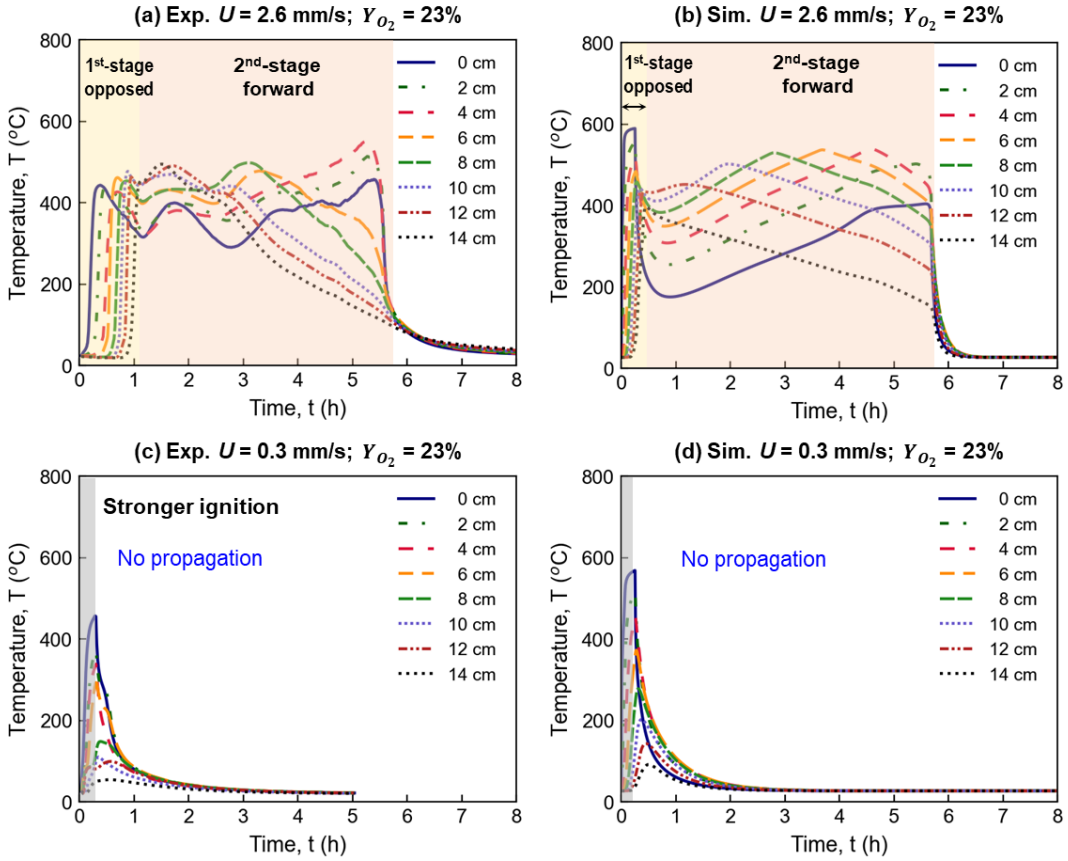

Fig. 4-2 Comparisons of temperature profiles from experimental measurement and simulations results. (a-b) successful two-stage smouldering propagation under flow velocity of 2.6 mm/s; and (c-d) failed smouldering propagation under insufficient oxygen supply of 0.3 mm/s.

When the imposed oxygen flux falls below the critical limit, neither the experiment nor the simulation yields self-sustained propagation Fig. 4-2(c-d). Under these oxygen-limited conditions, exothermic oxidation cannot sustain the endothermic drying and pyrolysis steps, so temperatures at all depths simply decay after ignition. Note that in Fig. 4.2a the “0-cm” thermocouple exhibits a delayed peak relative to Fig. 4-2b the experiment includes an additional 1 cm pre-ignited ignition layer (see Section 4.2.1). The fluctuations observed in the forward-front temperature (Fig. 4-2a) likely reflect spatial heterogeneity in fuel properties, uneven front geometry, and local collapses of char, where phenomena not captured by the model. The simulation also assumes constant fuel properties, neglects microscopic particle

structure and ash collapse [45], and cannot account for "O_2 leakage" from nonuniform packing [39]. Therefore, it is impossible to completely match the experimental and simulated results, especially the time-evolution temperature profile [45]. Nevertheless, the model successfully predicts profile shape, peak temperature, and overall spread duration.

Moreover, Fig. 4-3 presents simulated peak temperatures and smouldering durations (dashed lines) alongside experimental data (symbols). The model reproduces the experimental trends closely, confirming its validity. In particular, it captures the effect of oxidiser flow: as the airflow velocity increases, peak temperature rises and burning duration decreases, reflecting the higher reaction rates and heat release under improved oxygen supply. Conversely, lower flow rates yield extended burn times, indicating the persistence of deep underground smouldering fires that can last for weeks or months [9,16]. These near-limit smouldering dynamics merit further detailed study.

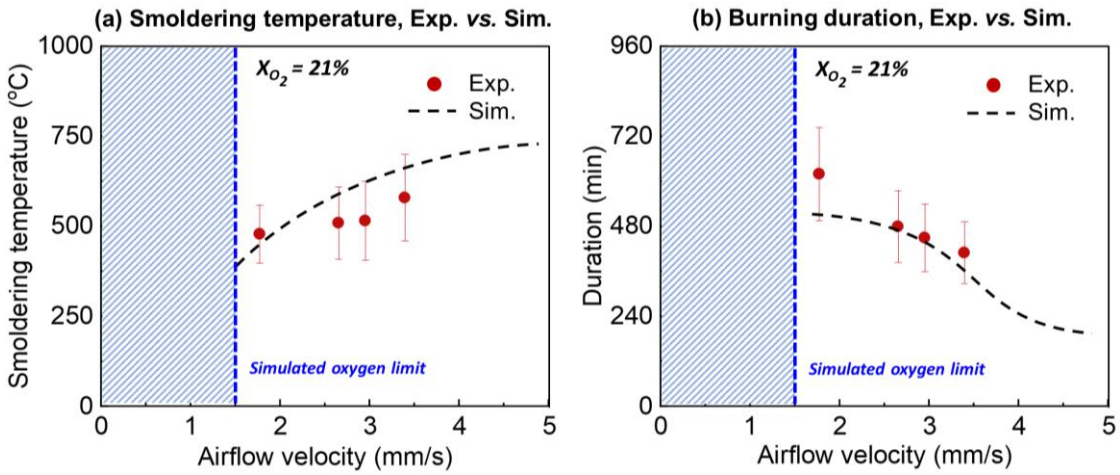

Fig. 4-3 Comparison of experimental and simulation data on (a) smouldering peak temperature and (b) burning duration. The satisfactory agreement validates the capability of computational model.

Comparisons in Fig. 4-2 and Fig. 4-3 show close alignment between experimental and simulated results in propagation mode, spread rate, peak temperature, and burn duration. This agreement confirms that our model reliably captures the oxygen-driven propagation and extinction behaviour of smouldering in porous pine-needle beds.

4.3.2 Roles of oxygen concentrations

Using the validated model and base cases, we then determined smothering limits by varying the oxygen mass fraction (Y_{O_2}) of internal oxidiser flow. Fig. 4-4a describes the simulated boundary trendlines for the smothering limits of smouldering combustion, i.e., the minimum

internal flow velocity (U_{min}) to sustain smouldering under various Y_{O_2}. A LOC of 3 % was identified: below this value, smouldering extinguishes regardless of flow rate. Afterwards, the predicted required flow velocity increased with the decreasing oxygen mass fraction, which was consistent with the trend shown in our previous experimental work on smouldering peat [42]. For example, the predicted required flow velocity increased from 1.6 mm/s to 12 mm/s, as Y_{O_2} decreased from 23% to 5%.

Based on previous work [42,57], at the extinction limit, the heat generated from the net heterogeneous smouldering reactions ($\dot{q}''_{sm}$) should just balance the heat loss from water evaporation ($\dot{q}''_{MC}$), internal flow convection ($\dot{q}''_{conv,in}$), and environmental heat losses ($\dot{q}''_{e}$) as

$$\dot{q}''_{sm,min} = \dot{q}''_{MC} + \dot{q}''_{conv,in} + \dot{q}''_{e} \tag{4.17}$$

By further organizing Eq. 4.17, we obtain

$$\dot{q}''_{sm,min} = S_{sm}\rho_w \Delta H_{ev} MC + \rho_g c_{p,g} U(T_{sm} - T_\infty) + (h_r + h_c)(T_{sm} - T_\infty) \tag{4.18}$$

where S_{sm} and T_{sm} refers to smouldering propagation rate and temperature. For simplicity, the radiative heat loss is linearized by using the radiation heat transfer coefficient (h_r) [83]. On the other hand, the minimum oxidation heat generated can be described as

$$\dot{q}''_{sm,min} = \dot{q}''_{ox} = \dot{m}''_{O_2,min} \Delta H_{ox} = \rho_g (U Y_{O_2})_{min} \Delta H_{ox} \tag{4.19}$$

where ρ_g is the density of oxidiser flow, and ΔH_{ox} is the heat of smouldering oxidation. Therefore, the minimum oxidiser flow velocity and can be derived as

$$U_{min} = \frac{S_{sm}\rho_w \Delta H_{ev} MC + (h_r + h_c)(T_{sm} - T_\infty)}{\rho_g Y_{O_2} \Delta H_{ox} - \rho_g c_{p,g}(T_{sm} - T_\infty)} \propto \frac{1}{Y_{O_2} - C} \quad (Y_{O_2} > 3\%) \tag{4.20}$$

where for a specific fuel with a particular MC and density, S_{sm} and T_{sm} can be regarded as constants at the limiting condition of smouldering propagation [45]. $C = \frac{c_{p,g}(T_{sm} - T_\infty)}{\Delta H_{ox}}$ is a constant relying on smouldering and ambient temperatures. Therefore, the minimum gas flow velocity is inversely proportional to the oxygen concentration ($U_{min} \propto \frac{1}{Y_{O_2} - C}$) in Eq. (4.20), and the overall trend of simulated results in Fig. 4-4a is successfully explained. Furthermore, the predicted oxygen supply rate was further calculated as $\dot{m}''_{O_2} = \rho_g Y_{O_2} U$, and the results are shown in Fig. 4-4b. It is found that $\dot{m}''_{O_2}$ increased from 0.45 g/m^2·s to 0.8 g/m^2·s when Y_{O_2} decreased from 23% to 4%. This trend also agreed well with the trend found in our previous experiments [42].

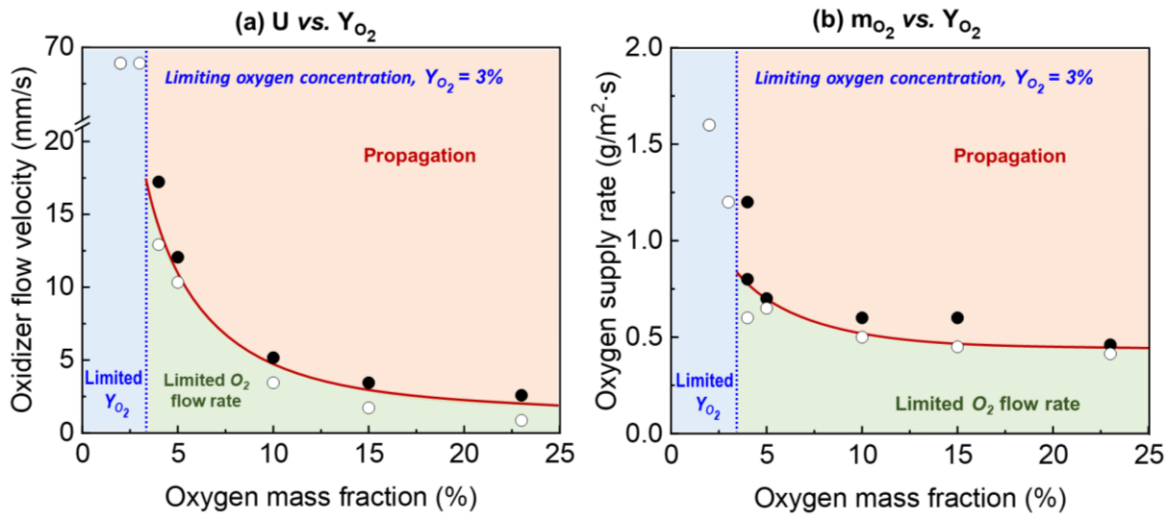

Fig. 4-4 Simulation results and boundary trendlines of (a) minimum internal flow velocity (U) *vs.* oxygen mass fraction (Y_{O_2}); (b) minimum oxygen supply rate (m_{O_2}) *vs.* oxygen mass fraction (Y_{O_2}).

4.3.3 Fuel density, Moisture and ambient temperature

Fuel dry bulk density (ρ_{dry}) and moisture content (MC) vary widely in applied smouldering systems and wildfire settings, and both parameters strongly affect smouldering propagation and extinction [128]. To assess the sensitivity of smothering limits to moisture, we varied MC from 5% to 120% on a dry basis while maintaining dry bulk density according to $\rho_{dry} = \rho_{wet}/(1 + \mathrm{MC})$ to account for volumetric expansion upon water uptake [128].

Simulation results demonstrate that the critical airflow velocity depends markedly on both fuel dry bulk density (Fig. 4-5a) and MC (Fig. 4-5b). In particular, increasing fuel dry bulk density reduces the minimum velocity required to sustain smouldering propagation, in agreement with earlier experiments (Fig. 4-5a) [39]. For example, when MC is 50%, as the fuel dry bulk density increases from 50 kg/m^3 to 300 kg/m^3, the airflow velocity required for sustaining smouldering was predicted to decrease from about 7 mm/s to 3 mm/s. This effect arises because higher density increases the effective thermal conductivity of the bed [83], thereby improving heat transfer from the reaction zone to unburnt fuel and reducing the oxygen flux needed for continuous smouldering [39].

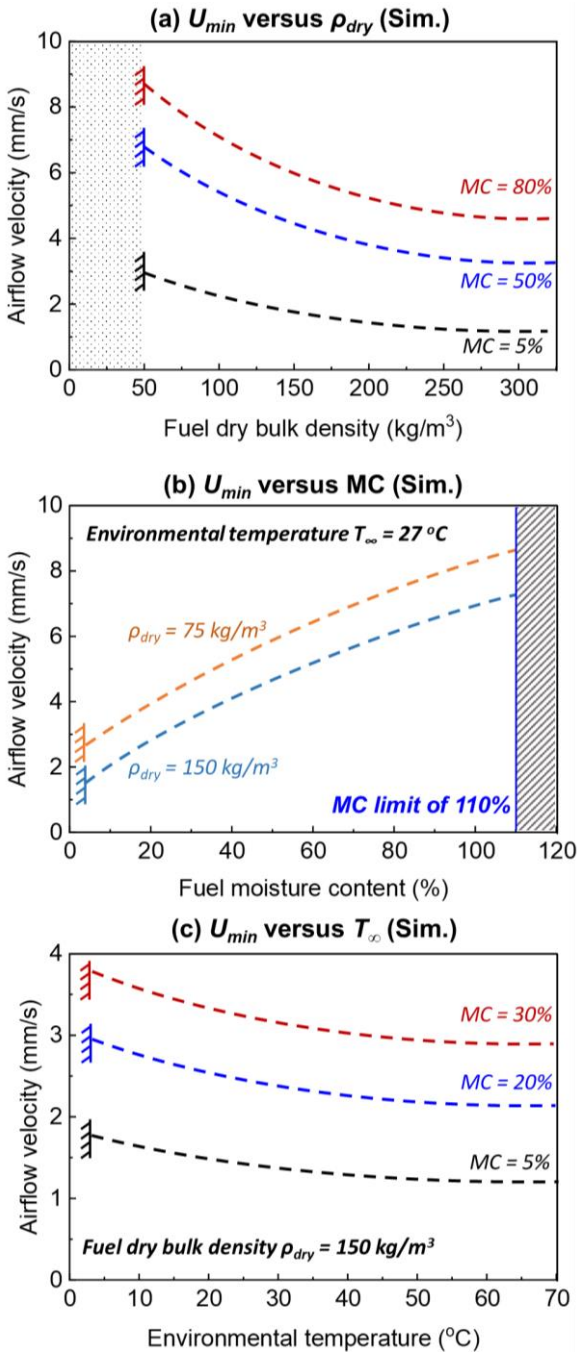

Fig. 4-5 Simulation results of the role of (a) fuel dry bulk density, (b) moisture content, and (c) ambient temperature on oxygen threshold of smouldering combustion.

Conversely, increasing moisture content raises the minimum flow velocity required for sustained smouldering (Fig. 4-5b). For example, when MC increased from 5% to 50%, the required U_{min} for high-density pine needles (ρ_{dry} = 150 kg/m^3) climbs from approximately 2 mm/s to about 5 mm/s. This trend follows Eq. 4.20, where U_{min} increases as $\dot{q}''_{MC}$ increases. In other words, it demands greater oxidiser velocities to supply sufficient exothermic heat release.

The model also predicts a maximum MC of about 110%, above which smouldering cannot be maintained regardless of flow rate.

In real fire scenarios, the ambient temperature can be much higher which may lead to a different oxygen threshold. Therefore, the effect of ambient temperature (T_∞) was also investigated and summarised in Fig. 4-5c. In order to focus on the T_∞, the process of water freezing caused by sub-zero temperature was out of the scope of this study. As a result, the temperature range under investigation was limited to 0-70 ^{o}C. Predicted results showed that the required airflow velocity decreases as T_∞ increases. For example, given a fixed fuel moisture content of 5%, as the ambient temperature increases from 10 ^{o}C to 70 ^{o}C, the predicted required airflow velocity decreases from about 1.7 mm/s to about 1.4 mm/s. This could be also explained by Eq. 4.17-4.18, which show that higher T_∞ lowers environmental heat losses and therefore decreases the oxygen flux needed for self-sustaining smouldering.

4.3.4 Smouldering temperature (T_{sm}) and propagation rate (S_{sm})

Smouldering temperature (T_{sm}) and propagation rate (S_{sm}) are two key parameters that describe the smouldering behaviours and reflect the intensities of reactions and the rates of fuel consumption. Therefore, Fig. 4-6 and Fig. 4-7 further compare the effects of moisture content and bulk density on the T_{sm} and S_{sm}, and each curve was controlled to have the same airflow mass supply rate (i.e., $\dot{m}''_{O_2}$). First of all, at the smothering limit, the minimum smouldering temperature and propagation rate were predicted to be around 300 ^{o}C and 0.5 cm/h, and the predicted T_{sm} and S_{sm} both increase as $\dot{m}''_{O_2}$ increases, agreeing well with the literature [29,32,129]. By considering a 1-step global smouldering reaction, the smouldering burning flux can be described as

$$\dot{m}''_F = \rho S_{sm} = \frac{\dot{m}''_{O_2}}{\nu} \propto T_{sm} \tag{4.21}$$

where ν is the stoichiometric factor. By further reorganizing Eq. 4.21, we obtain

$$S_{sm} = \frac{\dot{m}''_F}{\rho} = \frac{\dot{m}''_{O_2}}{\nu\rho} \tag{4.22}$$

Therefore, as the $\dot{m}''_{O_2}$ increases, the reaction rate of smouldering combustion increases, leading to a higher smouldering temperature and spread rate.

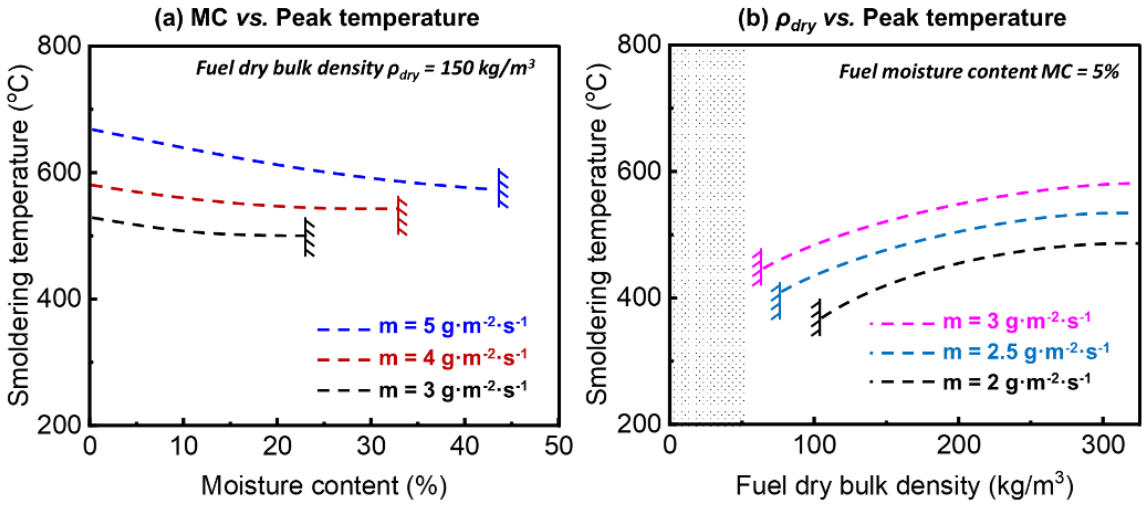

Fig. 4-6 The (peak) smouldering temperature (T_{sm}) as a function of (a) fuel moisture content and (b) fuel dry bulk density. All curves are trend lines with fixed oxygen supply of simulated results.

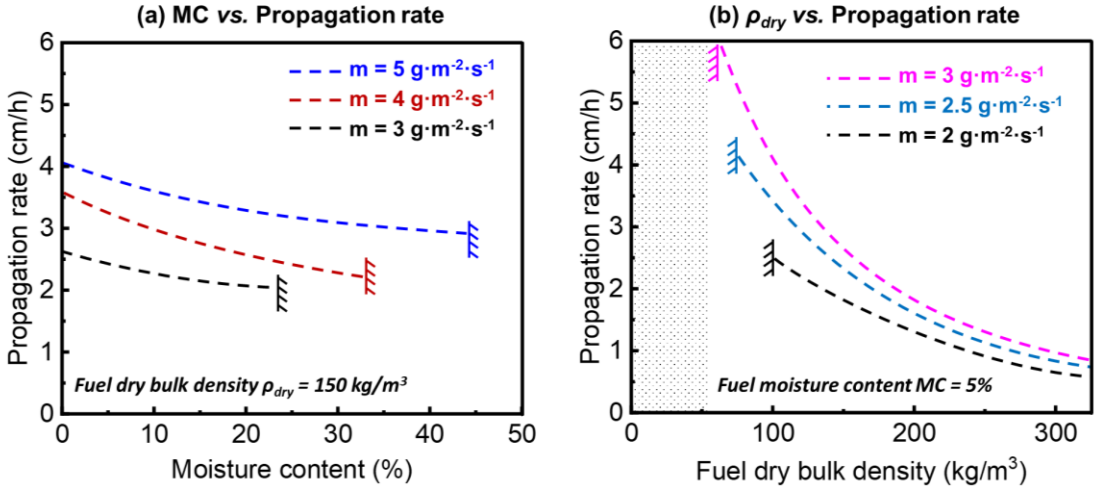

Fig. 4-7 The smouldering propagation rate (S_{sm}) as a function of (a) fuel moisture content and (b) fuel dry bulk density. All curves are trend lines with fixed oxygen supply of simulated results.

Fig. 4-6 illustrates that peak smouldering temperatures decline as (a) moisture content increases or (b) dry bulk density decreases in pine-needle beds, while Fig. 4-7 shows that propagation rates slow with higher moisture and lower bulk density. Increased moisture demands additional latent heat for drying, reducing both reaction-zone temperature and spread speed. Conversely, from Eq. 4.15, a higher solid density reduces the porosity factor γ and the intrinsic conductivity k_i. This leads to a higher smouldering temperature but a lower

propagation rate as the heat is easier to accumulate and more difficult to dissipate within the fuel due to a lower thermal conductivity [39], consistent with the trend shown in Fig. 4-6 and Fig. 4-7. Notably, smouldering temperature is more sensitive to oxygen flux than to moisture or density variations [128]. For example, when the air flow rate was stabilized at 3 g/m^2·s, as the moisture content was reduced from 20% to 5%, the smouldering temperature was only decreased by 20 ^{o}C. However, if the air flow rate was increased from 3 g/m^2-s to 5 g/m^2·s, the smouldering peak temperature was significantly increased by 100 ^{o}C. Further fundamental studies are required to elucidate the detailed mechanisms governing these behaviours.

4.4 Conclusions

In this chapter, we used a one-dimensional Gpyro model coupling heat–mass transfer with a five-step heterogeneous kinetic scheme to quantify smothering limits in pine-needle beds under forced internal oxidiser flow. Validation against controlled experiments confirmed the model's accuracy. We found that the minimum oxidiser velocity (or mass flux) needed for self-sustained smouldering rises as oxygen concentration falls, with a limiting oxygen concentration of approximately 3%, in agreement with both experiments and theoretical analysis.

Parametric studies revealed that this threshold velocity increases as fuel density or ambient temperature decreases and also increases with moisture content, which predicts a maximum tolerable MC of ~110 %. Moreover, peak smouldering temperatures drop, and propagation rates slow with increasing MC or decreasing bulk density, consistent with theoretical predictions. At the smothering limit, the model predicts a minimum reaction-zone temperature near 300 °C and a propagation speed of ~0.5 cm/h. These findings advance our understanding of smouldering resilience and offer guidance for both fire hazard assessment and the design of controlled smouldering applications.

Acknowledgments

This research is funded by the National Natural Science Foundation of China (No. 52322610), and RGC Hong Kong GRF Scheme (No. 15221523).

Chapter 5 Laboratory Large-scale Demonstrations: Persistent Smouldering Fires under In-depth Natural Diffusion

Summary

This chapter presents large-scale laboratory experiments demonstrating that smouldering fires can persist in deep peat layers for over ten days, regardless of ignition depth. As the ignition point moves deeper, four distinct propagation regimes appear: (I) downward-only spread, (II) bidirectional (downward + upward) spread, (III) in-depth lateral propagation, and (IV) localized burn. Modes III and IV produce neither visible smoke nor surface collapse, underscoring the challenge of detecting subsurface peat fires. For initial ignition depths shallower than -40 cm, peak reaction-zone temperatures decrease with increasing depth. However, for ignitions deeper than -40 cm, temperatures remain stable near 300 °C, highlighting oxygen transport as the dominant control. Despite the persistent combustion, total mass loss remains low due to incomplete oxidation at moderate temperatures. Near-surface CO levels range from 10 to 100 ppm, indicating that CO monitoring could be used for pilot detection of underground fire intensity.

This chapter is based on "Y. Qin, D. Musa, S. Lin* and X. Huang* (2022). Deep Peat Fire Persistently Smouldering for Weeks: A Laboratory Demonstration. ***International Journal of Wildland Fire***, 32, 86-98."

5.1 Introduction

Peat is a carbon-rich soil formed under anaerobic conditions through the accumulation of partially decomposed vegetation [11,130]. Peatlands serve as vital terrestrial carbon reservoirs, containing roughly one-third of global soil carbon (500–600 Gt C)—a stock comparable to all surface vegetation and approaching the size of the atmospheric carbon pool (~850 Gt C) [131,132]. As a naturally porous, char-forming material, peat readily undergoes smouldering: a slow, low-temperature, flameless combustion that can persist for extended periods [9,133] (Fig. 5-1 (a-b)). Climate change and human activities have heightened peatland fire susceptibility [134,135], and over recent decades, recurring peat fires have inflicted severe ecological and climatic damage alongside substantial economic losses [131,135,136]. For example, 2019 slash-and-burn fires in Southeast Asia triggered months-long peatland conflagrations, producing transboundary haze and serious health impacts [137,138].

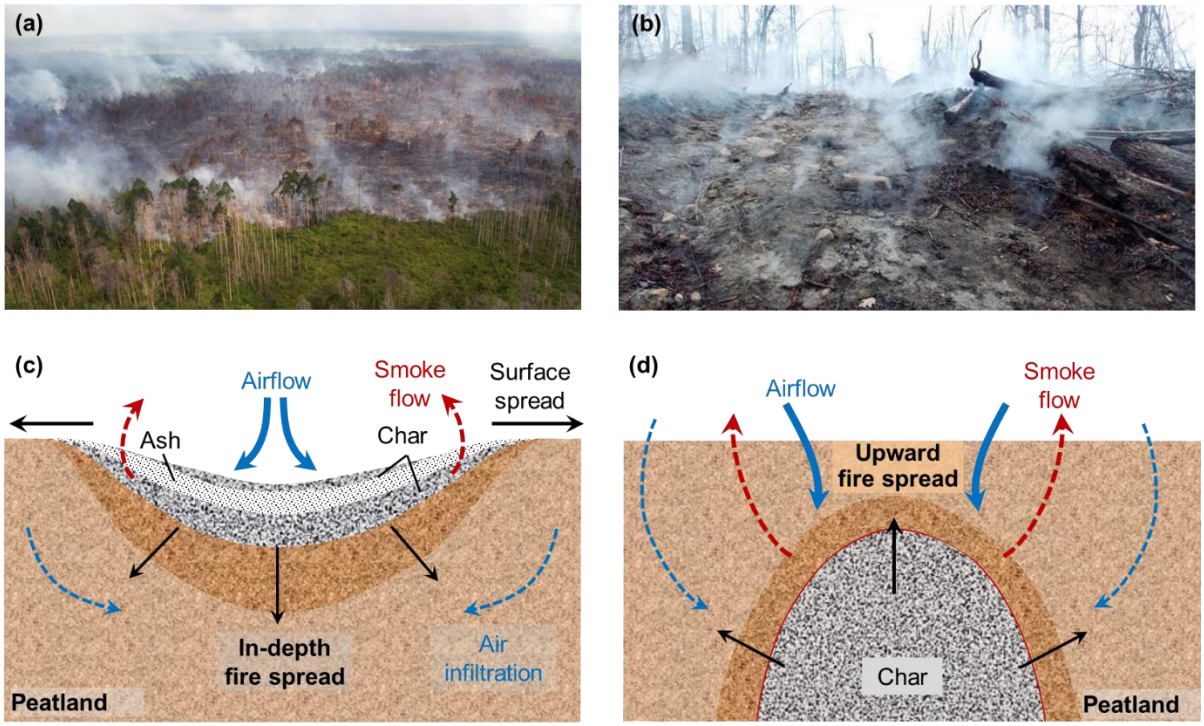

Fig. 5-1 (a) Smouldering peat fires from aerial view (courtesy: Reuters 2017) and (b) deep peat fire in the field (courtesy: WV News 2016), (c) lateral and downward peat fire spread after ignition on top surface, and (d) upward spread of deep-layer peat fires [82,128].

Although high moisture content normally inhibits peat ignition, drought (whether climatically driven or anthropogenic) increases fire risk [139]. Ignition sources range from natural causes such as lightning strikes (e.g., lightning [101,140], flaming wildfire [62], self-

heating ignition [141] and volcanic eruption [142]) or anthropogenic reasons (e.g., deforestation [143], poor land management [144], accidental ignition and arson [145]). Smouldering ignition needs less energy than flaming and can spread under wetter, low-oxygen conditions [40,62], propagating both vertically and horizontally to enlarge burn areas (Fig. 5-1c) [82]. These fires may smoulder for months or even years despite rain, weather changes or firefighting, making them among the Earth's longest-lasting fires [9].

Even when surface smouldering is controlled by rain or fire suppression, hidden subsurface hotspots can persist at low temperatures and spread slowly, making it difficult for detection by patrols and satellites [1,9]. With the return of dry, hot weather, these deep fires can migrate upward and reignite surface flames (Fig. 5-1d) [14,82]. Such "holdover" behaviour has been documented in peatlands across Southern Africa, Southeast Asia and the Arctic [9,13,146], yet the mechanisms and limiting conditions of deep-layer peat fires remain poorly understood.

Research to date has explored peat smouldering chemistry kinetics [147], ignition dynamics [62,141,148,149], fire spread [81,82,128,150,151], extinction [68,152,153] and fire emissions [80,154,155]. Small-scale laboratory trials show downward spread to ~30 cm depth [128,156], and airborne LiDAR has recorded real-world peat smoulder penetration of 50 cm over extended periods [132,157].

In our earlier pilot experiments, we demonstrated that coil-heated peat fires ignited at depths up to 15 cm can propagate upward to the surface [82]. However, both laboratory and field studies have been limited to depths ≤ 30 cm; large-scale experiments probing deeper soil layers are still needed. This study presents a series of metre-tall peat-column experiments to characterize underground peat fire behaviour. We quantify temperature profiles, spread dynamics, persistence and CO emissions over burn durations exceeding ten days. These findings provide insights on the mechanisms driving in-depth peat smoulder fires and lay groundwork for future larger-scale field investigations.

5.2 Experimental methods

5.2.1 Peat sample

Commercially sourced Estonian moss peat was chosen for its ~97 % organic content, uniform density, and consistent particle size, ensuring the experimental reproducibility [62,68,71,79,158]. Elemental analysis shows that its mass fraction of C/H/O/N/S is

45.6/6.0/48.0/0.5/0.3%, respectively. Samples were oven-dried at 75 °C for 48 h (Huang and Rein, 2017) and then equilibrated in ambient air to an equilibrium moisture content of ~10%. This dry peat was used for tests. The measured bulk density (ρ_p, kg m^{-3}) of dry peat was 128 ± 10 kg/m^3, and its porosity (Φ_p) was 0.90 ± 0.01.

To study the effects of moisture content, dried peat was blended with water to achieve the desired MC, packed into sealed containers, and allowed to homogenize for at least 48 h, during which natural volumetric expansion occurred [62,128]. Thermogravimetric analysis was performed on a PerkinElmer STA 6000 under both air and N_2 atmospheres; representative TGA curves are provided in Appendix 3. The full suite of chemical properties for the peat samples is summarised in Table 5-1.

Table 5-1 Properties of dried peat used in the experiments.

Bulk density (kg/m^3)	**Dried moisture (%)**	**Volatile content (%)**	**Ash content (%)**	**Fixed carbon (%)**	**Heat of combustion (MJ/kg)**	**C (%)**	**H (%)**	**O (%)**	**C/O (-)**	**H/O (-)**
127.8±10	<10	72.0	3.5	24.5	13.1	46.1	5.8	47.5	0.97	0.12

5.2.2 Experimental setup and procedure

Fig. 5-2 illustrates the 1 m-tall peat-column apparatus. The reactor walls are fabricated from 1 cm-thick ceramic fibreboard for its low thermal conductivity and non-flammability [33], and clad in two layers of aluminium foil to suppress radiative heat loss [83]. Similar setups of smaller sizes had been widely used for past lab-scale peat fire experiments [81,82,128,156,158–160]. The internal cross-section measures 24 cm × 24 cm to minimise cold-wall quenching effects [67]. However, the use of ceramic fibreboard makes it impossible for the infrared camera to capture the evolution and propagation of the smouldering front from the side view.

An array of K-type thermocouples (1.5 mm bead diameter) is inserted through the sidewall at 6 cm vertical intervals, under the assumption of predominantly one-dimensional front propagation, to monitor temperature and track the smouldering front. A 20 cm electrical coil heater, powered at 200 W for 60 minutes, serves as the ignition source; this protocol reliably establishes a uniform front in peat up to 150% moisture content [128]. Ignition depths vary from the surface (0 cm) down to -100 cm in 20 cm steps, allowing the front to initiate at different soil layers. A Testo 340 real-time sensor positioned 5 cm above the free surface

records CO emissions. Temperature and gas-phase data are logged every minute for up to 12 hours, until the column cools to ambient temperature. Each scenario is replicated at least twice, with three to four repeats when multiple propagation modes appear, ensuring the reproducibility owing to the peat's uniform commercial specifications [68].

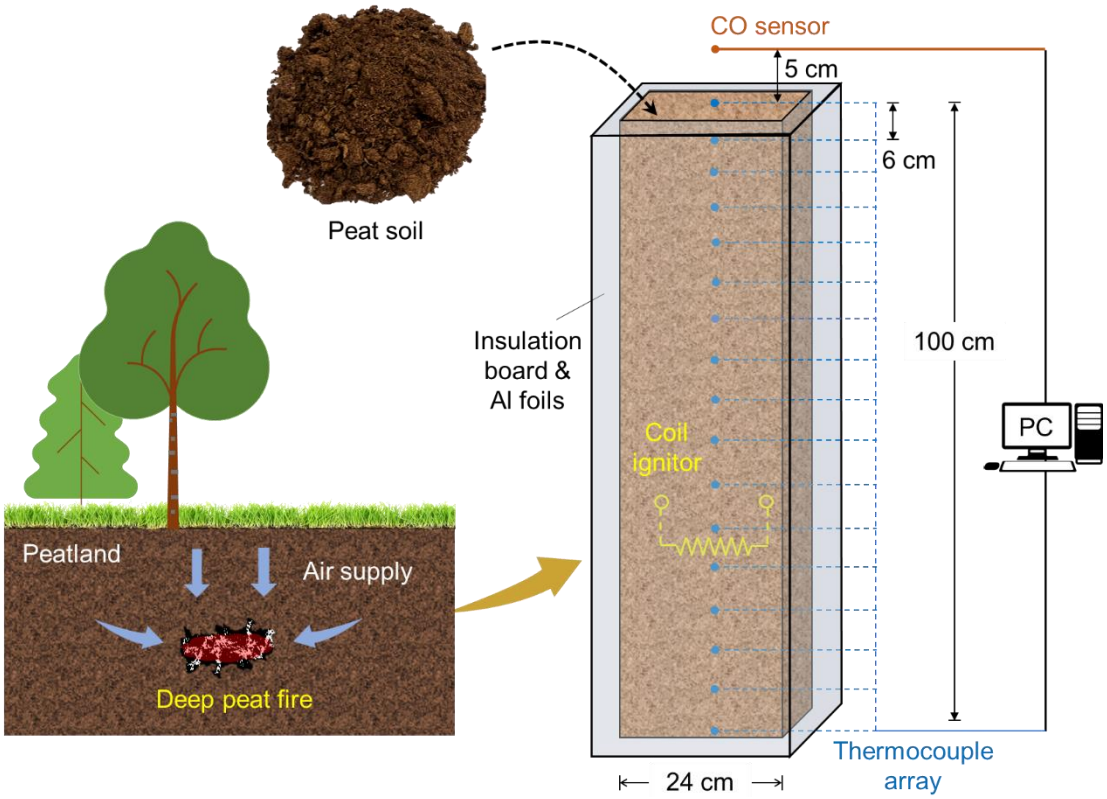

Fig. 5-2 Experimental setup for in-depth smouldering peat fire.

In our experiments, oxygen was supplied primarily through the open top surface of the peat column. Minor gas leakage around the thermocouple ports likely introduced a low level of lateral oxidiser ingress. In natural peat fires, oxygen likewise diffuses into the smouldering zone from the sides, as shown in Fig. 5-1 (c-d). These small lateral flows may therefore improve the laboratory setup's fidelity to field conditions.

5.3 Experimental phenomena and results

Surface and subsurface smouldering in peatlands has long been observed yet remains poorly characterized due to the inherent difficulty of direct observation. In this section, we compare the persistence and spread of smouldering peat fires (initial moisture content 10%) ignited at different depths. Representative temperature-time evolutions for each ignition depth are provided in the supplementary videos.

5.3.1 Base case of surface ignition

Fig. 5-3a presents thermocouple data for the base case, in which smouldering was initiated at the surface (z = 0) of an air-dried peat column (MC = 10%). After 60 min of coil heating, the surface temperature exceeded 500 °C, confirming the establishment of a robust smouldering front. The reaction then propagated downward, where a layer of black char and white ash layer was formed on the free surface due to environmental heat losses. Such phenomenon was also observed in other experiments and real scenarios [71,128]. As this insulating layer accumulated, oxygen transport to the deeper front became increasingly restricted, causing the reaction-zone temperature to fall from approximately 550 °C near the surface to about 350 °C at depth (see more discussion in Section 5.3.2).

After about 4 days, peak front temperatures had declined to roughly 300 °C which was insufficient to fully oxidise the char (see TGA in Appendix 3), and substantial char and unburnt peat remained. At this point the smouldering front stabilized at about -35 cm below the original surface, with no further surface regression.

Fig. 5-3b further plots the temperature profiles recorded at 24 h intervals, with the dashed black line marking the regressed surface position. As expected, after the ignition, a strong smouldering front gradually propagated downward with a regressing top surface. The hottest zone is not on the top surface but consistently below the top free surface. It was because the accumulating layers of unburnt char and ash on the top reduced the environmental cooling. Following the initial continuous front, the smouldering zone bifurcates into two distinct reaction fronts at separate depths.

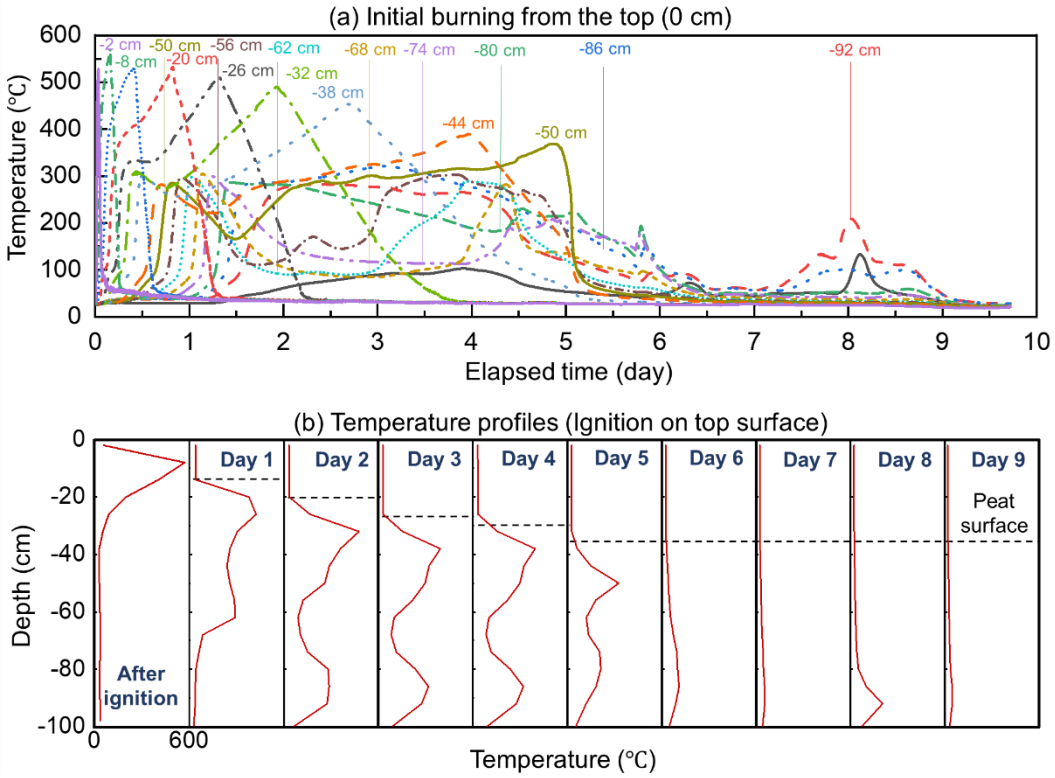

Fig. 5-3 Base case with peat fire ignited on top free surface, (a) thermocouples data and (b) evolution of temperature profile, where the negative sign means the distance below the initial free surface (z = 0).

The primary reason for the separated multi-depth burning was that the downward fire propagation was localised. In other words, the cross-section area of 24 cm × 24 cm was not entirely ignited because it was much larger than the size of the smouldering front (5~10 cm) [81]. By contrast, smaller 10 cm × 10 cm columns exhibited uniform front propagation across the cross section [71,128]. In natural peatlands, similar lateral oxygen supply likely generates multiple fronts, accelerating fire spread and complicating detection. In other words, extinguishing surface smouldering does not eliminate deeper burning.

Moreover, from Fig. 5-3b shows that the first front reached the column base by day 2, then persisted as a low-temperature, localized burn under limited oxygen. A secondary front formed thereafter, descending for an additional four days. The elevated peak temperature on day 8 reflects thermocouple placement outside the reaction zone on days 6–7 rather than increased combustion intensity. The overall smouldering persisted for more than ten days, with only 25 percent mass loss measured, which is the evidence of incomplete combustion due to oxygen restriction and moderate temperatures.

Afterwards, to simulate the in-depth burning and re-emerging behaviour of peat fires, we

initiate smouldering fires at different depths of the peat column (starting from -20 cm) to observe the smouldering burning and fire propagation behaviours.

5.3.2 Shallow peat fire propagation (upward-and-downward)

Fig. 5-4 (a-b) shows the temperature evolution for the case ignited at -20 cm depth. Following coil heating at z = -20 cm, the smouldering front propagated downwardly (also see Video S1). During this process, no smoke or volume change could be observed visually until the expanding smouldering front approached the peat surface. Roughly 12 hours after ignition, the front reached the surface, producing heavy smoke and elevated temperatures. A black char spot then formed and rapidly spread laterally across the surface under abundant ambient oxygen. These holdover, hibernation, and re-emergence stages reproduce the dynamics observed in our earlier pilot tests [82] and in field peatlands across Southern Africa, Southeast Asia and the Arctic [9,13,146]. Unlike mixed fuels on natural surfaces, pure peat did not transition to flaming [62]. Although in real fire scenarios, other surface fuels (e.g., leaves and branches) on the peatlands may be ignited or even trigger a flame. This process requires future investigations.

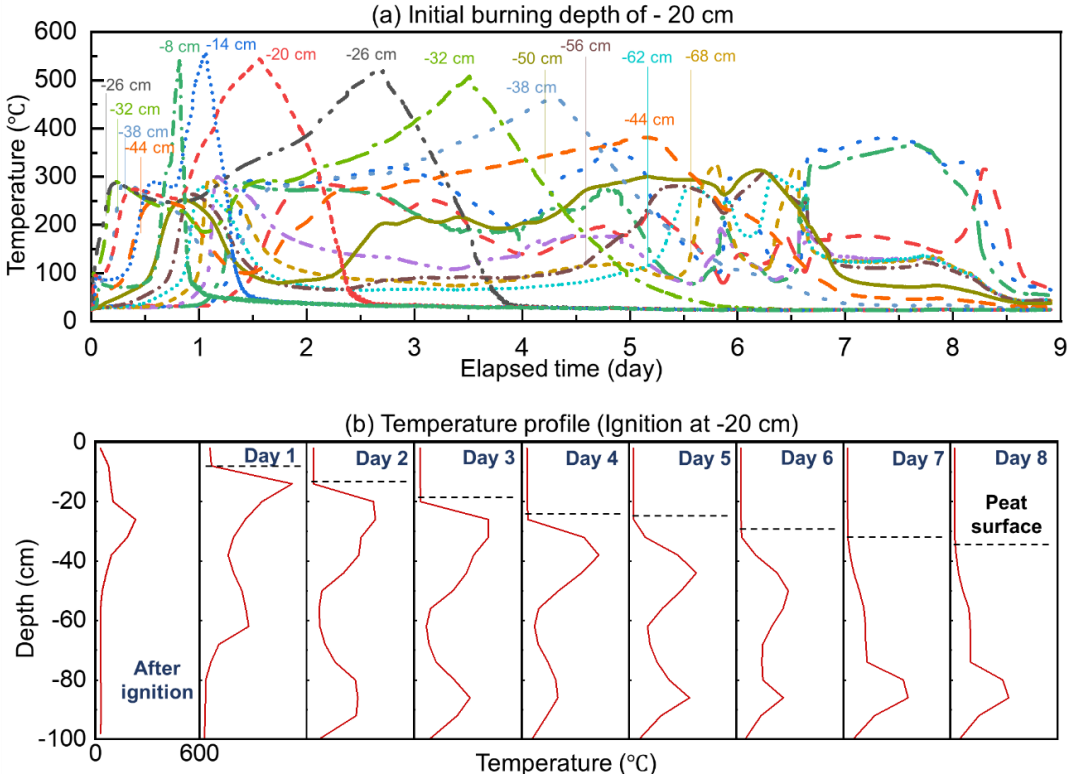

Fig. 5-4 Thermocouple measurement of smouldering peat fire ignited at the depth of -20 cm. The negative sign means the distance below the initial free surface (z = 0).

After surfacing, smouldering resumed downward propagation in a manner analogous to the surface-ignited case (Fig. 5-3), including the development of two distinct reaction fronts and roughly 35 cm of surface regression over nine days. The peak temperatures on Days 7 and 8 exceeded those on Day 6, reflecting localized deep layer burning under limited oxygen. Although the primary front appeared stationary at −80 cm for six days, lateral spread within the cross-section likely occurred, requiring further investigation.

5.3.3 Deep fire downward propagation

Ignition at depths of -40 cm and -60 cm below the surface produced a different burning phenomenon, as shown in Fig. 5-5. In both cases, the smouldering front persisted only within the deep peat layer; temperatures recorded above the ignition zone never exceeded 100 °C, and the overlying peat remained uncharred. These observations confirm that no upward propagation occurred.

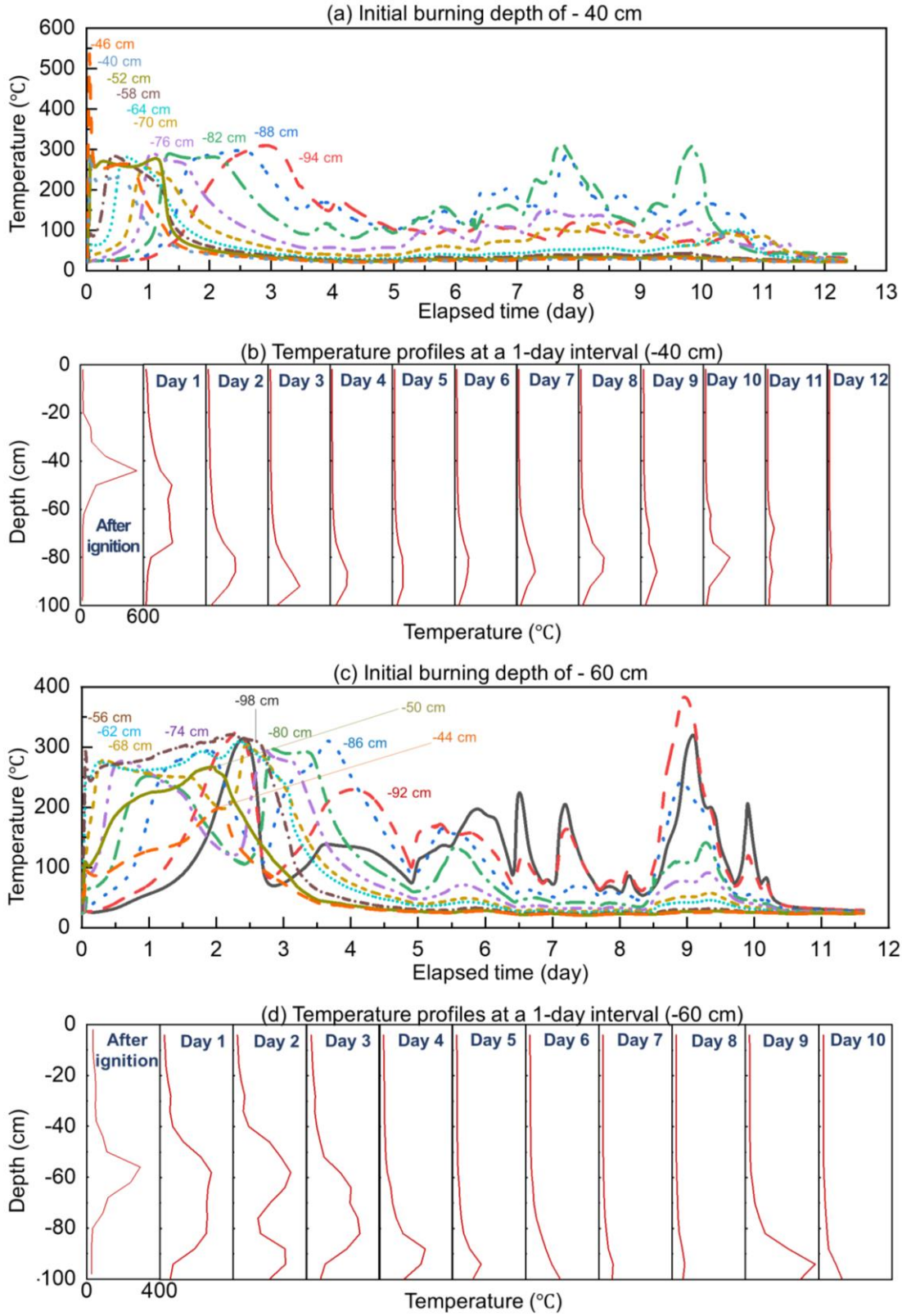

Fig. 5-5 Thermocouple data and temperature profile of smouldering peat fire ignited at depths of (a-b) -40 cm and (c-d) -60 cm, where the negative sign means the distance below the initial free surface (z = 0).

The peak temperatures below the ignition location barely reached 300 ºC, because the thermocouples were not in contact with the local burning fronts. Nevertheless, we can see the overall fire propagation was downward, and there must be multiple localised fire propagation in different directions. Due to the low smouldering temperature, even after burning for 10 days, the total mass loss was less than 10%. These local fire fronts were not stable that were easily extinguished under the limited oxygen supply. Therefore, even after burning for 10 days, the total mass loss was less than 10%. The residual in the deep layer also included some uncharred fresh peat soil. Therefore, the burning of deep peat fire was incomplete, which is another reason for forming multiple burning fronts in deep layers. These deep local fire fronts were unstable under limited oxygen supply, so they may not always be self-sustained. Moreover, during the entire burning process of 10 days, No visible smoke, surface collapse or regression occurred throughout the burn, highlighting the difficulty of detecting in-depth peat fires. A further three-day observation post-cooling revealed no re-ignition.

5.3.4 No fire propagation (local partial burning)

In tests with ignition depths of -80 cm and -100 cm (Fig. 5-6), different behaviours were observed. After 60 minutes of coil heating, temperatures in the ignition zone rose above 400 °C, confirming robust smouldering reaction front. Once heating ceased, temperatures settled around 300 °C, which is close to the peat's minimum smouldering threshold [62]. However, the fire was successfully initiated because there was some clear temperature increase from time to time.

During the first two to three days, the active combustion zone expanded only marginally, with no clear upward or downward migration of the front. Afterwards, the burning was only sustained in these small regions, and a clear fluctuation of temperature was also observed over the next several days because of the limited and uneven oxygen supply. By day 10, all probes fell to ambient temperature and no surface regression was detected. Post-test inspection revealed that peat above the ignition depth remained essentially unaltered, while at and below the ignition plane the soil was heavily charred but showed little white ash formation, indicating incomplete oxidation under severe oxygen restriction.

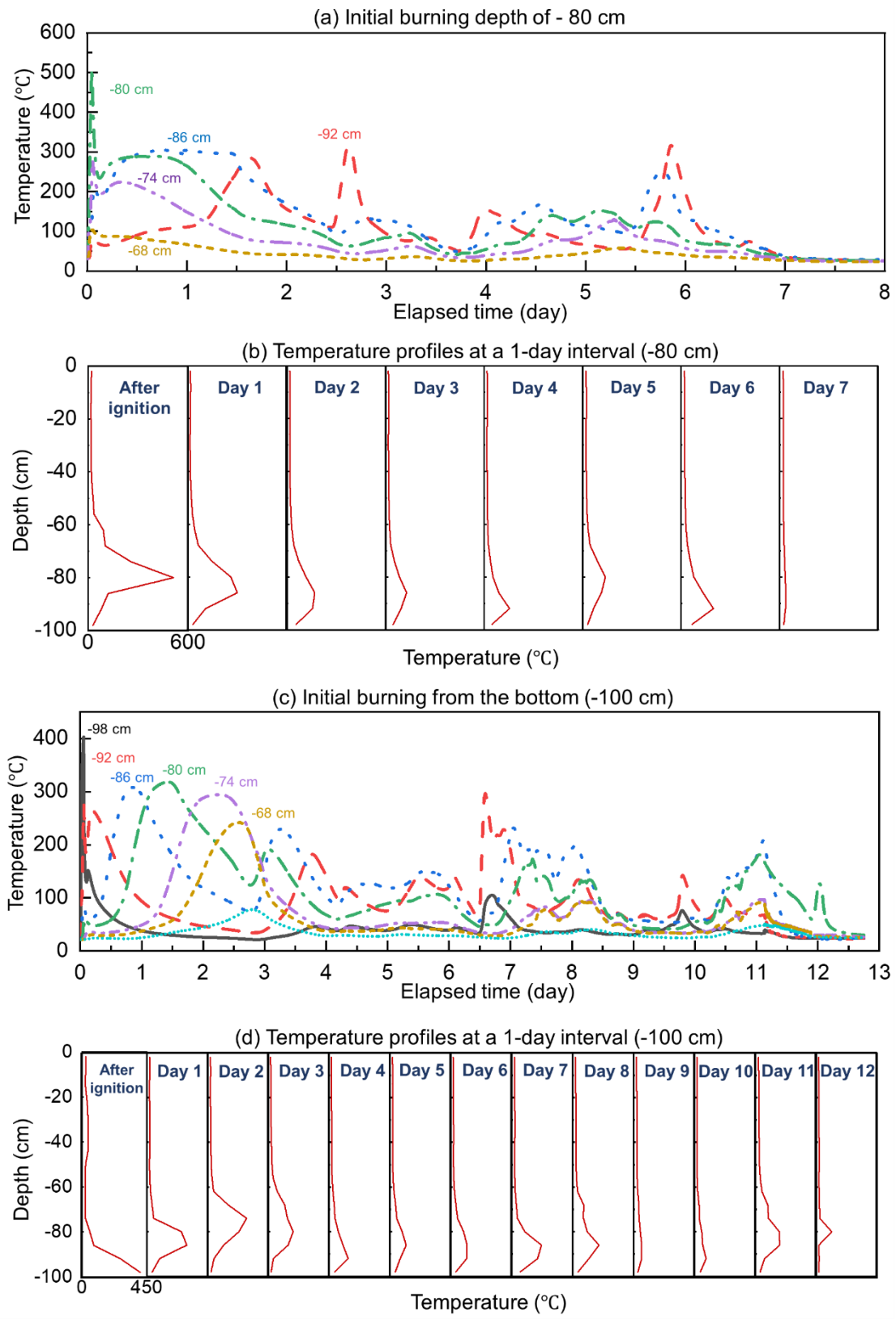

Fig. 5-6 Thermocouple measurement of smouldering peat fire ignited at the depth of (a-b) -80 cm, (c-d) -100 cm. The negative sign means the distance below the initial free surface (z = 0).

The overall burning was so weak that it was both a long-term burning process and a

prolonged extinction process. It is worth noting that the moisture redistribution likely played a role: water evaporated from the deep-layer burn zone may have migrated upward and condensed in cooler peat, raising moisture content in the overlying layer and inhibiting further spread. Future field experiments should investigate how such moisture dynamics contribute to self-suppression of deep smouldering fires.

5.4 Analysis and Discussion

5.4.1 Smouldering temperature

Fig. 5-7 shows the peak smouldering temperatures measured at different ignition depths. Because thermocouples sample only a single point, they may miss the local hot spot, so some reported peaks below 250 °C likely underestimate the true maximum and do not indicate sustainable smouldering at those lower values.

When the fire starts at the surface (0 cm), peak temperature falls from about 550 °C down to 350 °C at -40 cm depth. Beyond -40 cm, it remains stable near 300 °C, just above the minimum smouldering threshold. The same trend appears for ignition at -20 cm: temperatures decline to 300 °C by -40 cm and then remain essentially constant at greater depths. In other words, once the front propagates below approximately -40 cm, peak smouldering temperatures are depth-independent at roughly 300 °C.

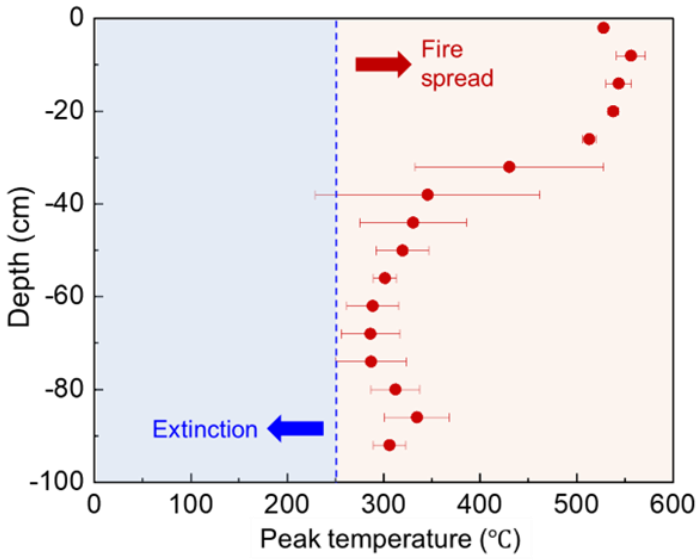

Fig. 5-7 Measured peak smouldering temperature at different depths of the peat fires (the error bar represents the standard deviation of the measured data).

In peat columns ventilated only from the surface, peak smouldering temperature declines with depth because the growing ash weakens the oxygen diffusion to the reaction zone [128]. This agrees well with the trend of smouldering temperatures above -40 cm, as shown in Fig. 5-7. This decline continues down to about -40 cm. Below that depth, temperatures stabilize near 300 °C, indicating that surface-driven oxygen ingress has become negligible and lateral diffusion dominates. As a result, fires ignited deeper than -40 cm remain localised or spread downward without breaking through to the surface. Further experimental and numerical work will be essential to clarify how lateral oxygen supply and ash insulation govern deep-layer smouldering.

5.4.2 Burnt mass loss

After fire extinctionwe measured residual mass in the one-metre column to quantify total peat consumption. A 20% mass loss corresponds to complete combustion of a -20 cm layer. Fig. 5-8 plots mass loss and equivalent burnt thickness versus ignition depth. Surface ignition (z = 0 cm) consumed roughly 25% of the peat, consistent with ~35 cm of surface recession (Fig. 5-3). With ignition below -40 cm, mass loss fell below 10%, and no surface regression or collapse was observed. Thus, despite burn durations exceeding ten days, deep-layer smouldering remains highly incomplete: only a small fraction of the peat undergoes pyrolysis to char, and only a portion of that char oxidises, as evidenced by low reaction-zone temperatures (~300 °C). Because chemical-reaction rates rise exponentially with temperature, prolonged low-temperature smouldering yields minimal mass loss.

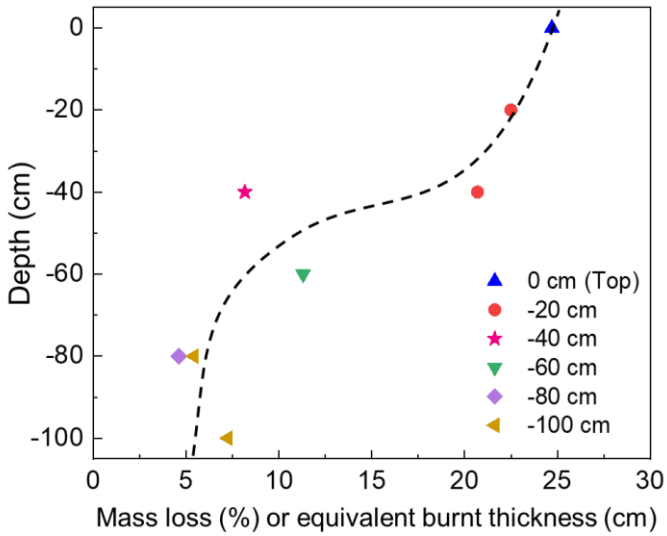

Fig. 5-8 Measured burnt mass loss (or equivalent burnt thickness) vs. initial peat fire depth.

5.4.3 Smouldering CO emission

As smouldering is an incomplete combustion process, carbon monoxide emissions warrant particular attention. CO arises both from peat pyrolysis and from char oxidation [155]. Therefore, Fig. 5-9 summarises CO concentrations measured 5 cm above the original surface for varying ignition depths.

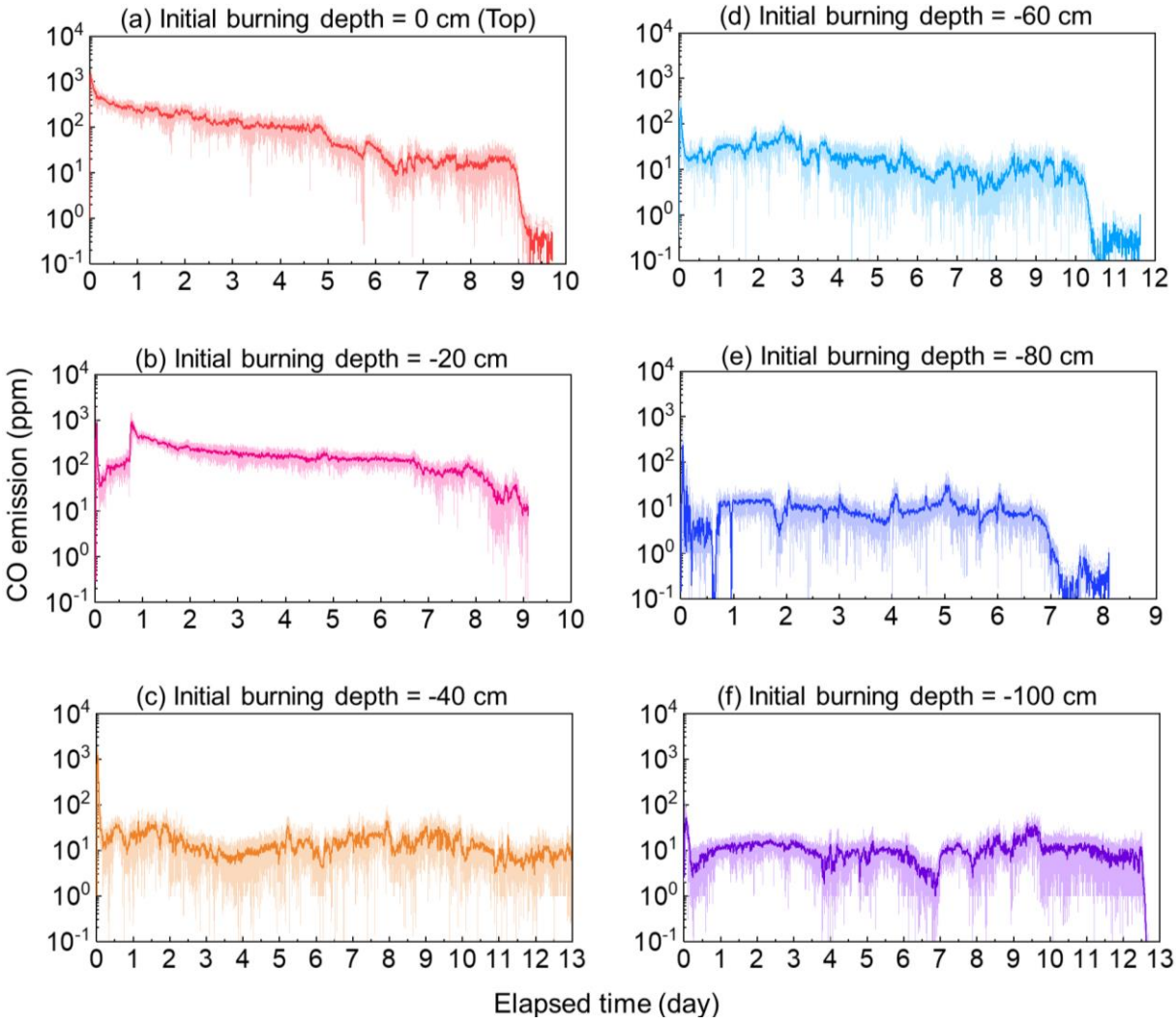

Fig. 5-9 Measured CO concentrations 5 cm above the top surface for peat fires at different depths.

During the 60 min coil-heater ignition, CO levels reached a high level (~10^3 ppm) for all ignition depths. For surface (0 cm) and -20 cm ignition in Fig. 5-9 (a-b), concentrations initially sat around 10^2 ppm, then climbed to about 10^3 ppm as the fire spread upward and laterally across the surface. Such high CO levels pose potentially lethal risks to firefighters and nearby residents [161,162]. By contrast, in-depth or localized smouldering scenarios (Fig. 5-9 (c-f)) yielded CO concentrations on the order of 10 ppm. Although these deep fires are difficult to

detect by satellite or visual patrol, the elevated surface CO indicates that continuous CO monitoring could provide an effective early detection for hidden underground peat fires.

5.4.4 Effect of moisture content

Moisture content strongly influences peat properties [80,128,149,150,163]. To assess its impact on deep smouldering, we ignited a peat column at -60 cm with 50% MC and compared it to a dry (~10% MC) case (Fig. 5-10). Raising MC from ~10% to50 % halved the burn duration from approximately 11 days to 5 days, despite using the same ignition protocol (200 W, 60 min).

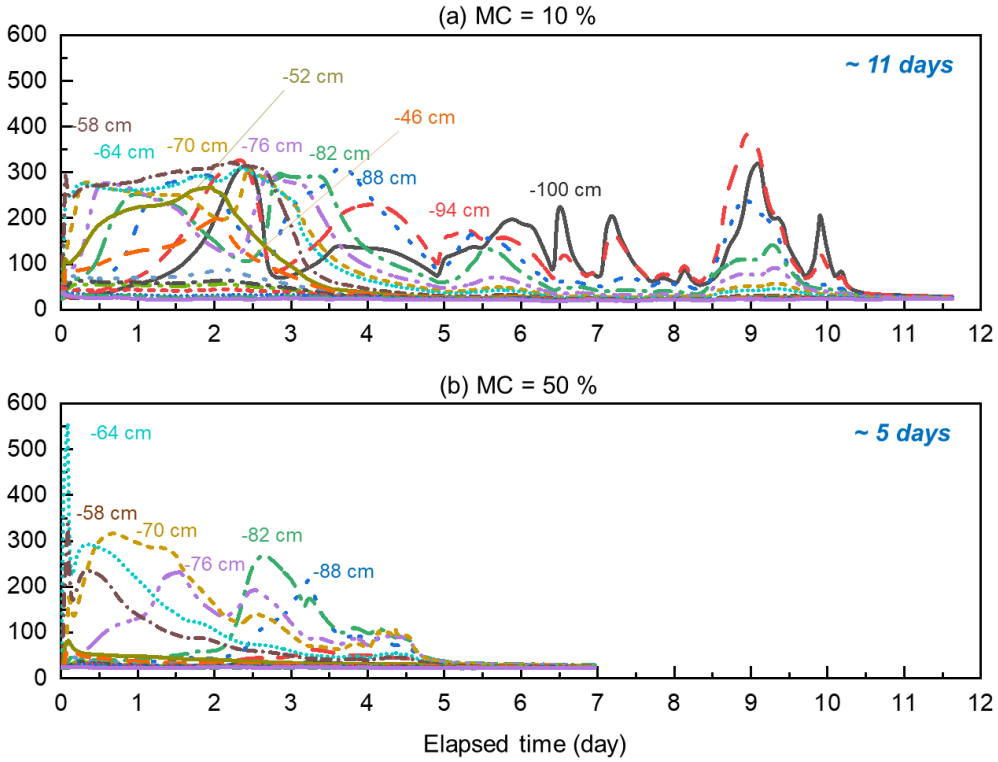

Fig. 5-10 Comparison of smouldering dry peat (MC = 10%) and wet peat (MC = 50%) in the same ignition position of -60 cm. The negative sign means the distance below the initial free surface (z = 0).

In the wet sample, the smouldering front advanced only to -80 cm and exhibited lower peak temperatures. This reduced persistence arises from three moisture-related effects: altered thermal properties, enhanced heat transfer via vapor diffusion, and a strong evaporative heat sink [62,164]. Moreover, evaporated water may re-condense above the reaction zone, further inhibiting spread. These findings highlight the importance of maintaining high peat moisture

in fire-prone areas. Systematic future studies should explore moisture-dependent smouldering behaviour in greater detail.

5.5 Conclusions

This chapter demonstrates that once ignited at any depth, peat smouldering can persist for over ten days in deep soil layers. As ignition moves deeper, four different fire regimes arise: (I) downward spread, (II) bidirectional (downward + upward) spread, (III) deep-layer propagation, and (IV) localized burning. In regimes III and IV, the absence of visible smoke, surface collapse, or regression underscores how difficult these deep fires are to detect.

Temperature-depth profiles reveal that for ignition depths shallower than 40 cm, peak smouldering temperatures fall with increasing depth. Beyond -40 cm, peak temperatures remain stable at approximately 300 °C, indicating that oxygen transport governs fire dynamics in deep layers. Prolonged smouldering at these moderate temperatures produces only minor mass loss due to incomplete combustion. Near-surface CO concentrations span roughly 10 to 10^2 ppm, suggesting a practical monitoring possibility for hidden fires. Finally, elevated peat moisture content is found to slow deep-layer propagation and shorten overall burn duration.

Acknowledgments

This research is funded by the National Natural Science Foundation of China (NSFC) No. 51876183.

Chapter 6 Conclusions of this Thesis

Smouldering is the slow, low-temperature, and flameless combustion which primarily controlled by two mechanisms: system heat loss and **oxygen supply**. The path and rate of oxygen supply are crucial for the heterogeneous oxidations that generate the required heat to balance endothermic processes such as drying, pre-heating, environmental cooling, and endothermic pyrolysis reactions during propagation. Therefore, this thesis focuses on the fundamental problem of oxygen thresholds in near-limit smouldering, and the influence of fuel properties and environmental conditions. Experimental and computational studies were carried out to explore characteristics of limiting oxygen supply under forced internal flow. Large-scale laboratory experiments (1 metre in height) were conducted to demonstrate persistent smouldering phenomena under oxygen-limited conditions. The findings and conclusions in this thesis contribute to an in-depth understanding of smouldering combustion, which enriching prevention strategies for smouldering fires, and assists in optimising the applied smouldering systems.

6.1 Outcomes of the present research

First, *Chapter 1* comprehensively reviewed the background, research motivation, current methodologies and insights in literature. Several knowledge gaps were identified: (1) the fundamental research problem of the actual minimum oxygen rate required to sustain smouldering remains unclear. (2) the roles of fuel properties and environmental conditions are still not well understood. (3) Even for the same fuel, varying values of LOC are reported due to different setup and boundary conditions. The general research objectives and methodologies were determined to address these gaps.

In *Chapter 2*, the limiting oxygen supply to sustain different smouldering propagation modes is experimentally quantified with a forced internal flow in a novel reactor. Smouldering propagation in peat soil under varying internal oxidiser flow velocities (up to 14.7 mm/s) and oxygen concentrations ranging from 2% to 21% were investigated. The findings reveal a transition in smouldering behaviour: at higher velocities, smouldering propagates bidirectionally (forward and opposed), while reducing the velocity results in unidirectional propagation. At a velocity as low as 0.3 mm/s, smouldering ceases, with the minimum temperature recorded at around 300°C. As internal flow velocity increases, the limiting oxygen concentration for sustaining smouldering decreases, reaching a minimum value below 2%.

When the oxygen concentration exceeds 10%, the minimum oxygen supply rate stabilizes at 0.08 ± 0.01 g/m^2·s. However, for oxygen concentrations below 10%, the required oxygen supply rate rises sharply due to enhanced convective cooling caused by the higher internal flow velocities.

Furthermore, the role of fuel bulk density and particle size were determined and analysed in *Chapter 3*. Pine needles of bulk density (55–120 kg/m^3) and wood samples of particle size (1–50 mm) were selected for experiments. Our results show that the minimum airflow velocity required to sustain smouldering increases as bulk density decreases or particle size increases. At higher airflow velocities, smouldering initially propagates unidirectionally (opposed), transitioning to bidirectional propagation (opposed + forward). However, when the pore size is large (due to larger fuel particles or lower bulk density), bidirectional propagation consistently occurs because oxygen can penetrate through the opposed smouldering front. A simplified thermochemical analysis was conducted to highlight the role of interparticle heat transfer in determining the minimum oxygen supply rate for sustaining smouldering propagation.

In *Chapter 4*, a physics-based 1-D computational model was build integrating heat-and-mass transfer and 5-step heterogeneous chemistry to investigate the oxygen threshold of smouldering propagation in porous pine needle beds subjected to forced internal oxidiser flow. Simulation results revealed that, the required oxidiser flow velocity or oxygen supply rate increased as the oxygen concentration decreased, and the predicted LOC about 3%, agreeing well with the experimental observations and theoretical analysis. Moreover, the required airflow velocity was predicted to increase as the fuel density and environmental temperature decreased, or the moisture content increased, and the predicted maximum moisture content capable of supporting smouldering was about 110 %. At the smothering limit, the modelled minimum smouldering temperature and propagation rate were around 300 ^{o}C and 0.5 cm/h.

In *Chapter 5*, the smouldering underground fires are experimentally demonstrated to be able to sustain in deep soil layers for more than 10 days, regardless of the initial burning position. As the initial burning position becomes deeper, four smouldering burning modes can be observed: (I) downward propagation, (II) upward-and-downward propagation, (III) in-depth propagation, and (IV) no propagation (local burning). For the in-depth fire propagation and localised burning, no visual smoke, noticeable collapse, or regression was observed, indicating the difficulty of detecting deep peat fire. For peat fires shallower than 40 cm, the peak smouldering temperature decreases as the depth increases. Otherwise, the smouldering

temperature remains at about 300 ^{o}C and becomes insensitive to the depth, revealing the dominant role of oxygen supply in peat fire dynamics in deep soil layers. Despite long-term burning, the mass loss fraction is small because the low smouldering temperature causes incomplete combustion. The CO concentration near the surface varies on the order of 10 and 10^2 ppm, so it can be used to detect underground fires and monitor their intensity. High peat moisture content can slow down in-depth fire propagation and reduce the burning duration.

6.2 Future work

This thesis has conducted foundational experimental and computational studies to systematically explore the oxygen supply thresholds and critical oxygen supply characteristics of smouldering combustion. However, smouldering is a complex process, and smouldering fire phenomenon on Earth is an interdisciplinary topic involving combustion science, geoscience, and ecology. Therefore, future research is necessary to gain a deeper understanding of smouldering phenomena and its impacts in Earth ecosystems.

6.1.1 Equivalence in Realistic and Complex Oxygen Supply Scenarios

From a fundamental research perspective, this study employed a forced internal flow oxygen supply model to determine the minimum oxygen required to sustain smouldering combustion. However, apart from certain applied smouldering systems that process biowaste using forced flow, the results obtained under these conditions are difficult to directly apply to realistic smouldering scenarios, such as underground smouldering fires. Therefore, future research requires additional experiments, simulations, and theoretical analyses to compare and establish connections between the oxygen thresholds identified in fundamental studies under forced flow and those in realistic fire scenarios. This will help contribute laboratory-based research findings into practical applications for fire safety management.

6.1.2 Field Experiments to Verify Oxygen Threshold Findings

Full-scale smouldering peat fire experiment will be performed in the field. The maximum burning depth and minimum oxygen supply should be investigated by conducting real-scale field experiments. In addition, it contributes to verify the results from laboratory experiment and numerical simulations. Eventually, the whole series of multi-scale smouldering research

will contribute to understanding the dynamics of persistent underground smouldering fires.

6.1.3 Development of AI Models to Predict Oxygen Thresholds in Smouldering

Since numerous experimental and numerical data have been obtained, a comprehensive dataset can be compiled with varying fuel types and composition, fuel properties (e.g., bulk density, particle size, moisture content) and environmental conditions (e.g., temperature, gravity). Artificial intelligence models such as neural networks can be trained to predict LOC and minimum oxygen supply rate of smouldering combustion and fires. This approach can systematically leverage the existing insights and new methods, which not only conserves additional experimental and computational resources but also facilitates the application of current results to a broader range of scenarios.

References

[1] G. Rein, X. Huang, Smouldering wildfires in peatlands, forests and the arctic: Challenges and perspectives, Curr. Opin. Environ. Sci. Heal. 24 (2021) 100296.

[2] Y. Chen, Z. Wang, S. Lin, Y. Qin, X. Huang, A review on biomass thermal-oxidative decomposition data and machine learning prediction of thermal analysis, Clean. Mater. 9 (2023) 100206.

[3] J.G. Quintiere, Principles of fire behavior, Second Edi, Taylor & Francis Group, Boca Raton, 2016.

[4] G. Rein, N. Cleaver, C. Ashton, P. Pironi, J.L. Torero, Smoldering combustion, in: SFPE Handb. Fire Prot. Eng. Fifth Ed., Elsevier, New York, NY, 2016: pp. 581–603.

[5] Y. Chen, S. Lin, Y. Qin, N.C. Surawski, X. Huang, Carbon distribution and multi-criteria decision analysis of flexible waste biomass smouldering processing technologies, Waste Manag. 167 (2023) 183–193.

[6] F. Richter, F.X. Jervis, X. Huang, G. Rein, Effect of oxygen on the burning rate of wood, Combust. Flame. 234 (2021) 111591.

[7] O. Fujita, Solid combustion research in microgravity as a basis of fire safety in space, Proc. Combust. Inst. 35 (2015) 2487–2502.

[8] C. Wu, X. Huang, S. Wang, F. Zhu, Y. Yin, Opposed Flame Spread over Cylindrical PMMA Under Oxygen-Enriched Microgravity Environment, Fire Technol. 56 (2020) 71–89.

[9] G. Rein, Smouldering Fires and Natural Fuels, in: Claire M. Belcher (Ed.), Fire Phenom. Earth Syst. An Interdiscip. Guid. to Fire Sci., Wiley–Blackwell: London, 2013: pp. 15–33.

[10] S.N. Koplitz, L.J. Mickley, M.E. Marlier, J.J. Buonocore, P.S. Kim, T. Liu, M.P. Sulprizio, R.S. DeFries, D.J. Jacob, J. Schwartz, M. Pongsiri, S.S. Myers, Public health impacts of the severe haze in Equatorial Asia in September-October 2015: Demonstration of a new framework for informing fire management strategies to reduce downwind smoke exposure, Environ. Res. Lett. 11 (2016).

[11] S.E. Page, F. Siegert, J.O. Rieley, H.D. V. Boehm, A. Jayak, S. Limink, A. Jaya, S. Limin, The amount of carbon released from peat and forest fires in Indonesia during 1997, Nature. 420 (2002) 61–65.

[12] A. Heil, J.G. Goldammer, Smoke-haze pollution: a review of the 1997 episode in Southeast Asia, Reg. Environ. Chang. 2 (2001) 24–37.

[13] R.C. Scholten, R. Jandt, E.A. Miller, B.M. Rogers, S. Veraverbeke, Overwintering fires in boreal forests, Nature. 593 (2021) 399–404.

[14] J.L. McCarty, T.E.L. Smith, M.R. Turetsky, Arctic fires re-emerging, Nat. Geosci. 13 (2020) 658–660.

[15] W. Xu, R.C. Scholten, T.D. Hessilt, Y. Liu, S. Veraverbeke, Overwintering fires rising in eastern Siberia, Environ. Res. Lett. 17 (2022).

[16] Y. Qin, D.N.S. Musa, S. Lin, X. Huang, Deep peat fire persistently smouldering for weeks : a laboratory demonstration, Int. J. Wildl. Fire. 32 (2022) 86–98.

[17] Y. Zhang, Y. Shu, Y. Qin, Y. Chen, X. Huang, M. Zhou, Resurfacing of Underground Peat Fire: Smoldering Transition to Flaming Wildfire on Litter Surface, Int. J. Wildl. Fire. 33 (2024) WF23128.

[18] L. Hermesdorf, B. Elberling, L. D'Imperio, W. Xu, A. Lambæk, P.L. Ambus, Effects of fire on CO2, CH4, and N2O exchange in a well-drained Arctic heath ecosystem, Glob. Chang. Biol. 28 (2022) 4882–4899.

[19] E.E. Webb, M.M. Loranty, J.W. Lichstein, Surface water, vegetation, and fire as drivers of the terrestrial Arctic-boreal albedo feedback, Environ. Res. Lett. 16 (2021).

[20] K.N. Palmer, Smouldering combustion in dusts and fibrous materials, Combust. Flame. 1 (1957) 129–154.

[21] M. Toledo, A. Arriagada, N. Ripoll, E.A. Salgansky, M.A. Mujeebu, Hydrogen and syngas production by hybrid filtration combustion: Progress and challenges, Renew. Sustain. Energy Rev. 177 (2023).

[22] T.L. Rashwan, J.L. Torero, J.I. Gerhard, Heat losses in a smouldering system: The key role of non-uniform air flux, Combust. Flame. 227 (2021) 309–321.

[23] J. Li, Q. Zhao, M. Si, Z. Dong, J. Huang, Y. Li, X. Hu, S. Tian, Removal of cadmium in contaminated soils by self-sustaining smoldering, J. Environ. Chem. Eng. 11 (2023) 109869.

[24] C.R. Lohri, S. Diener, I. Zabaleta, A. Mertenat, C. Zurbrügg, Treatment technologies for urban solid biowaste to create value products: a review with focus on low- and middle-income settings, Rev. Environ. Sci. Biotechnol. 16 (2017) 81–130.

[25] W. and the E. Department of Agriculture, J. Pickin, C. Wardle, K. O'farrell, P. Nyunt, S. Donovan, National waste report 2020, 2020.

[26] IPCC, 2006 IPCC guidelines for national greenhouse gas inventories, (2006).

[27] Y. Chen, S. Lin, Z. Liang, X. Huang, Clean smoldering biowaste process : Effect of burning direction on smoke purification by self-sustained flame, Fuel Process. Technol.

237 (2022) 107453.

[28] J.L. Torero, J.I. Gerhard, M.F. Martins, M.A.B. Zanoni, T.L. Rashwan, J.K. Brown, Processes defining smouldering combustion: Integrated review and synthesis, Prog. Energy Combust. Sci. 81 (2020) 100869.

[29] W. Zhang, Q. Song, X. Wang, X. Wang, H. Li, Z. Yang, Experimental study and modeling analysis of sewage sludge smoldering combustion at different airflow rates, Waste Manag. 168 (2023) 126–136.

[30] Z. Song, M.A.B. Zanoni, T.L. Rashwan, Modelling oxygen-limited and self-sustained smoldering propagation: Thermochemical treatment of food waste in an inert porous medium, Chem. Eng. J. 468 (2023) 143539.

[31] H.K. Wyn, M. Konarova, J. Beltramini, G. Perkins, L. Yermán, Self-sustaining smouldering combustion of waste: A review on applications, key parameters and potential resource recovery, Fuel Process. Technol. 205 (2020) 106425.

[32] L. Yermán, H. Wall, J. Torero, J.I. Gerhard, Y.L. Cheng, Smoldering Combustion as a Treatment Technology for Feces: Sensitivity to Key Parameters, Combust. Sci. Technol. 188 (2016) 968–981.

[33] E. Christensen, H. Y., F. Restuccia, M.A.M.A. Santoso, X. Huang, G. Rein, Y. Hu, F. Restuccia, M.A.M.A. Santoso, X. Huang, G. Rein, Experimental methods and scales in smouldering wildfires, in: P. Pereira (Ed.), Fire Eff. Soil Prop., CSIRO, 2019: pp. 267–280.

[34] A. Anca-Couce, N. Zobel, A. Berger, F. Behrendt, Smouldering of pine wood: Kinetics and reaction heats, Combust. Flame. 159 (2012) 1708–1719.

[35] D. Cancellieri, V. Leroy-Cancellieri, E. Leoni, A. Simeoni, A.Y. Kuzin, A.I. Filkov, G. Rein, Kinetic investigation on the smouldering combustion of boreal peat, Fuel. 93 (2012) 479–485.

[36] B. Zhou, S. Yang, X. Jiang, J. Cai, Q. Xu, W. Song, Q. Zhou, The reaction of free radicals and functional groups during coal oxidation at low temperature under different oxygen concentrations, Process Saf. Environ. Prot. 150 (2021) 148–156.

[37] O. Kadowaki, M. Suzuki, K. Kuwana, Y. Nakamura, G. Kushida, Limit conditions of smoldering spread in counterflow configuration: Extinction and smoldering-to-flaming transition, Proc. Combust. Inst. 38 (2021) 5005–5013.

[38] R.M. Hadden, G. Rein, C.M. Belcher, Study of the competing chemical reactions in the initiation and spread of smouldering combustion in peat, Proc. Combust. Inst. 34 (2013) 2547–2553.

[39] Y. Qin, Y. Zhang, Y. Chen, S. Lin, X. Huang, Minimum oxygen supply rate for smouldering propagation : Effect of fuel bulk density and particle size, Combust. Flame. 261 (2024) 113292.

[40] X. Huang, G. Rein, Interactions of Earth's atmospheric oxygen and fuel moisture in smouldering wildfires, Sci. Total Environ. 572 (2016) 1440–1446.

[41] C.M. Belcher, J.M. Yearsley, R.M. Hadden, J.C. McElwain, G. Rein, Baseline intrinsic flammability of Earth's ecosystems estimated from paleoatmospheric oxygen over the past 350 million years, Proc. Natl. Acad. Sci. U. S. A. 107 (2010) 22448–22453.

[42] Y. Qin, Y. Chen, S. Lin, X. Huang, Limiting oxygen concentration and supply rate of smoldering propagation, Combust. Flame. 245 (2022) 112380.

[43] H. Yan, O. Fujita, Experimental investigation on the smoldering limit of scraps of paper initiated by a cylindrical rod heater, Proc. Combust. Inst. 37 (2019) 4099–4106.

[44] M.A. Santoso, E.G. Christensen, H.M.F. Amin, P. Palamba, Y. Hu, D.M.J.M.J. Purnomo, W. Cui, A.S. Pamitran, F. Richter, T.E.L. Smith, Y.S. Nugroho, G. Rein, GAMBUT field experiment of peatland wildfires in Sumatra: from ignition to spread and suppression, Int. J. Wildl. Fire. (2022) 949–966.

[45] S. Lin, H. Yuan, X. Huang, A computational study on the quenching and near-limit propagation of smoldering combustion, Combust. Flame. 238 (2022) 111937.

[46] X. Huang, G. Rein, H. Chen, Computational smoldering combustion: Predicting the roles of moisture and inert contents in peat wildfires, Proc. Combust. Inst. 35 (2015) 2673–2681.

[47] C. Lautenberger, C. Fernandez-Pello, Generalized pyrolysis model for combustible solids, Fire Saf. J. 44 (2009) 819–839.

[48] S. Wolfram, Statistical mechanics of cellular automata, Rev. Mod. Phys. 55 (1983) 601.

[49] D.M.J. Purnomo, E.G. Christensen, N. Fernandez-Anez, G. Rein, BARA: cellular automata simulation of multidimensional smouldering in peat with horizontally varying moisture contents, Int. J. Wildl. Fire. 33 (2024) 1–11.

[50] D.M.J. Purnomo, S. Apers, M. Bechtold, P. Sofan, G. Rein, KAPAS II: Simulation of peatland wildfires with daily variations of peat moisture content, Int. J. Wildl. Fire. 32 (2023) 823–835.

[51] D.M.J. Purnomo, M. Bonner, S. Moafi, G. Rein, Using cellular automata to simulate field-scale flaming and smouldering wildfires in tropical peatlands, Proc. Combust. Inst. 38 (2021) 5119–5127.

[52] N. Fernandez-Anez, K. Christensen, V. Frette, G. Rein, Simulation of fingering behavior

in smoldering combustion using a cellular automaton, Phys. Rev. E. 99 (2019) 1–13.

[53] A.J. Watson, J.E. Lovelock, The dependence of flame spread and probability of ignition on atmospheric oxygen: an experimental investigation, Fire Phenom. Earth Syst. an Interdiscip. Guid. to Fire Sci. (2013) 273–287.

[54] M.C. Johnston, J.S. T'ien, Gravimetric measurement of solid and liquid fuel burning rate near and at the low oxygen extinction limit, Fire Saf. J. 91 (2017) 140–146.

[55] A. Kumar, J. T'Ien, Numerical modeling of limiting oxygen index apparatus for film type fuels, Int. J. Spray Combust. Dyn. 4 (2012) 299–322.

[56] H. Wang, P.J. van Eyk, P.R. Medwell, C.H. Birzer, Z.F. Tian, M. Possell, Effects of Oxygen Concentration on Radiation-Aided and Self-sustained Smoldering Combustion of Radiata Pine, ENERGY & FUELS. 31 (2017) 8619–8630.

[57] A. Bar-Ilan, G. Rein, D. C.walther, A.C. Fernandez-Pello, J.L. Torero, D.L. Urban, The effect of buoyancy on opposed smoldering, Combust. Sci. Technol. 176 (2004) 2027–2055.

[58] E.R. Carvalho, C.A. Gurgel Veras, J.A. Carvalho, Experimental investigation of smouldering in biomass, Biomass and Bioenergy. 22 (2002) 283–294.

[59] T.J. Ohlemiller, Modeling of smoldering combustion propagation, Prog. Energy Combust. Sci. 11 (1985) 277–310.

[60] S. Lin, T.H. Chow, X. Huang, Smoldering propagation and blow-off on consolidated fuel under external airflow, Combust. Flame. 234 (2021) 111685.

[61] M.A. Santoso, E.G. Christensen, J. Yang, G. Rein, Review of the Transition From Smouldering to Flaming Combustion in Wildfires, Front. Mech. Eng. 5 (2019) 49.

[62] S. Lin, P. Sun, X. Huang, Can peat soil support a flaming wildfire?, Int. J. Wildl. Fire. 28 (2019) 601–613.

[63] S. Wang, P. Ding, S. Lin, J. Gong, X. Huang, Smoldering and Flaming of Disc Wood Particles Under External Radiation: Autoignition and Size Effect, Front. Mech. Eng. 7 (2021) 1–11.

[64] J. Quintiere, Principles of Fire Behaviour, Alar Elken, New York, 1997.

[65] Y. Chen, Z. Liang, S. Lin, X. Huang, Limits of sustaining a flame above smoldering woody biomass, Combust. Sci. Technol. 195 (2022) 2801–2819.

[66] L. Yermán, H. Wall, J.L. Torero, Experimental investigation on the destruction rates of organic waste with high moisture content by means of self-sustained smoldering combustion, Proc. Combust. Inst. 36 (2017) 4419–4426.

[67] S. Lin, X. Huang, Quenching of smoldering: Effect of wall cooling on extinction, Proc.

Combust. Inst. 38 (2021) 5015–5022.

[68] S. Lin, Y. Liu, X. Huang, How to build a firebreak to stop smouldering peat fire: Insights from a laboratory-scale study, Int. J. Wildl. Fire. 30 (2021) 454–461.

[69] X. Huang, G. Rein, Computational study of critical moisture and depth of burn in peat fires, Int. J. Wildl. Fire. 24 (2015) 798–808.

[70] R. Hadden, G. Rein, Chapter 18 - Burning and Water Suppression of Smoldering Coal Fires in Small-Scale Laboratory Experiments, in: G.B. Stracher, A. Prakash, E.V.B.T.-C. and P.F.A.G.P. Sokol (Eds.), Elsevier, Amsterdam, 2011: pp. 317–326.

[71] S. Lin, Y.K. Cheung, Y. Xiao, X. Huang, Can rain suppress smoldering peat fire?, Sci. Total Environ. 727 (2020) 138468.

[72] M.L. Ramadhan, P. Palamba, F.A. Imran, E.A. Kosasih, Y.S. Nugroho, Experimental study of the effect of water spray on the spread of smoldering in Indonesian peat fires, Fire Saf. J. 91 (2017) 671–679.

[73] N. a. Moussa, T.Y. Toong, C. a. Garris, Mechanism of smoldering of cellulosic materials, Symp. Combust. 16 (1977) 1447–1457.

[74] M. Schmidt, C. Lohrer, U. Krause, Self-ignition of dust at reduced volume fractions of ambient oxygen, J. Loss Prev. Process Ind. 16 (2003) 141–147.

[75] M. Malow, U. Krause, Smouldering combustion of solid bulk materials at different volume fractions of oxygen in the surrounding gas, Fire Saf. Sci. (2008) 303–314.

[76] D.C. Walther, A. Carlos Fernandez-Pello, D.L. Urban, Small-scale smoldering combustion experiments in microgravity, Proc. Combust. Inst. 26 (1996) 1361–1368.

[77] T. Yamazaki, T. Matsuoka, Y. Nakamura, Near-extinction behavior of smoldering combustion under highly vacuumed environment, Proc. Combust. Inst. 37 (2019) 4083–4090.

[78] T. Yamazaki, T. Matsuoka, Y. Li, Y. Nakamura, Applicability of a Low-Pressure Environment to Investigate Smoldering Behavior Under Microgravity, Fire Technol. (2020).

[79] S. Lin, X. Huang, An experimental method to investigate the water-based suppression of smoldering peat fire, MethodsX. 7 (2020).

[80] Y. Hu, E.G. Christensen, H.M.F. Amin, T.E.L. Smith, G. Rein, Experimental study of moisture content effects on the transient gas and particle emissions from peat fire, Combust. Flame. 209 (2019) 408–417.

[81] X. Huang, F. Restuccia, M. Gramola, G. Rein, Experimental study of the formation and collapse of an overhang in the lateral spread of smouldering peat fires, Combust. Flame.

168 (2016) 393–402.

[82] X. Huang, G. Rein, Upward-and-downward spread of smoldering peat fire, Proc. Combust. Inst. 37 (2019) 4025–4033.

[83] F.P. Incropera, Principles of heat and mass transfer, Hoboken, NJ : Wiley. U.S., 2007.

[84] S. Wang, S. Lin, Y. Liu, X. Huang, M.J. Gollner, Smoldering ignition using a concentrated solar irradiation spot, Fire Saf. J. 129 (2022) 103549.

[85] G. Rein, Smoldering Combustion, in: SFPE Handb. Fire Prot. Eng., Springer, New York, 2016: pp. 581–603.

[86] T.J. Ohlemiller, Smoldering combustion, National Institute of Standards and Technology, Gaithersburg, MD, 1986.

[87] Russell A. Ogle, S.E. Dillon, M. Fecke, Explosion from a Smoldering Silo Fire, Process Saf. Prog. 33 (2013) 94–103.

[88] Z. Liang, S. Lin, X. Huang, Smoldering ignition and emission dynamics of wood under low irradiation, Fire Mater. 47 (2023) 514–524.

[89] T.J. Ohlemiller, Smoldering combustion propagation on solid wood, Fire Saf. Sci. Proc. Third Int. Symp. (2006) 565–574.

[90] S. Wang, P. Ding, S. Lin, X. Huang, A. Usmani, Deformation of wood slice in fire: Interactions between heterogeneous chemistry and thermomechanical stress, Proc. Combust. Inst. 38 (2021) 5081–5090.

[91] D. Wu, X. Huang, F. Norman, F. Verplaetsen, J. Berghmans, E. Van Den Bulck, Experimental investigation on the self-ignition behaviour of coal dust accumulations in oxy-fuel combustion system, Fuel. 160 (2015) 245–254.

[92] E. Villacorta, I. Haraldseid, R.F. Mikalsen, B.C. Hagen, S. Erland, G. Kleppe, U. Krause, V. Frette, Onset of smoldering fires in storage silos: Susceptibility to design, scenario, and material parameters, Fuel. 284 (2021).

[93] Z. Song, T. He, M. Li, D. Wu, F. You, Self-sustaining smoldering as a novel disposal approach for food waste with high moisture content, Fuel Process. Technol. 228 (2022) 107144.

[94] Y. Chen, S. Lin, Z. Liang, N.C. Surawski, X. Huang, Smouldering organic waste removal technology with smoke emissions cleaned by self-sustained flame, J. Clean. Prod. 362 (2022) 132363.

[95] T.L. Rashwan, J.L. Torero, J.I. Gerhard, Heat losses in applied smouldering systems: Sensitivity analysis via analytical modelling, Int. J. Heat Mass Transf. 172 (2021) 121150.

[96] G. B.Starcher, A. Prakash, E. V.Sokol, Coal and Peat Fires:A Global Perspective, 1st ed., Elsevier, Oxford, 2011.

[97] A. Ronda, M. Della Zassa, A. Biasin, M.A. Martin-Lara, P. Canu, S.Z. Miry, M.A.B. Zanoni, T.L. Rashwan, J.L. Torero, J.I. Gerhard, Experimental investigation on the smouldering of pine bark, Fuel. 193 (2017) 81–94.

[98] L. Yermán, R.M. Hadden, J. Carrascal, I. Fabris, D. Cormier, J.L. Torero, J.I. Gerhard, M. Krajcovic, P. Pironi, Y.L. Cheng, Smouldering combustion as a treatment technology for faeces: Exploring the parameter space, Fuel. 147 (2015) 108–116.

[99] I. Fabris, D. Cormier, J.I. Gerhard, T. Bartczak, M. Kortschot, J.L. Torero, Y.L. Cheng, Continuous, self-sustaining smouldering destruction of simulated faeces, Fuel. 190 (2017) 58–66.

[100] X. Huang, J. Gao, A review of near-limit opposed fire spread, Fire Saf. J. 120 (2021) 103141.

[101] H. Zhang, Y. Qiao, H. Chen, N. Liu, L. Zhang, X. Xie, Experimental study on flaming ignition of pine needles by simulated lightning discharge, Fire Saf. J. (2020) 103029.

[102] R.J. Yokelson, D.W.T. Griffith, D.E. Ward, Open-path fourier transform infrared studies of large-scale laboratory biomass fires, J. Geophys. Res. Atmos. 101 (1996) 21067–21080.

[103] J.L. Torero, A.C. Fernandez-Pello, Forward smolder of polyurethane foam in a forced air flow, Combust. Flame. 106 (1996) 89–109.

[104] C. Lautenberger, Gpyro Technical Reference, 2014.

[105] X. Huang, G. Rein, Thermochemical conversion of biomass in smouldering combustion across scales: The roles of heterogeneous kinetics, oxygen and transport phenomena, Bioresour. Technol. 207 (2016) 409–421.

[106] F. Yu, G. Wei, X. Zhang, K. Chen, Two effective thermal conductivity models for porous media with hollow spherical agglomerates, Int. J. Thermophys. 27 (2006) 293–303.

[107] Z. Song, Modelling oxygen-limited and self-sustained smoldering propagation: Underground coal fires driven by thermal buoyancy, Combust. Flame. 245 (2022).

[108] Z. Song, C. Kuenzer, Coal fires in China over the last decade: A comprehensive review, Int. J. Coal Geol. 133 (2014) 72–99.

[109] J. Yang, H. Wang, R. Wang, Z. Fu, Y. Hu, Experimental study of smouldering combustion and transient emissions from forest duff with dual layers, Proc. Combust. Inst. 40 (2024) 105354.

[110] J. Yang, G. Rein, H. Chen, M. Zammarano, Smoldering propensity in upholstered furniture: Effects of mock-up configuration and foam thickness, Appl. Therm. Eng. 181 (2020) 115873.

[111] H. Mitchell, R. Amin, M. Heidari, P. Kotsovinos, G. Rein, Structural hazards of smouldering fires in timber buildings, Fire Saf. J. 140 (2023) 103861.

[112] M.A. Decker, D.A. Schult, Dynamics of smoulder waves near extinction, Combust. Theory Model. 8 (2004) 491–512.

[113] J. Yang, N. Liu, H. Chen, W. Gao, R. Tu, Effects of atmospheric oxygen on horizontal peat smoldering fires: Experimental and numerical study, Proc. Combust. Inst. 37 (2019) 4063–4071.

[114] J.L. Dupuy, Slope and fuel load effects on fire behaviour :Laboratory experiments in pine needles fuel beds, Int. J. Wildl. Fire. 5 (1995) 153–164.

[115] P.A. Santoni, P. Bartoli, A. Simeoni, J.L. Torero, Bulk and particle properties of pine needle fuel beds-influence on combustion, Int. J. Wildl. Fire. 23 (2014) 1076–1086.

[116] Y. Qiao, H. Zhang, J. Yang, H. Chen, N. Liu, Transition from smouldering to flaming combustion of pine needle fuel beds under natural convection, Proc. Combust. Inst. 40 (2024) 105343.

[117] J.C. Thomas, A. Simeoni, M. Gallagher, N. Skowronski, An experimental study evaluating the burning dynamics of pitch pine needle beds using the FPA, Fire Saf. Sci. 11 (2014) 1406–1419.

[118] S. Benkorichi, T. Fateh, F. Richard, J.L. Consalvi, A. Nadjai, Investigation of thermal degradation of pine needles using multi-step reaction mechanisms, Fire Saf. J. 91 (2017) 811–819.

[119] H. Wang, P.J. van Eyk, P.R. Medwell, C.H. Birzer, Z.F. Tian, M. Possell, Effects of Oxygen Concentration on Radiation-Aided and Self-sustained Smoldering Combustion of Radiata Pine, Energy and Fuels. 31 (2017) 8619–8630.

[120] J.P. Valdivieso, J. de D. Rivera, Effect of Wind on Smoldering Combustion Limits of Moist Pine Needle Beds, Fire Technol. 50 (2014) 1589–1605.

[121] D. Morvan, M. Larini, Modeling of one dimensional fire spread in pine needles with opposing air flow, Combust. Sci. Technol. 164 (2001) 37–64.

[122] J. Yang, H. Wang, R. Wang, J. Xu, W. Huang, Y. Hu, Experimental and theoretical study on the smoldering combustion of size-fractioned forest duff particles, Int. J. Heat Mass Transf. 231 (2024) 125883.

[123] W. Gong, J. Cuevas, P. Reszka, A. Simeoni, The role of smoldering in the ignition of

Pinus palustris needles, Fire Saf. J. 143 (2024) 104053.
[124] A.K. Rana, S. Guleria, V.K. Gupta, V.K. Thakur, Cellulosic pine needles-based biorefinery for a circular bioeconomy, Bioresour. Technol. 367 (2023) 128255.
[125] H. Yuan, F. Restuccia, F. Richter, G. Rein, A computational model to simulate self-heating ignition across scales, configurations, and coal origins, Fuel. 236 (2019) 1100–1109.
[126] C. Lautenberger, Gpyro-A Generalized Pyrolysis Model for Combustible Solids:Technical Reference, Berkeley, 2014.
[127] S. Lin, S. Wang, X. Huang, Modeling smoldering ignition by an irradiation spot, Fire Saf. J. 134 (2022) 103708.
[128] X. Huang, G. Rein, Downward spread of smouldering peat fire: The role of moisture, density and oxygen supply, Int. J. Wildl. Fire. 26 (2017) 907–918.
[129] Z. Song, B. Dang, H. Zhang, C. Zhao, Y. Xiao, S. Ren, Gas-solid oxygen and thermal nonequilibria of reverse smoldering combustion wave, Proc. Combust. Inst. 40 (2024) 105422.
[130] S. Hugron, J. Bussières, L. Rochefort, Tree plantations within the context of ecological restoration of peatlands: practical guide, Peatland Ecology Research Group, Université Laval, Québec, 2013. http://www.gret-perg.ulaval.ca/uploads/tx_centrerecherche/Tree_Plantation_guide.pdf.
[131] M.R. Turetsky, B. Benscoter, S. Page, G. Rein, G.R. Van Der Werf, A. Watts, Global vulnerability of peatlands to fire and carbon loss, Nat. Geosci. 8 (2015) 11–14.
[132] U. Ballhorn, F. Siegert, M. Mason, S. Limin, Derivation of burn scar depths and estimation of carbon emissions with LIDAR in Indonesian peatlands, Proc. Natl. Acad. Sci. U. S. A. 106 (2009) 21213–21218.
[133] G. Rein, Smouldering Combustion Phenomena in Science and Technology, Int. Rev. Chem. Eng. 1 (2009) 3–18.
[134] A. Witze, The Arctic is burning like never before — and that's bad news for climate change, Nature. 585 (2020) 336–337.
[135] W.M. Jolly, M.A. Cochrane, P.H. Freeborn, Z.A. Holden, T.J. Brown, G.J. Williamson, D.M.J.S. Bowman, Climate-induced variations in global wildfire danger from 1979 to 2013, Nat. Commun. 6 (2015) 1–11.
[136] M.C. Mack, M.S. Bret-Harte, T.N. Hollingsworth, R.R. Jandt, E.A.G. Schuur, G.R. Shaver, D.L. Verbyla, Carbon loss from an unprecedented Arctic tundra wildfire, Nature. 475 (2011) 489–492.

[137] J.E. Goldstein, L. Graham, S. Ansori, Y. Vetrita, A. Thomas, G. Applegate, A.P. Vayda, B.H. Saharjo, M.A. Cochrane, Beyond slash-and-burn: The roles of human activities, altered hydrology and fuels in peat fires in Central Kalimantan, Indonesia, Singap. J. Trop. Geogr. (2020) 1–19.

[138] D. Normile, Indonesia's fires are bad, but new measures prevented them from becoming worse, Science (80-.). (2019).

[139] A.L. Sinclair, L.L.B. Graham, E.I. Putra, B.H. Saharjo, G. Applegate, S.P. Grover, M.A. Cochrane, Effects of distance from canal and degradation history on peat bulk density in a degraded tropical peatland, Sci. Total Environ. 699 (2020).

[140] K. Anderson, A model to predict lightning-caused fire occurrences, Int. J. Wildl. Fire. 11 (2002) 163–172.

[141] F. Restuccia, X. Huang, G. Rein, Self-ignition of natural fuels: Can wildfires of carbon-rich soil start by self-heating?, Fire Saf. J. 91 (2017) 828–834.

[142] H. Svensen, D.K. Dysthe, E.H. Bandlien, S. Sacko, H. Coulibaly, S. Planke, Subsurface combustion in Mali: Refutation of the active volcanism hypothesis in West Africa, Geology. 31 (2003) 581.

[143] C.A. Silva, G. Santilli, E.E. Sano, G. Laneve, Fire occurrences and greenhouse gas emissions from deforestation in the Brazilian Amazon, Remote Sens. 13 (2021) 1–18.

[144] M.B. Dickinson, K.C. Ryan, Introduction: Strengthening the foundation of wildland fire effects prediction for research and management, Fire Ecol. 6 (2010) 1–12.

[145] J. Prestemon, D. Butry, Time to Burn: Modeling Wildland Arson as an Autoregressive Crime Function, Am. J. Agric. Econ. 87 (2005) 756–770.

[146] T. Gumbricht, T. Mccarthy, J. McCarth, D. Roy, P.E. Frost, K. Wessels, Remote sensing to detect sub-surface peat fires and peat fire scars in the Okavango Delta, Botswana, S. Afr. J. Sci. 98 (2002) 851–858.

[147] X. Huang, G. Rein, Smouldering combustion of peat in wildfires: Inverse modelling of the drying and the thermal and oxidative decomposition kinetics, Combust. Flame. 161 (2014) 1633–1644.

[148] W.H. Frandsen, Ignition probability of organic soils, Can. J. For. Res. 27 (1997) 1471–1477.

[149] W.H. Frandsen, The influence of moisture and mineral soil on the combustion limits of smouldering forest duff, Can. J. For. Res. 16 (1987) 1540–1544.

[150] N. Prat-Guitart, G. Rein, R.M. Hadden, C.M. Belcher, J.M. Yearsley, Effects of spatial heterogeneity in moisture content on the horizontal spread of peat fires, Sci. Total

Environ. 572 (2016) 1422–1430.

[151] J. Yang, H. Chen, Natural Downward Smouldering of Peat : Effects of Inorganic Content and Piled Bed, Fire Technol. (2018).

[152] M.A. Santoso, W. Cui, H.M.F. Amin, E.G. Christensen, Y.S. Nugroho, G. Rein, Laboratory study on the suppression of smouldering peat wildfires: effects of flow rate and wetting agent, Int. J. Wildl. Fire. 30 (2021) 378–390.

[153] H. Mulyasih, L.A. Akbar, M.L. Ramadhan, A.F. Cesnanda, R.A. Putra, R. Irwansyah, Y.S. Nugroho, Experimental study on peat fire suppression through water injection in laboratory scale, Alexandria Eng. J. 61 (2022) 12525–12537.

[154] G. Rein, S. Cohen, A. Simeoni, Carbon emissions from smouldering peat in shallow and strong fronts, Proc. Combust. Inst. 32 II (2009) 2489–2496.

[155] Y. Hu, N. Fernandez-Anez, T.E.L.L. Smith, G. Rein, Review of emissions from smouldering peat fires and their contribution to regional haze episodes, Int. J. Wildl. Fire. 27 (2018) 293–312.

[156] B.W. Benscoter, D.K. Thompson, J.M. Waddington, M.D. Flannigan, B.M. Wotton, W.J. De Groot, M.R. Turetsky, Interactive effects of vegetation, soil moisture and bulk density on depth of burning of thick organic soils, Int. J. Wildl. Fire. 20 (2011) 418–429.

[157] G. Rein, N. Cleaver, C. Ashton, P. Pironi, J.L. Torero, The severity of smouldering peat fires and damage to the forest soil, Catena. 74 (2008) 304–309.

[158] S. Lin, Y. Liu, X. Huang, Climate-induced Arctic-boreal peatland fire and carbon loss in the 21st century, Sci. Total Environ. 796 (2021) 148924.

[159] N. Prat-Guitart, G. Rein, R.M. Hadden, C.M. Belcher, J.M. Yearsley, Propagation probability and spread rates of self-sustained smouldering fires under controlled moisture content and bulk density conditions, Int. J. Wildl. Fire. 25 (2016) 456–465.

[160] T. Depci, M. Karta, Peat and lignite leaching process with tetralin in autoclave to produce oil, Physicochem. Probl. Miner. Process. 54 (2018) 334–342.

[161] A. Ernst, J.D. Zibrak, Carbon monoxide poisoning, N. Engl. J. Med. 339 (1998) 1603–1608.

[162] J.C. Norris, S.J. Moore, A.S. Hume, Synergistic lethality induced by the combination of carbon monoxide and cyanide, Toxicology. 40 (1986) 121–129.

[163] N.C. Dadap, A.R. Cobb, A.M. Hoyt, C.F. Harvey, A.G. Konings, Satellite soil moisture observations predict burned area in Southeast Asian peatlands, Environ. Res. Lett. 14 (2019).

[164] S. McAllister, I. Grenfell, a. Hadlow, W.M. Jolly, M. Finney, J. Cohen, Piloted ignition

of live forest fuels, Fire Saf. J. 51 (2012) 133–142.

Appendices

Appendix 1

Thermogravimetric analysis was performed using a PerkinElmer STA6000 instrument under varying oxygen levels, achieved by blending air and nitrogen (N_2). The tested oxygen concentrations included 21% (ambient air), 10%, 5%, 2%, and 0% (pure N_2). Samples weighing 2–3 mg were subjected to a heating rate of 30 °C/min, increasing from ambient temperature to 800 °C. To ensure reproducibility, each condition was tested at least twice.

Figure A1(a) presents the derivative thermogravimetric (DTG) curves for organic peat soils across different oxygen concentrations. The initial mass reduction below 200 °C corresponds primarily to moisture evaporation, contributing to less than 10% of the total weight loss. Beyond the drying phase (<100 °C), two distinct peaks appear, indicating rapid mass loss. The first peak, occurring near 270 °C, signifies pyrolysis, where the peat undergoes thermal decomposition, releasing volatile gases and forming char. Notably, the pyrolysis temperatures remained consistent across all oxygen levels.

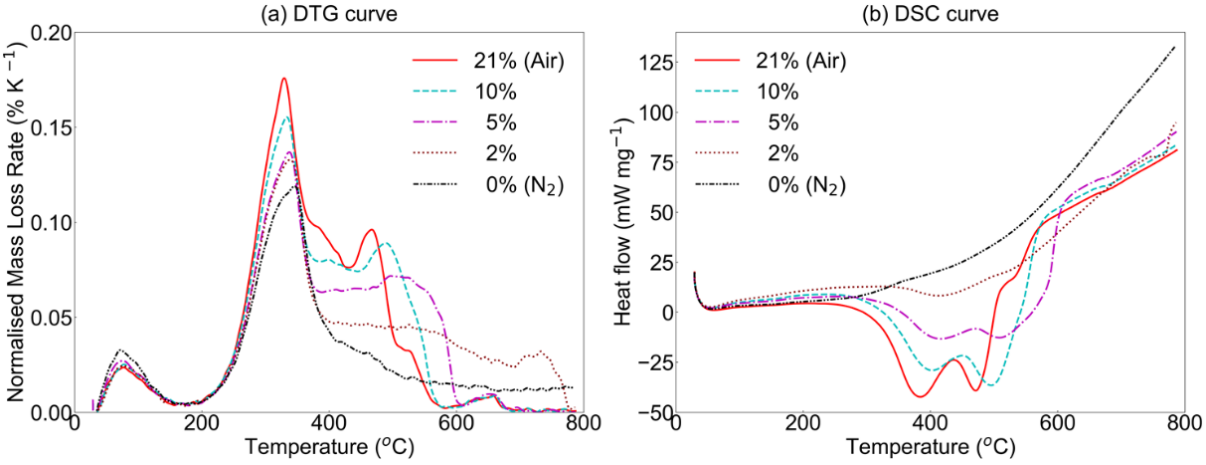

Fig. A1 (a) DTG and (a) DSC curves of tested peat soil in different oxygen concentrations.

The peak mass loss rate exhibits a positive correlation with oxygen concentration, suggesting the occurrence of oxidation near 320°C, where reaction kinetics intensify under higher O_2 levels. As temperatures rise, thermal decomposition releases flammable volatiles, and oxidation becomes the dominant mass loss mechanism. Notably, oxidative reactions were detected even at minimal oxygen concentrations (as low as 2%), confirming that smouldering combustion can occur under oxygen-limited conditions (see Fig. 2-5).

Figure A1(a) further reveals that the cumulative mass loss remains consistent across all oxygen concentrations except in pure N_2, where oxidative processes are entirely suppressed. However, reduced O_2 levels significantly decelerate both oxidation rates and smouldering propagation. The heat flux required for sample heating (see Fig. A1(b)), serves as an indicator of reaction temperatures and associated energy release. Lower oxygen concentrations elevate the ignition temperature while diminishing the peak exothermic rate. Despite these variations, the total heat release over the full temperature range (up to 800°C) remains stable at approximately 12.6 MJ/kg.

Appendix 2

Thermogravimetric analysis was performed using a PerkinElmer STA6000 analyser under both oxidative (air) and inert (N_2) conditions. Small fuel samples (2-3 mg) were subjected to controlled heating from ambient temperature to 800 °C at a constant rate of 20 K/min, enabling precise monitoring of mass variations and heat transfer characteristics. Throughout the experiments, sample mass and heat flux were continuously recorded with high precision. To ensure reproducibility, each experimental condition was repeated at least three times, with representative data presented in Figure A2.

The derivative thermogravimetric (DTG) profiles in Figure A2(a) reveal distinct thermal decomposition patterns for wood and pine needles under nitrogen. Following initial moisture removal (< 100°C), both materials exhibit rapid mass loss starting at approximately 250 °C, reaching maximum decomposition rates between 300-350 °C. This primary devolatilization phase corresponds to endothermic pyrolysis, where organic components thermally degrade into volatile gases and solid char. Comparative analysis demonstrates that wood samples consistently display lower peak decomposition rates than pine needles across all temperature regimes.

Under oxidative conditions (Figure A2(b)), a secondary mass loss peak emerges near 460°C, characteristic of heterogeneous oxidation of the char. This exothermic process occurs significantly above the primary pyrolysis zone, confirming the thermal separation of these distinct reaction mechanisms. Notably, the oxidative degradation rates for wood remain systematically lower than those observed for pine needles.

The differential heat flow profiles (Figures A2(c) and (d)) quantify the thermal energy exchange during heating. Integration of these curves under air and nitrogen atmospheres enabled determination of the net heat of combustion, yielding values of 15.7 MJ/kg for wood and 14.7 MJ/kg for pine needles. These measurements provide fundamental thermochemical parameters essential for understanding the combustion behaviour of smouldering fuels.

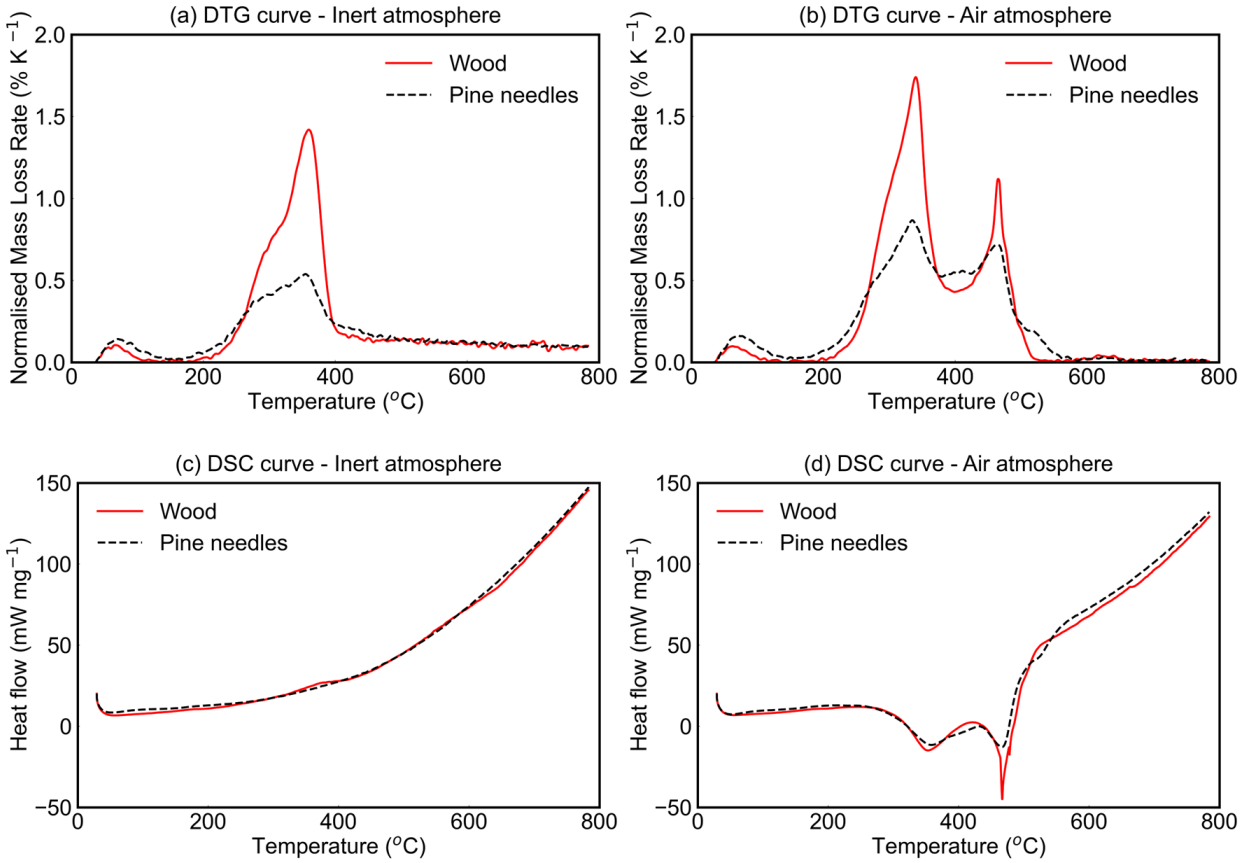

Fig. A2 (a) and (c) show the DTG and DSC curves of wood samples and pine needles in N_2 atmosphere, while (b) and (d) present the comparison in air atmosphere.

Appendix 3

The peat sample was first pulverised into powders and dried at 90 ^{o}C for 48 h. The thermal analysis of the peat sample was performed using a PerkinElmer STA 6000 Simultaneous Thermal Analyser in both air and nitrogen atmospheres. The initial mass was around 2-3 mg, and the sample was heated at a relatively low heating rate of 10 K/min. Fig. A3 shows the remaining mass fraction and mass-loss rate curves of this peat. As expected, the mass-loss rate rapidly increases at about 250 ^{o}C, which could be defined as the pyrolysis temperature.

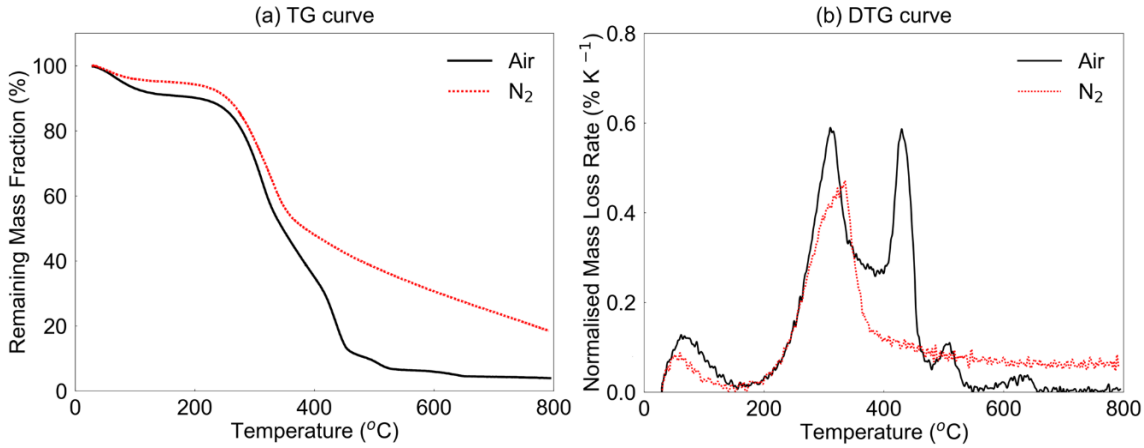

Fig. A3 TGA results of the peat sample at a heating rate of 10 K/min.